(12)
12

FINAL REPORT

INTEGRITY OF WEAR COATING SUBJECTED TO HIGH-SPEED ASPERITY EXCITATION

By

Frederick D. Ju
Presidential Professor

and

Jew-Chyi Liu
Research Assistant

Mechanical Engineering Department
The University of New Mexico
Albuquerque, NM 87131

May, 1990

Work performed under ONR Grant
No. N00014-84-K-0252 and 89-J-1325

Jan. 1985 - Sept. 1989

ABSTRACT

When hard coatings are designed to protect substrates against the high speed frictional excitation of asperities, it is important to consider parameters that would affect the integrity of the coating. Thermo-mechanical cracking and coating delamination are the major failures of hard coating. In analytical modeling, it is important to know the limitation of the model and the validity of the conclusions drawn from the analysis. The report addresses the postulation of a two-dimensional model, which is used for the mathematical simplicity to study the effects of various parameters. For high speed asperity excitation, thermal stress dominates the analytical criteria. The report considers the effect of coating thickness and its critical value. Material parameters are grouped into those of mechanical properties and those of thermal properties. The differences of those properties between the coating and the substrate directly affect the integrity of the coating. Irregularities, especially in the neighborhood of the coating/substrate interface, are introduced to study their damaging effects to the coating integrity. The report also addresses the significance of some unavoidable randomness in coating and the resulting effect on the coating integrity.

TABLE OF CONTENTS

	Page
ABSTRACT	II
TABLE OF CONTENTS	III
LIST OF FIGURES	IV
NOMENCLATURE	VII
1.0 INTRODUCTION	1
2.0 MATHEMATICAL FORMULATION	4
3.0 ASPERITY EXCITATION OVER A HARD WEAR MEDIUM	7
4.0 PARAMETRIC EFFECT IN A COATED MEDIUM	13
5.0 IRREGULARITIES	21
5.1 EFFECTS OF THE CAVITY	21
5.1.1 ANALYTICAL MODEL	22
5.1.2 SOLUTION TECHNIQUE	24
(i) Perturbation Method	24
(ii) Difference Equations	26
(iii) Special Element At Cavity Corner	26
5.1.3 NUMERICAL RESULTS	27
5.1.4 SUMMARY	43
5.2 EFFECTS OF THE LINE CRACK	44
5.2.1 ANALYTICAL MODEL	45
5.2.2 SOLUTION TECHNIQUE	47
(i) Temperature Field	47
(ii) Stress Field	49
(iii) Special Crack Tip Elements	50
5.2.3 NUMERICAL RESULTS	51
5.2.4 SUMMARY	59
5.3 EFFECTS OF THE RANDOM VARIATION IN COATING THICKNESS	61
5.3.1 Formulation Of The Problem	62
5.3.2 Method of Solution	64
5.3.3 Numerical Results	69
5.3.5. SUMMARY	77
6.0. CONCLUSIONS	85
REFERENCES	86

LIST OF FIGURES

Figure		Page
1.	Two-dimensional asperity configuration	3
2.	Stress fields for varying contact area and load distribution	8
3.	Stress field corresponding to varying aspect ratio	9
4.	Critical depth versus Peclet number in two-dimensional case	12
5.	Maximum principal thermal stresses in coating layer versus coating thickness for different mechanical mismatches (surface material properties are constant)	14
6.	Maximum principal thermal stresses in substrate versus coating thickness for different mechanical mismatches (surface material properties are constant)	15
7.	Maximum principal thermal stresses in coating layer versus coating thickness for different mismatches in thermal conductivity (surface material properties are constant)	17
8.	Maximum principal thermal stresses in substrate versus coating thickness for different mismatches in thermal conductivity (surface material properties are constant)	18
9.	Maximum principal thermal stresses versus coating thickness for different mismatches of thermal capacity (surface material properties are constant)	19
10.	Interface shear stress ($\sigma_{\xi\eta}$) versus coating thickness for different mismatches in thermal conductivity (surface material properties are constant)	20
11.	Two-dimensional model of a coated wear surface with a cavity	23
12.	Thermal, mechanical and combined principal stress (cases 7A, 7B, 7C), L=0.094 and η=0.06 above the top edge of the cavity for all cases.	28
13.	Thermal principal stress, η=0.06 above the top edge off the cavity for all cases	30
14.	The effect of Peclet number on the critical depth and the critical ligament thickness	31

15. Thermal principal stress, L=0.094 and η=0.06 above the top edge of the cavity for all cases 32

16. Thermal principal stress L=0.094 and η=0.06 above the top edge of the cavity for all cases 33

17. Thermal principal stress, L=0.094 and η=0.06 above the top edge of the cavity for all cases 34

18. Thermal principal stress L=0.094 and η=0.06 above the top edge of the cavity for all cases 36

19. Thermal principal stress, L=0.094 and η=0.06 above the top edge of the cavity for all cases 37

20. The effect of the ligament thickness on the angle of principal direction of the thermal stress field 38

21. The effect of Young's modulus of the coating layer on the angle of principal direction of the thermal stress field 39

22. The effect of Young's modulus of the substrate on the angle of principal direction of the thermal stress field 40

23. The effect of thermal conductivity of the coating layer on the angle of principal direction of the thermal stress field 41

24. The effect of thermal conductivity of the substrate on the angle of principal direction of the thermal stress field 42

25. Two-dimensional model 46

26. Energy balance at crack tip 48

27. Temperature distribution, L=0.022 52

28. Effect of the location of the moving heat source on stress intensity factors 54

29. Stress intensity factors vs Young's modulus 55

30. Stress intensity factors vs the coefficient of thermal expansion 56

31. Stress intensity factors vs thermal conductivity 57

32. Stress intensity factors vs thermal capacity 58

33. Effect of ligament thickness on stress intensity factors 60

34. Mean temperature as a function of η with coating thickness d_0=0.03 for thermal conductivity impedance 71

35. Mean temperature as a function of η with coating thickness d_0=0.05 for thermal conductivity impedance 72

36. Standard deviation as a function of η with coating thickness d_0=0.03 for thermal conductivity impedance 73

37. Standard deviation as a function of η with coating thickness d_0=0.05 for thermal conductivity impedance 74

38. Mean temperature at the coating/substrate interface as a function of mean coating thickness d_0 for thermal conductivity impedance 75

39. Standard deviation at the coating/substrate interface as a function of mean coating thickness d_0 for thermal conductivity impedance 76

40. Mean temperature as a function of the frequency p with coating thickness d_0=0.05 for thermal conductivity impedance 78

41. Standard deviation as a function of the frequency p with coating thickness d_0=0.05 for thermal conductivity impedance 79

42. Mean temperature as a function of η with coating thickness d_0=0.03 for thermal capacity impedance 80

43. Mean temperature as a function of η with coating thickness d_0=0.05 for thermal capacity impedance 81

44. Standard deviation as a function of η with coating thickness d_0=0.03 for thermal capacity impedance 82

45. Standard deviation as a function of η with coating thickness d_0=0.05 for thermal capacity impedance 83

NOMENCLATURE

a	asperity characteristic dimension, the half width of the contact area
c	specific heat
$C(t)$	distance from x_1 origin to the trailing edge of the moving heat source
c_1	dilatational wave speed
c_2	shear wave speed
d	the dimensionless coating thickness (= H/a)
d_0	the dimensionless mean coating thickness (= H_0/a)
e	depth of the cavity
E_I, E_{II}	Young's modulus of the coating layer and the substrate, respectively
$E_\alpha[\cdot]$	the expected value
$f(\alpha)$	the random fluctuation function
H	the coating thickness
H_0	the mean coating thickness
k	thermal conductivity
K_I	mode I stress intensity factor
K_{II}	mode II stress intensity factor
L'	ligament thickness
L	dimensionless ligament thickness (=L'/d)
M	Mach number
P	center of the finite difference cell
N,S,W,Z	surrounding point of P
$P(x)$	load distribution over the contact area
P_0	average pressure over the contact area
$q(x)$	heat flux distribution through the contact area
q_0	average heat flux through the contact area
R_I,R_{II}	Peclet numbers of the surface layer and the substrate, respectively
T	temperature field
U	internal energy
u_1, u_2	displacement in x_1 and x_2 direction, respectively
u, v	dimensionless displacement in ξ and η direction (=u_i/d), respectively
V	traversing speed of asperity (in x direction)
$Var_\alpha[\cdot]$	variance
$\{x', y'\}$	material coordinate fixed to the medium
$\{x, y\}$	convective coordinate fixed to the moving asperity
α	the sample random variable

β	the material region: I for the coating layer; II for the substrate
δ	mass density ratio ($=\rho_\beta/\rho_I$)
δ_{ij}	Kronecker delta
ϕ	dimensionless temperature field ($=(T-T_0)k/q_0a$)
κ	thermal diffusivity
λ, μ	Lame constants
σ_{11}, σ_{12}, σ_{22}	stress field
$\sigma_{\xi\xi}$, $\sigma_{\xi\eta}$, $\sigma_{\eta\eta}$	dimensionless stresses ($=\sigma_{ij}/\mu$)
∂_x^n, ∂_y^n	n^{th} partial derivative with respect to x or y
(ξ, η)	dimensionless coordinate (=x/a, y/a)
ρ	mass density
Ω	statistical sample space
τ	dimensionless time (Vt/d)
$(\sigma_{ij})_i$	the perturbative order for the stress components

1.0 INTRODUCTION

The present report addresses the integrity of a coated medium, which is subjected to the frictional excitation of a high-speed asperity. Break-down of the coating integrity occurs principally in the form of cracking of the coating or delamination of the coating from the substrate. With Coulomb friction predominates in asperity excitation, the stress state in the coated medium and particularly in the neighborhood of the coating/substrate interface is governed by the thermo-mechanical field. The thermal field results from the dissipative frictional power, which manifests as thermal load traversing over the wear surface of the coated medium. The thermal component of the stress state dominates with increase of the asperity speed. These high thermal stresses will then initiate fracture in the coated material, inasmuch as the coating is introduced as a surface modification to improve the surface wear property of the contacting bodies.

The integrity of the coating relies first on the choice of the coating material, which would reduce friction as well as resist thermal cracking. The integrity of the coating also depends on the interaction between the coating and its substrate, which it is designed to protect. The design of an effective coating is, therefore, depending on the property of the coating, its geometry, and its property matching, or mismatching, with the substrate.

For the purpose of a fundamental understanding of the parametric effects which can best adapt to later application to design, the study adopted an analytical formulation. The mathematical model is represented by differential equations, which govern the thermo-mechanical field of the coated medium and the substrate. The dynamic boundary conditions are described by the boundary values of the field. From the analytical formulation, mechanical and thermal properties that affect in a dominant way the thermo-mechanical field can be identified. The effect of the coating thickness and their irregularities can be quantified. In the analyses, emphasis has been placed on the coating being a hard deposition over the substrate. The mathematical

model is thus simplified to allow the use of thermoelastic formulation. For hard coatings, it is postulated that failures will initiate by thermo-mechanical cracking. The crack may occur with cohesive failure. The criterion is the maximum tensile stress to reach a limit. Shear crack may exist in the coating/substrate interface. The limiting shearing stress will then be the cause of coating delamination.

The report will first address the coating as a single material in its response to the asperity excitation. The purpose is to identify those important characteristics of the coating material. The deterministic effect of coating thickness will be established, especially when the coating is thin, in the neighborhood of from 20 to 100 μ. The interfacial relationship between the coating and the substrate will be studied in detail for both the mechanical properties and the thermal properties of both materials. The interfacial irregularities, defects and random thickness, will then be discussed.

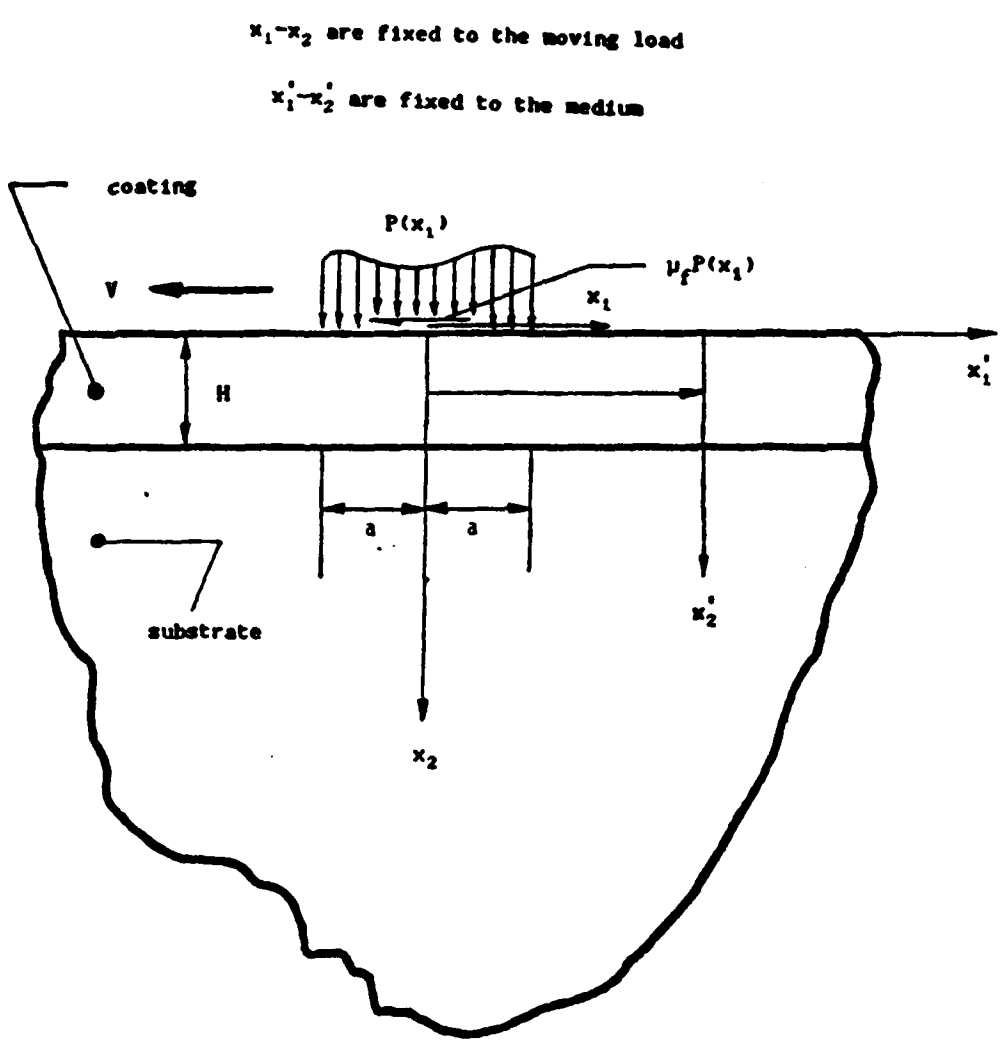

Figure 1. Two–dimensional asperity configuration

2.0 MATHEMATICAL FORMULATION

The traversing asperity imposes a moving traction over the surface as well as a moving heat source caused by the rate of frictional work. The stress field caused by the traction, normal and frictional, is the mechanical portion of the response, while that of the heat source is the thermal portion of the response. In numerical computations, the size of the asperities are of the order of 1 mm. The total thickness of the medium including both the coating layer and the substrate is at least an order of magnitude larger than the asperity size. Mathematically, the material is represented by a half space with the asperity traversing over the surface boundary at a uniform speed (V) as shown in Figure 1.

The asperity is characterized by the contact pressure $p(x_1)$, distributed over a contact width of 2a. The coefficient of friction μ_f is postulated at the steady state value corresponding to that of the surface temperature. For hard coating surface, Blau (1980) and Ruff and Blau (1980), demonstrated that the surface yield, due to the asperity excitation, are sub-granular. The plastic deformation and surface shear for hard wear material are restricted to a very thin surface layer of 4-7 microns. If the depth at which cracks initiate is of an order larger than that of the plastic zone, the thermo-elastic theories for crack initiation may apply. The energy loss due to plastic deformation is thus incorporated into the frictional energy loss on the wear surface.

The governing differential equations are the Fourier equation[1] and the thermo-elastic Navier's equation, respectively expressed in the material coordinates (fixed to the coated medium):

$$\kappa_\beta \partial_{ii} T^\beta = \partial_t T^\beta, \tag{1}$$

$$(\lambda_\beta + \mu_\beta)\partial_{ij} u_j^\beta = \rho_\beta \ddot{u}_i^\beta + (3\lambda_\beta + 2\mu_\beta)\alpha_\beta \partial_i T^\beta, \tag{2}$$

[1]The Fourier equation holds provided that the asperity speed is lower than the speed of thermal wave.

where (λ, μ) are the Lame's elastic coefficients, u_i is the displacement field, T is the temperature field, ρ is the mass density, α is the coefficient of thermal expansion, κ is the thermal diffusivity, i and j index the coordinates and β indexes I and II for the coating layer and the substrate respectively, and where ∂_t denotes a time derivative. The indicial summation convention and Schouten's partial derivative notation, $\partial_i = \partial/\partial x_i$, are used. Both governing equations (1, 2) require explicit time-dependent solutions. The analytical complexity may be alleviated by using the convective coordinates (fixed to the asperity), provided that the asperity parameters are uniform and that the geometry is uniform in the traversing direction and the solutions are of steady--state. Equations in (1, 2) become

$$\kappa_\beta \partial_{jj} T^\beta = V \partial_1 T^\beta, \tag{3}$$

$$\partial_{ij} u_j^\beta + (1-2\nu_\beta)\partial_{jj} u^\beta = G_\beta M^2 (1-2\nu_\beta)\partial_{11} u_i^\beta + 2(1+\nu_\beta)\alpha_\beta \partial_i T^\beta, \tag{4}$$

where ν_β is the Poisson's ratio, $M=V/C_2$ ($= [V^2\rho_{II}/\mu_{II}]^{1/2}$), is the Mach number of shear in Region II, and $G_\beta = \mu_{II}\rho_\beta/\mu_\beta\rho_{II}$. The stress field $\{\sigma_{ij}\}$ is computed from the solved displacement field $\{u_i\}$ through the thermoelastic Hookian law given by:

$$\sigma_{ij}^\beta = \lambda_\beta \partial_k u_k^\beta \delta_{ij} + \mu_\beta(\partial_j u_i^\beta + \partial_i u_j^\beta) + (3\lambda_\beta + 2\mu_\beta)\alpha_\beta T^\beta \delta_{ij}, \tag{5}$$

where δ_{ij} is the Kronecker delta.

On the surface boundary, the rate of friction work done by the asperity's traversing over the wear surface manifests as heat input. The asperity excitation also exerts a pressure and friction force on the boundary. Hence at $x_2 = 0$,

$$k_1 \partial_2 T^I = -q_o = -\mu_f P(x_1) V, \tag{6}$$

$$\sigma_{22}^I = -P(x_1), \tag{7}$$

$$\sigma_{12}^{I} = \mu_f P(x_1),$$

where k is the thermal conductivity, x_1 is the coordinate in the traversing direction of the asperity, and $p(x_1)$ is the asperity pressure in the contact zone and zero elsewhere on the surface boundary. The temperature and the stress field satisfy the regularity conditions at infinity. At the coating/substrate interface, the continuity conditions hold for temperature, heat flux, traction, and displacement components at $x_2 = H$,

$$T^{I} = T^{II}, \quad k_I \partial_2 T^{I} = k_{II} \partial_2 T^{II},$$

$$\sigma_{2j}^{I} = \sigma_{2j}^{II}, \quad u_j^{I} = u_j^{II}.$$

For the steady state solution of the homogeneous wear medium, equations (3, 4) are solved with the boundary and continuity conditions using the method of Fourier transform. The method facilitates the parametric study of the properties.

When irregularities occur in the medium, homogeneity condition in the traversing direction of the asperity no longer holds. The condition for transformation to equations in (3, 4) cannot be justified. Hence more complex equations in (1, 2), which are defined in the material coordinates, must be used. With the explicit time variable, finite difference method is applied for the solution of specific materials and specific geometries.

3.0 ASPERITY EXCITATION OVER A HARD WEAR MEDIUM

From the governing equations, the boundary conditions and the continuity conditions (1 - 9), it is noticed that the thermo-mechanical state (σ_{ij}, u_i) is influenced by the asperity parameters (a, t, P, V) and the material parameters (λ, μ, ρ, α, k, κ, μ_f). The coefficient of Coulomb friction μ_f affects as a material parameter on the wear surface only. The asperity parameter (t) is the aspect ratio of the asperity contact area, the length perpendicular to the traverse direction to the width in the traverse direction. The three dimensional characteristics of the moving asperity was solved by Huang and Ju (1985).

The asperity parameters involve those excitation-related (V, P) and those contact area configuration-related (a, t). Larger half-width (a) leads to longer period of heat input. The thermo-mechanical field does not depend on the shape of contact area, Figure 2 (Huang and Ju, 1987). Yet its aspect ratio affects the temperature and the thermal stress states, Figure 3 (Huang and Ju, 1987). It is noticed that at the critical depth, at which the maximum value of principal thermal stress in tension occurs, a square or a circular contact area (t = 1) could result in almost six times the value of a two-dimension solution (t = ∞). Two dimensional modeling is therefore useful for the determination of the characteristics of the wear coating, but not in the actual evaluation of the stress state. The asperity velocity (V) influences the thermo-mechanical field in both the heat input, Equation (6) and the convective terms in Equations (3, 4). The latter, occurring in the differential equation, can be combined with the material parameters, forming the Peclet Number ($R = Va/\kappa$) in Equation (3) and the Mach Number ($M = V/C$) in Equation (4). The former, being the surface rubbing speed, directly determines the rate of heat input. It is conceivable that at low rubbing speed the mechanical portion of the stress dominates. The static case of $V = 0$ is indeed the limiting case. At high speed, however, the thermal stress prevails. Huang and Ju (1987) demonstrated that at a rubbing speed of 15 m/s the thermal stress is more than six time that of the mechanical portion of the stress. It was noted that the maximum values of the thermal and the mechanical components of the

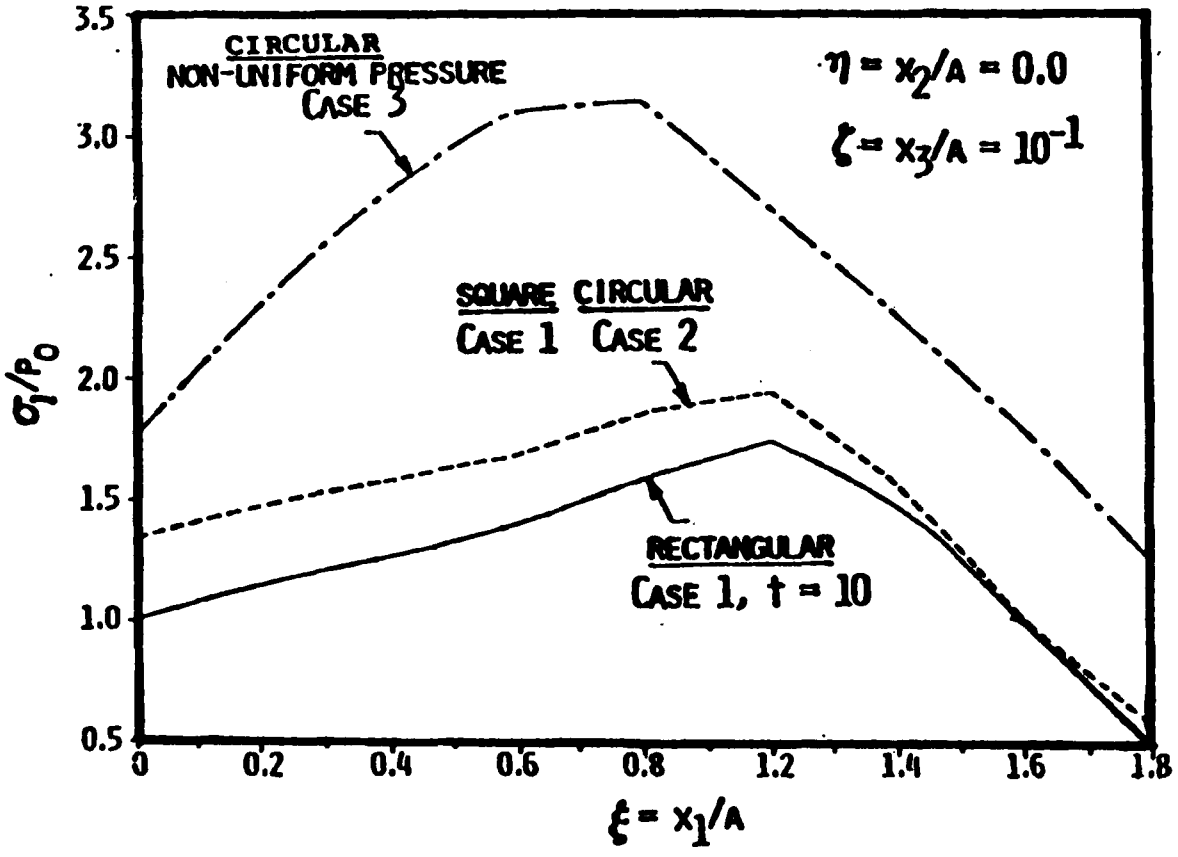

Figure 2. **Stress fields for varying contact area and load distribution**

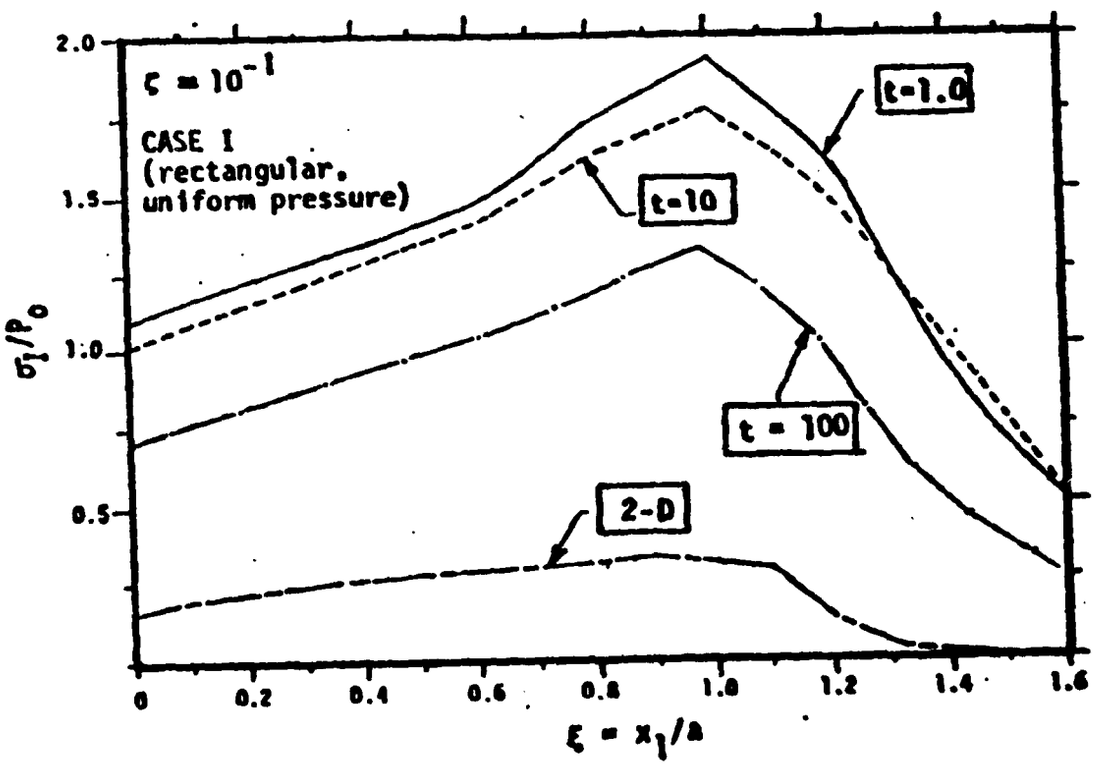

Figure 3. Stress field corresponding to varying aspect ratio

stress do not occur at the same location nor do they have the same principal directions. Hence, the estimate of the wear characteristics, due to high speed asperity excitation, shall be based on the thermal stress state.

In the material parameters, the mass density occurs in the inertial term in Equations (2, 4). However, since the asperity traversing speed is much below the Rayleigh wave speed, its effect there is essentially perturbative. In Equations (1, 3), the mass density is combined with the specific heat (c) as the thermal capacity (ρc), contributing to the thermal diffusivity (κ) of the material. The thermal conductivity (k), because of its presence in the boundary condition, Equation (6), and the continuity condition, Equation (9), is an independent parameter. The material parameters are therefore grouped as the mechanical constitutive coefficient [λ, μ, or ν, E] and the thermal parameter [α, k, κ]. The coefficient of expansion is the principal excitation in Navier's Equations (2, 4). The mechanical property is therefore dominated by a single parameter [$\alpha E/(1-\nu)$]. The thermal properties are grouped in dual parameters, [k, κ] or [k, ρc]. Using the latter, Huang and Ju (1987) concluded that, for materials of comparable thermal conductivity, materials of high thermal capacity are definitely preferred for the resulting lower temperature field. However, for materials of comparable thermal capacity, those of high thermal conductivity yield lower thermal stress state. Moreover, because of its correspondingly lower Peclet number, the critical depth η_{cr} is thus accordingly larger. The critical depth η_{cr} is the dimensionless depth η at which the maximum principal thermal stress occurs, where η is the depth coordinate x_2 modulated by the asperity half width (a). Ju and Liu (1988a) found that the critical depth depends predominantly on the Peclet Number. In their study, the critical depth was computed directly by maximizing the thermal tensile stress with respect to positions under the asperity inside the material. The relationship between critical depth and the Peclet Number for all materials in the two dimensional formulation may be simplified to satisfy the exponential form

$$R(\eta_{cr})^{2.275} = 20.4368. \qquad (10)$$

The relation is depicted in Figure 4. The square symbols in the figure represent actual materials; they are Aluminum (Al), Silicon Carbon (SiC), Aluminum Oxide (Al_2O_3), Stellite III (St), and Zirconium (Zr) with the same asperity speed of 15 m/s, and the same asperity width of 0.254 mm. The traversing speed has been varied for Aluminum Oxide and Stellite III. The results all fall on the same curve. Invariably, the critical depth is located at the cold side in the neighborhood where the large temperature gradient occurs. Because of the combined effect maximum tensile stress and a discontinuity in material property, the critical depth shall characterize the material chosen for the coating when the thickness of coating becomes critical.

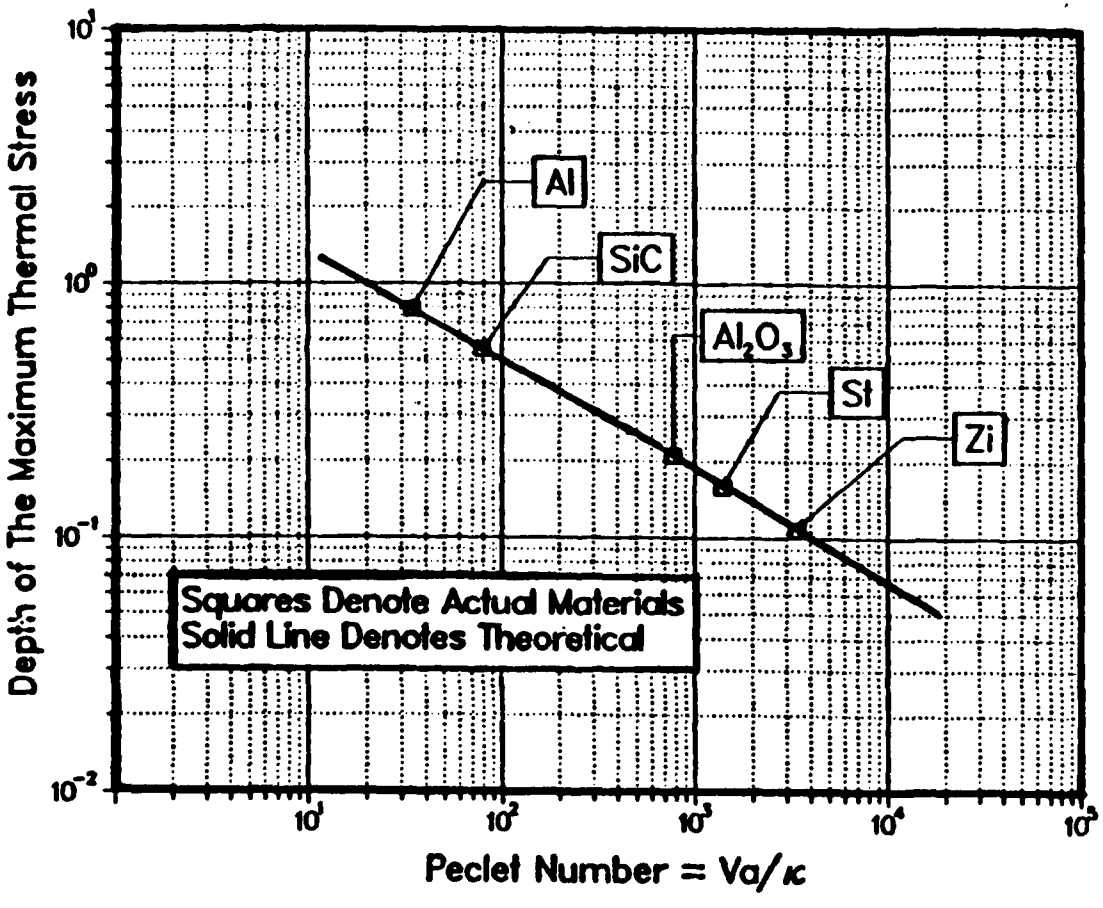

Figure 4. **Critical depth versus Peclet number in two–dimensional case**

4.0 PARAMETRIC EFFECT IN A COATED MEDIUM

It was pointed out by Ju and Chen (1984), that the phenomenon of thermo-mechanical cracking will be the same as a single material of the coating if the coating thickness is of the same order of magnitude as the asperity width. The interaction between coating and the substrate becomes significant only for coating thickness being of order of magnitude smaller than the asperity width. Ju and Liu (1988b) studied the effect of coating thickness in the neighborhood of the critical depth for various property differences between the coating and the substrate. In Figure 5 through Figure 9, the principal stresses in both the coating and the substrate are shown for the parametric variances of $[\alpha E/(1-\nu)]$, as the dominant mechanical property, and the thermal parameters [k] and $[\rho c]$. The variances are designated as:

$$\Pi_M = [\alpha E/(1-\nu)]_I/[\alpha E/(1-\nu)]_{II}, \tag{11}$$

$$\Pi_k = k_I/k_{II}, \tag{12}$$

$$\Pi_{\rho c} = [\rho c]_I/[\rho c]_{II}. \tag{13}$$

For all those variances, since the interest was essentially in the effect of parametric matching (or mismatching) between the coating and the substrate, the numerical values of the coating is set for the Stellite III with the Peclet Number R=1400. The corresponding critical depth for the coating is at $\eta_{cr} = 0.16$. Invariably, the worst case occurs in the neighborhood of the critical depth. Figures 5 and 6 show the principal stresses in the coating and the substrate respectively for various variances of mechanical parameter. For the variance of one, the coating and the substrate are of the same material. For variances larger than one, the substrate is of softer material; while less than one denotes stiffer substrate. For thick coatings ($\eta > 0.16$), the maximum stress in the coating occurs at the critical depth. The figures demonstrate that softer substrate provides less support for the coating. The thermal stress is thus higher. Stiffer substrate reduces the stress in the coating but takes on more stress especially for very thin

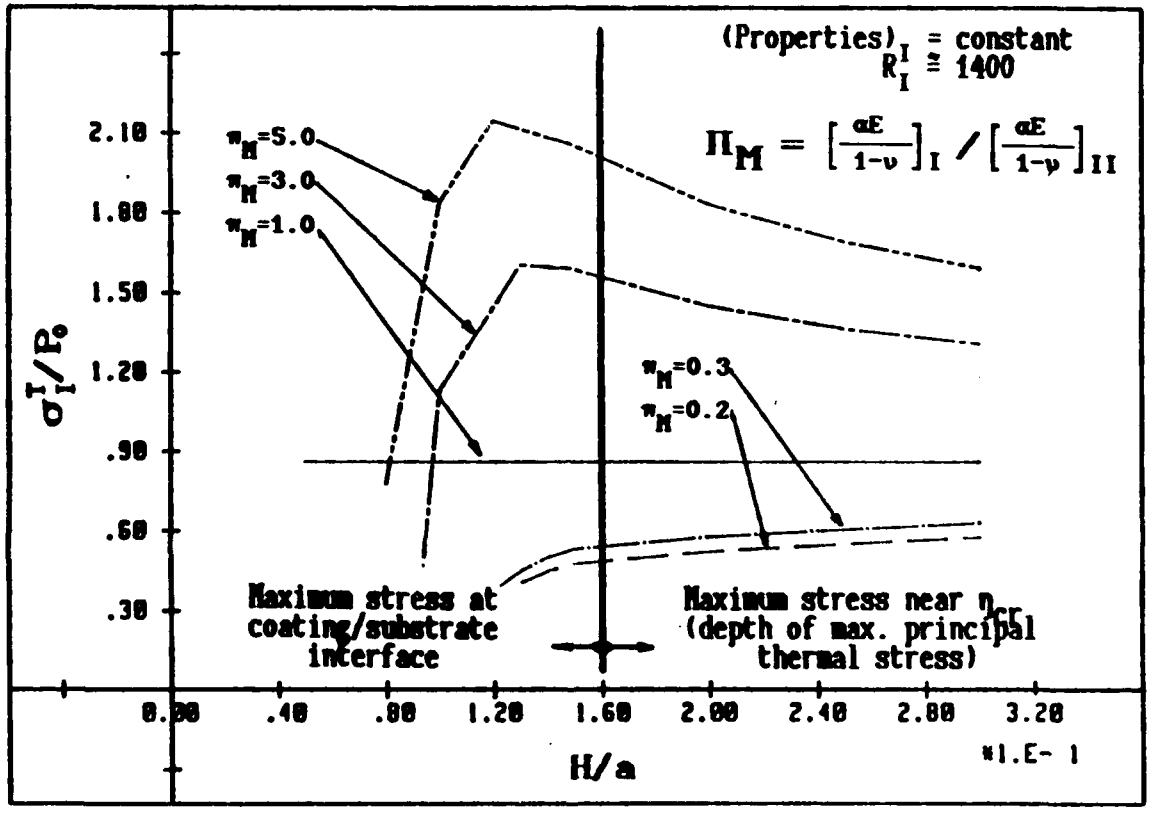

Figure 5. **Maximum principal thermal stresses in coating layer versus coating thickness for different mechanical mismatches (surface material properties are constant)**

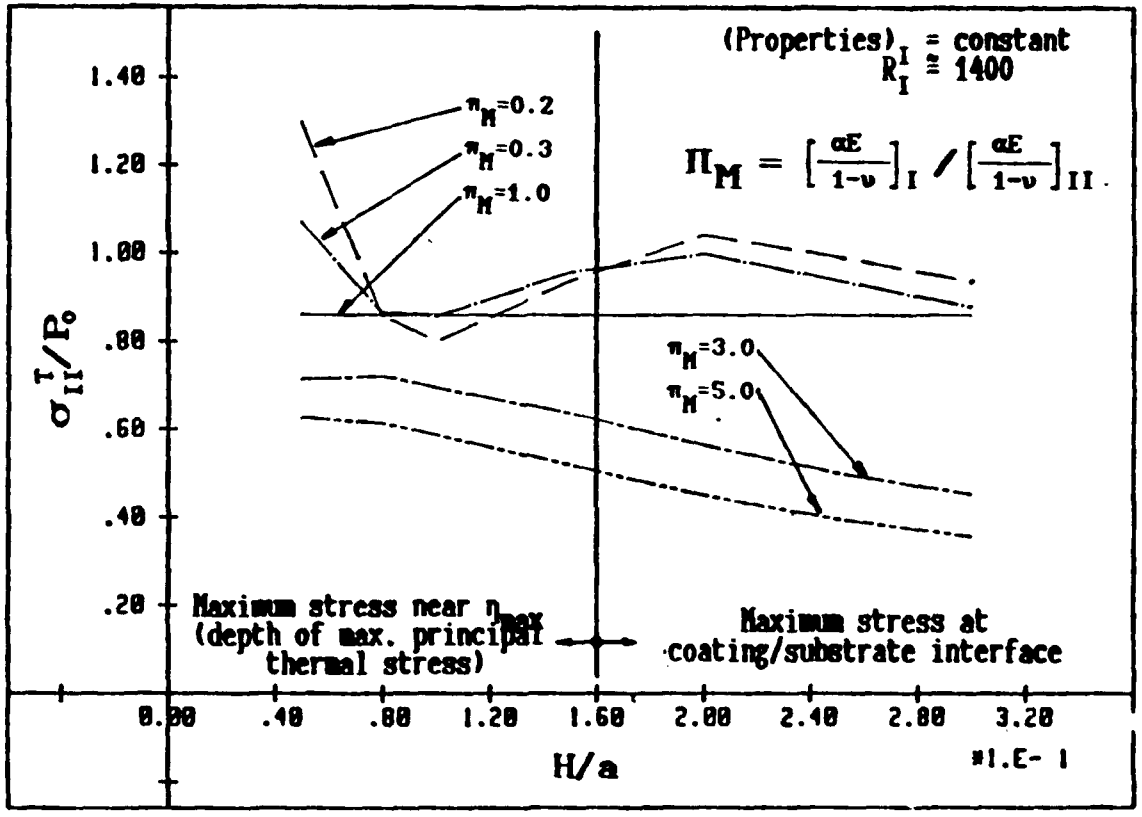

Figure 6. Maximum principal thermal stresses in substrate versus coating thickness for different mechanical mismatches (surface material properties are constant)

coatings. Figures 7 and 8 show the effect of the thermal conductivity variance. For less conductive substrate (Π_k = 10), the thermal stress is higher in the coating, especially at the coating/substrate interface for thin coatings. When the substrate is more conductive (the variance is 0.5), more heat is readily transferred to the substrate. The thermal stress is correspondingly reduced. Figure 9 illustrates a combined curve for maximum principal thermal stresses in the coating and in the substrate due to variance in thermal capacity. In both cases, the stresses are evaluated at the critical depth.

To study the criterion for coating delamination, Ju and Liu (1988b) also showed the effect of the shearing stress at the coating/ substrate interface, Figure 10. The existence of the interfacial shearing stress results when the principal direction is not parallel to the wear surface. Theoretically, when the principal angle is zero, the interfacial shearing stress vanishes. Figure 10 uses the variance in thermal conductivity without loss of generality. For a single material, Π_k = 1.0, the principal angle is small at locations closer to the wear surface. As a result, the shearing stress is correspondingly small. Significantly, the interfacial shearing stress reaches a maximum in the neighborhood of the critical depth of the coating. The existence of the interfacial shearing stress could cause interfacial shear cracks that would lead to coating delamination. The interfacial shearing stress can be controlled by proper selection of coatings to match the substrate.

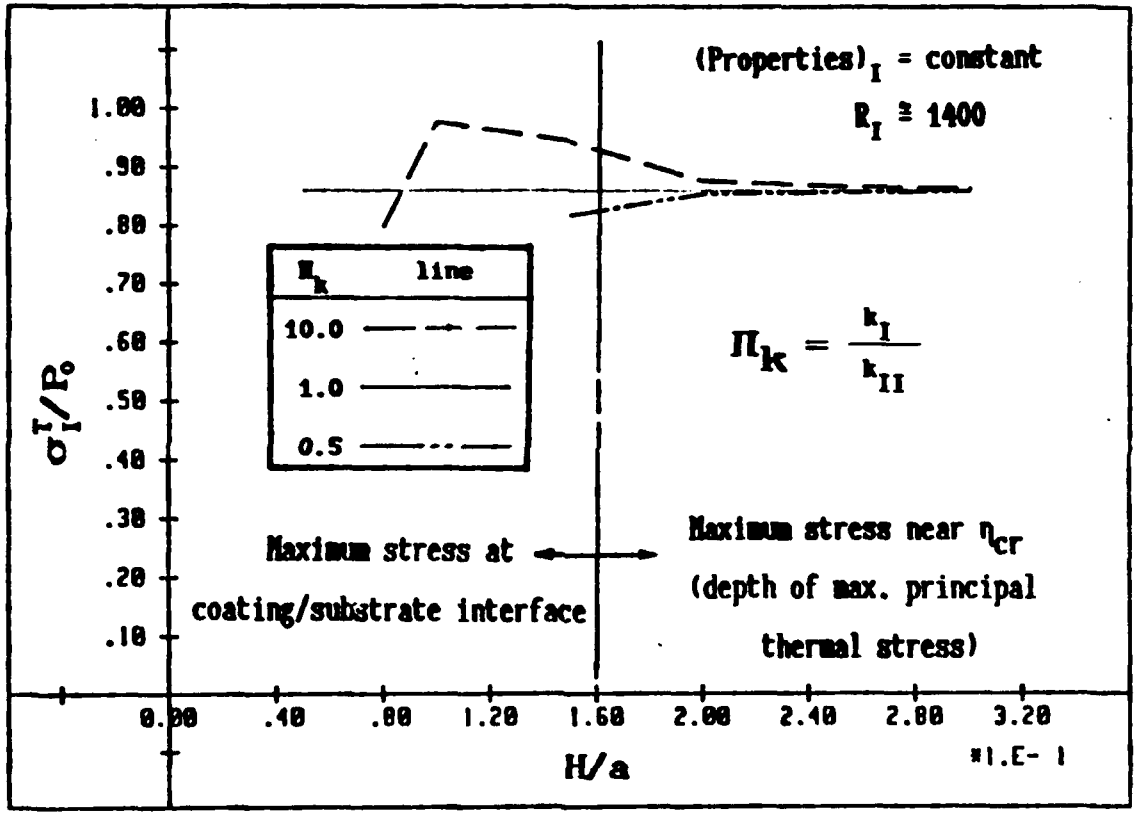

Figure 7. Maximum principal thermal stresses in coating layer versus coating thickness for different mismatches in thermal conductivity (surface material properties are constant)

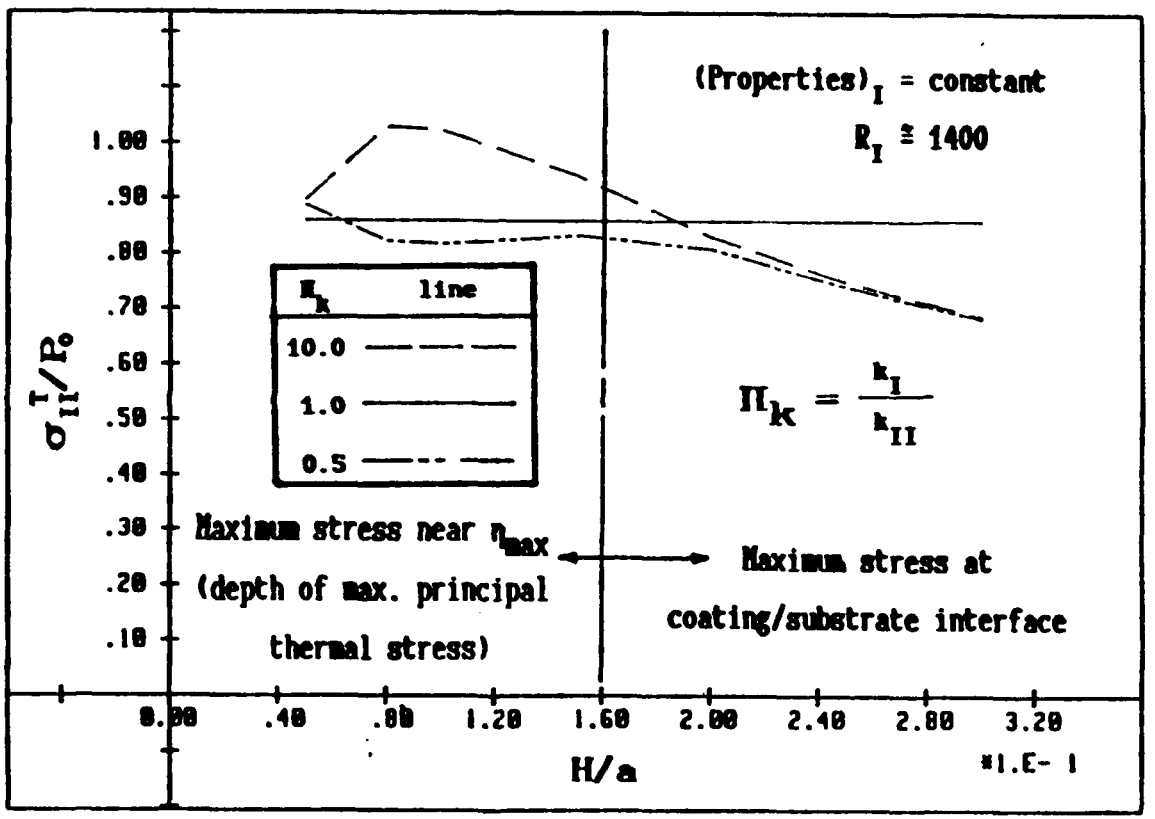

Figure 8. **Maximum principal thermal stresses in substrate versus coating thickness for different mismatches in thermal conductivity (surface material properties are constant)**

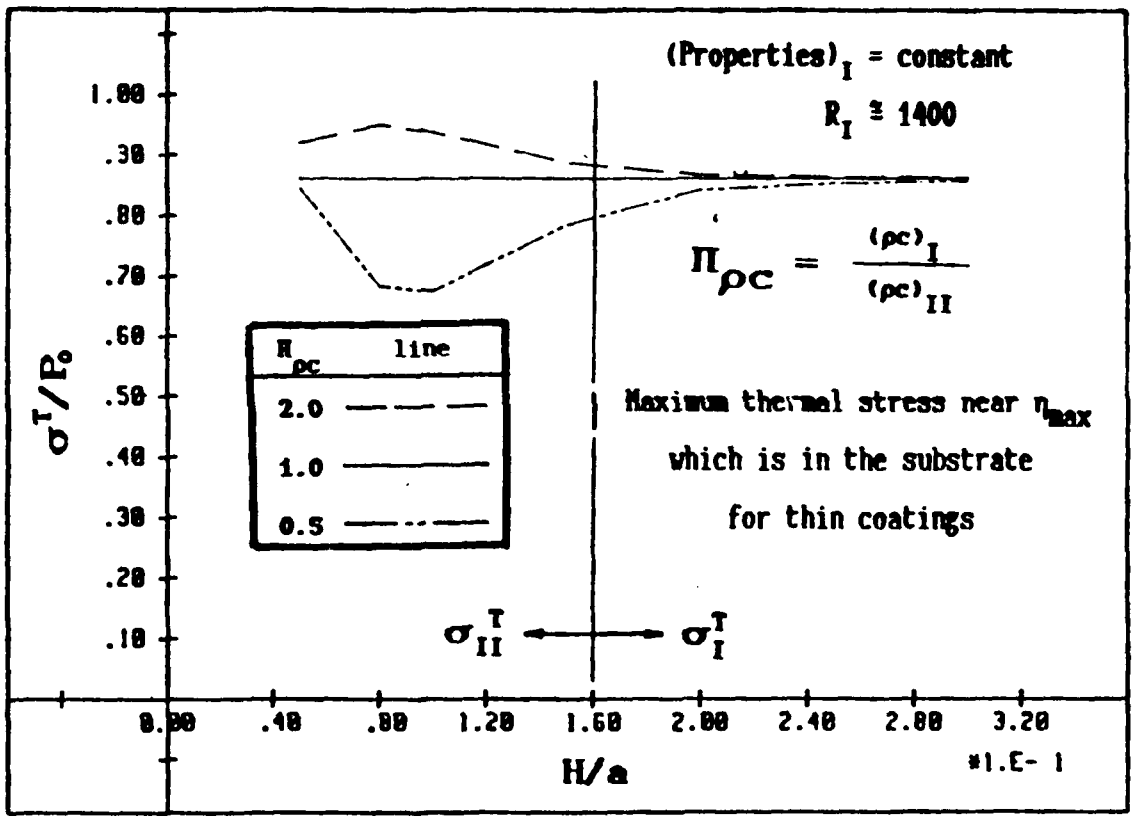

Figure 9. Maximum principal thermal stresses versus coating thickness for different mismatches of thermal capacity (surface material properties are constant)

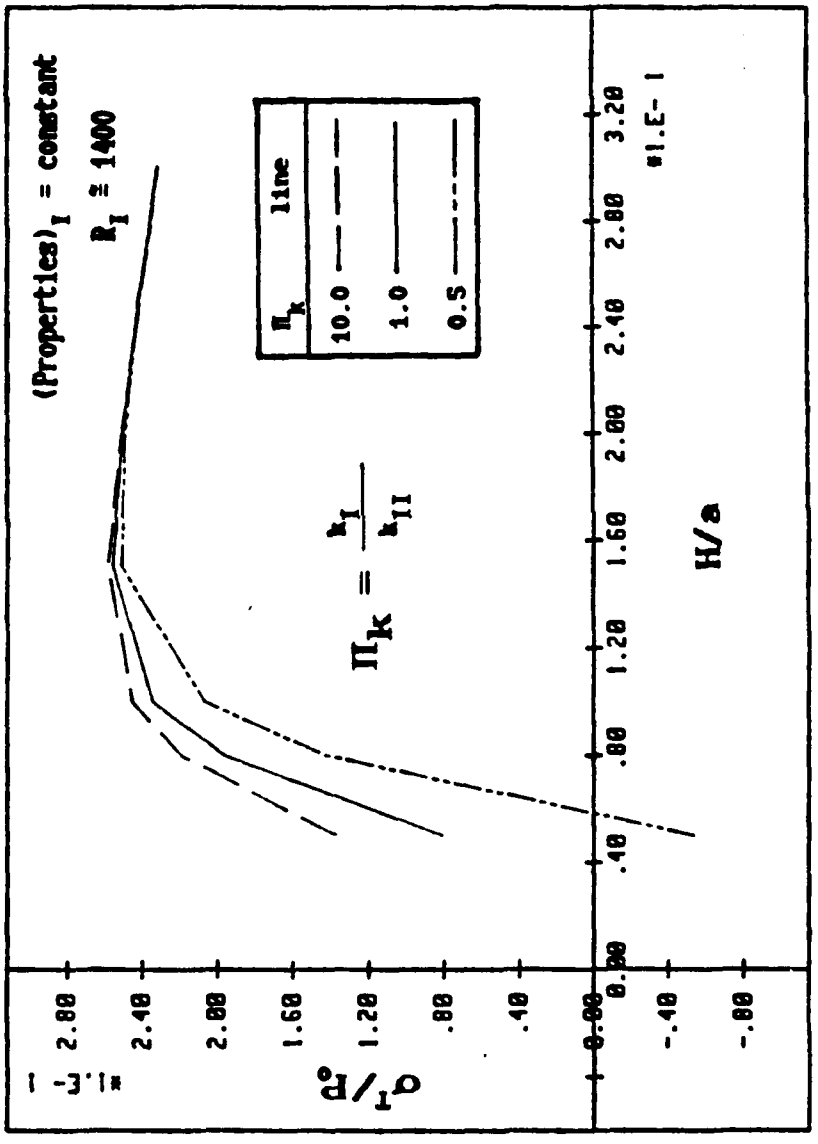

Figure 10. Interface shear stress ($\sigma_{\xi\eta}$) versus coating thickness for different mismatches in thermal conductivity (surface material properties are constant)

5.0 IRREGULARITIES

In the mathematical idealization, the coating is postulated to be of a known uniform thickness and to be smoothly and coherently bonded to the substrate. Such idealization, however feasible, would be too expensive to fabricate. Irregularities would eventually occur through wear. Inclusions do exist in the neighborhood of the interface. The thickness of the coating may vary either through manufacturing tolerance or through wear. Chen and Ju (1987, 1988, 1989a, 1989b) considered the effects of a small void cavity at the coating/substrate interface, and also an interfacial crack to simulate weak bonds. Liu and Ju (1989) studied the effect of random coating thickness on the temperature field. In both areas of studies, emphasis is placed on the effect of coating irregularities to estimate the integrity of the coating.

5.1 EFFECTS OF THE CAVITY

This section studies the thermo-mechanical cracking in a coated medium with a near surface void. It is one of a series of papers on the thermo-mechanical cracking phenomenon. The physical observations of the asperity friction are based on the works of Archard (1959), Bannerjee and Burton (1979) and Kennedy (1984a). Analytical solutions of thermo-mechanical cracking in a single material with no cavity were obtained by Ling et al (1965,1973), Mow and Cheng (1967), Kennedy (1981,1982), Ju (1982) and Huang and Ju (1985). Research on asperity excitation over coated surfaces with no cavity was first solved by Ju and Chen (1984) for moderately thick coating layers. Later, Ju and Liu (1988b) completed the investigation of the problem of a layered medium with no cavity for thin coatings. Based on these previous works on the problem of thermomechanical cracking from high-speed asperity friction, it was observed that the thermal stress field dominates the stress field and contributes principally to the failure by cracking. Among these works, Ju and Liu (1988a) also established that, at uniform asperity excitation, the Peclet number ($R=Va/\kappa$) dominates the determination of the critical depth (at which the tensile thermal stress reaches a maximum) for the case of no defect. In the analysis, they obtained a

simple relationship between critical depth and Peclet number for the two-dimensional problem which can be written as $R(\eta_{cr})^{2.275} = 20.4368$.

All previous work on the moving asperity problem dealt with uniform solid media. Chen and Ju (1987) first solved the transient temperature solution in a coated medium with a rectangular cavity, for which the material coordinates must be used. Later on, Chen and Ju (1988) also obtained the stress solutions of a single material with a rectangular cavity near the wear surface. They concluded that: (i) because of the cavity's poor heat transfer characteristics, the maximum tensile thermal stress in the case of a single material with a rectangular cavity is much higher than the maximum tensile stress in the case of no cavity, and (ii) the occurrence of the maximum tensile stress is at the trailing corner of the cavity, which defines a critical ligament thickness L_{cr}, closer to the wear surface than the critical depth (Ju and Liu, 1988a) of the material. For instance, for the case of a single material of Stellite III with a cavity, the critical ligament thickness is approximately 40 percent of the critical depth of the same material. This established that not only the Peclet number, but also the existence of the defect will influence the location at which the maximum tensile stress occurs. The present research will discuss the effects of a cavity in the neighborhood of the interface of a coated medium. The effect of the location of the cavity on stress field will also be discussed.

5.1.1 ANALYTICAL MODEL

In the problem of cavity, or void inclusion, the homogeneity condition in the traversing direction of the asperity no longer hold in the vicinity of the cavity, Figure 11. Hence, the governing differential equations, given in Equations (1, 2), must be used. Regularity conditions are still to be satisfied at infinity. The boundary conditions (6, 7, 8) remain. The continuity conditions (9) hold at interface, except at cavity. Heat transfer at cavity is negligible in comparison to that of the connected region. Small contact

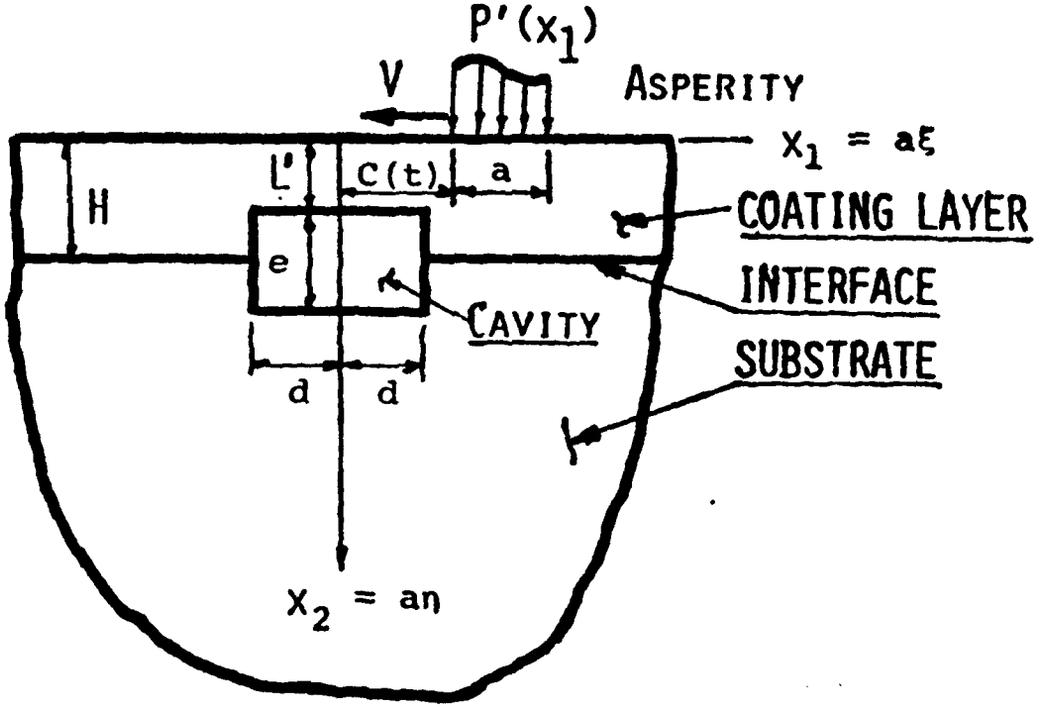

Figure 11. **Two–dimensional model of a coated wear surface with a cavity**

is ignored, allowing a traction-free condition at the cavity boundary. Small contact is ignored, allowing a traction-free condition at the cavity boundary. Because of the complexity of the geometry and the boundary conditions, the finite difference method was employed to solve the problem. The finite difference equation and the energy balance method applied on the surface boundary and the cavity boundaries for the temperature field are discussed by Chen and Ju (1987).

Ju and co-workers established that, for a moderately high-speed asperity excitation, the thermal stress effect dominates the stress field and eventually leads to failure in the no cavity case. Liu (1986) also showed that, if the asperity speed is larger than 0.127 m/s in Stellite III, the thermal stress dominates the failure, and the mechanical stress becomes less important. However, the mechanical stress may not be trivial when a cavity exists. Therefore, both the mechanical and thermal stress field will be studied.

5.1.2 SOLUTION TECHNIQUE

(i) Perturbation Method

For hard wear materials, such as Stellite III, and for a moderately high asperity speed, the Mach number M is of the order of 10^{-3}. Since the parameter M^2 is sufficiently small, Equations (2, 3) can be solved by the perturbation method.

The solutions to Equations (2, 3) can be expressed as a power series in $\epsilon = M^2$; that is

$$u^{\beta}(\xi,\eta,\tau,\epsilon) = u_0^{\beta}(\xi,\eta,\tau) + \epsilon u_1^{\beta}(\xi,\eta,\tau) + \epsilon^2 u_2^{\beta}(\xi,\eta,\tau) + \cdots, \quad (14)$$

$$v^{\beta}(\xi,\eta,\tau,\epsilon) = v_0^{\beta}(\xi,\eta,\tau) + \epsilon v_1^{\beta}(\xi,\eta,\tau) + \epsilon^2 v_2^{\beta}(\xi,\eta,\tau) + \cdots, \quad (15)$$

when Equation (14) and Equation (15) are substituted into Equations (2, 3), the terms with the same power of ϵ are grouped, leading to recursive

equations for displacements. The recurrence formulas can be written as:

$$\frac{\partial}{\partial\xi}\left(N_1^\beta \frac{\partial u_i^\beta}{\partial\xi}\right) + \frac{\partial}{\partial\xi}\left(N_2^\beta \frac{\partial v_i^\beta}{\partial\xi}\right) + \frac{\partial}{\partial\eta}\left(N_3^\beta \frac{\partial v_i^\beta}{\partial\xi}\right) + \frac{\partial}{\partial\eta}\left(N_3^\beta \frac{\partial u_i^\beta}{\partial\eta}\right) =$$
$$= \delta_{i0} \frac{\partial}{\partial\xi}\left(\frac{b_\beta^2 \gamma_\beta}{c_2^2} \phi^\beta\right) + (1-\delta_{i0})\, \delta \frac{\partial^2 u_{i-1}^\beta}{\partial\tau^2}, \qquad (16)$$

$$\frac{\partial}{\partial\xi}\left(N_3^\beta \frac{\partial v_i^\beta}{\partial\xi}\right) + \frac{\partial}{\partial\eta}\left(N_2^\beta \frac{\partial u_i^\beta}{\partial\xi}\right) + \frac{\partial}{\partial\xi}\left(N_3^\beta \frac{\partial u_i^\beta}{\partial\eta}\right) + \frac{\partial}{\partial\eta}\left(N_1^\beta \frac{\partial v_i^\beta}{\partial\eta}\right) =$$
$$= \delta_{i0} \frac{\partial}{\partial\eta}\left(\frac{b_\beta^2 \gamma_\beta}{c_2^2} \phi^\beta\right) + (1-\delta_{i0})\, \delta \frac{\partial^2 v_{i-1}^\beta}{\partial\tau^2}, \qquad (17)$$

where $N_1^\beta=(\lambda_\beta+2\mu_\beta)/\rho_{II}c_2^2$; $N_2^\beta=\lambda_\beta/\rho_{II}c_2^2$; $N_3^\beta=\mu_\beta/\rho_{II}c_2$; $b_\beta=(3\lambda_\beta+2\mu_\beta)/\rho_{II}$; $\gamma_\beta=(q_0 a\alpha_\beta)/k_I$; $\delta=\rho_\beta/\rho_{II}$; $c_1=[(\lambda_{II}+2\mu_{II})/\rho_{II}]^{1/2}$; $c_2=[\mu_{II}/\rho_{II}]^{1/2}$; δ_{i0} is the Kronecker delta; and i denotes the perturbative order.

Similarly, one can obtain the recurrence formulas for the stress field as follows:

$$(\sigma_{\xi\xi}^\beta)_i = \frac{\mu_{II}}{P_0}\, \delta \left(N_1^\beta \frac{\partial u_i^\beta}{\partial\xi} + N_2^\beta \frac{\partial v_i^\beta}{\partial\eta} - \frac{b_\beta^2 \gamma_\beta}{c_2^2} \phi^\beta\right), \qquad (18)$$

$$(\sigma_{\xi\eta}^\beta)_i = \frac{\mu_{II}}{P_0}\, \delta\, N_3^\beta \left(\frac{\partial u_i^\beta}{\partial\eta} + \frac{\partial v_i^\beta}{\partial\xi}\right), \qquad (19)$$

$$(\sigma_{\eta\eta}^\beta)_i = \frac{\mu_{II}}{P_0}\, \delta \left(N_2^\beta \frac{\partial u_i^\beta}{\partial\xi} + N_1^\beta \frac{\partial v_i^\beta}{\partial\eta} - \frac{b_\beta^2 \gamma_\beta}{c_2^2} \phi^\beta\right), \qquad (20)$$

where $(\cdot)_i$ denotes the perturbative order for the stress components. The solutions of each perturbative order can be obtained by applying the finite difference method.

(ii) Difference Equations

Because of the complexity of the geometry and the boundary conditions, the finite difference method was employed to solve the problem. The finite difference equations and the energy balance method applied on the surface boundary and the cavity boundaries for the temperature field are discussed by Chen and Ju (1987). According to the numerical results by Chen and Ju (1987,1988), a high temperature and high stress concentrations will be found in the vicinity of the cavity. Therefore, a very fine mesh must be used near the cavity and a relative coarse mesh can be used in the regions far away from the cavity. This non-uniform mesh can be transformed to a uniform mesh and the solution may be obtained in the transformed plane. The difference equations of the thermoelastic Navier's equation for the zeroth order solution can be written as

$$A_1 v(i-1,j-1,n) + A_2 u(i-1,j,n) + A_3 v(i-1,j+1,n) + A_4 u(i,j-1,n) + A_5 u(i,j,n) + A_6 u(i,j+1,n) + A_7 v(i+1,j-1,n) + A_8 u(i+1,j,n) + A_9 v(i+1,j+1,n) = \frac{\partial}{\partial \xi}\left(\frac{b_\beta^2 \gamma_\beta}{c_2^2}\phi^\beta\right), \qquad (21)$$

and

$$B_1 u(i-1,j-1,n) + B_2 v(i-1,j,n) + B_3 u(i-1,j+1,n) + B_4 v(i,j-1,n) + B_5 v(i,j,n) + B_6 v(i,j+1,n) + B_7 u(i+1,j-1,n) + B_8 v(i+1,j,n) + B_9 u(i+1,j+1,n) = \frac{\partial}{\partial \eta}\left(\frac{b_\beta^2 \gamma_\beta}{c_2^2}\phi^\beta\right), \qquad (22)$$

where $A_1, A_2, \ldots, B_1, B_2, \ldots$ are given in Chen and Ju (1989b), and the temperature gradients are derived from the temperature field.

(iii) Special Element At Cavity Corner

The scheme in this case is to devise special elements in which the approximation simulates the diverging rate in the vicinity of the singular point. However, this method can be used only when the behavior

of the singularity is known. The procedure of this method is to assume a series which consists of both the regular terms and the singular terms. For the current problem, the stress singularity at the cavity corner should be the same as those used by Williams (1952) and Sih (1962). The series form for the displacement in the neighborhood of the cavity corner can be written as

$$u(r,\theta) = \text{regular term} + \sum A_n \, r^{n\pi/\zeta} \, f(\theta), \qquad (23)$$

where r is the distance from the corner point and $\zeta = 3\pi/2$.

5.1.3 NUMERICAL RESULTS

Numerical results are obtained by using the finite difference non-uniform rectangular mesh and material properties for Stellite III. Numerical results of a coated medium with no cavity were compared with the analytic solutions (Ju and Chen, 1984), the error for the temperature field is less than 1%, and the error for the stress field is less than 5%; this confirms the accuracy of the numerical scheme. The details of the numerical results for the temperature field are referred to Chen and Ju (1987). Only the numerical results of the stress field will be discussed in the present section. When the cavity is located entirely in the surface layer, because the coating layer is much thicker than the ligament thickness, the effect is similar to that of a single material (Ju et al, 1984,1988). However, when the top edge of the cavity is at the interface, both the coating layer and the substrate will influence the stress field. Therefore, all figures are plotted for the worst cases when the top edge of the cavity is at the interface, and when the asperity is right over the cavity.

The effect of the cavity on the magnitude of the mechanical stress field can be seen in Figure 12, which shows the principal thermal stress field (case 7A), mechanical stress field (case 7B), and combined stress field (case 7C). In this figure, the material of the substrate is Stellite III, and the material properties of the coating layer are the

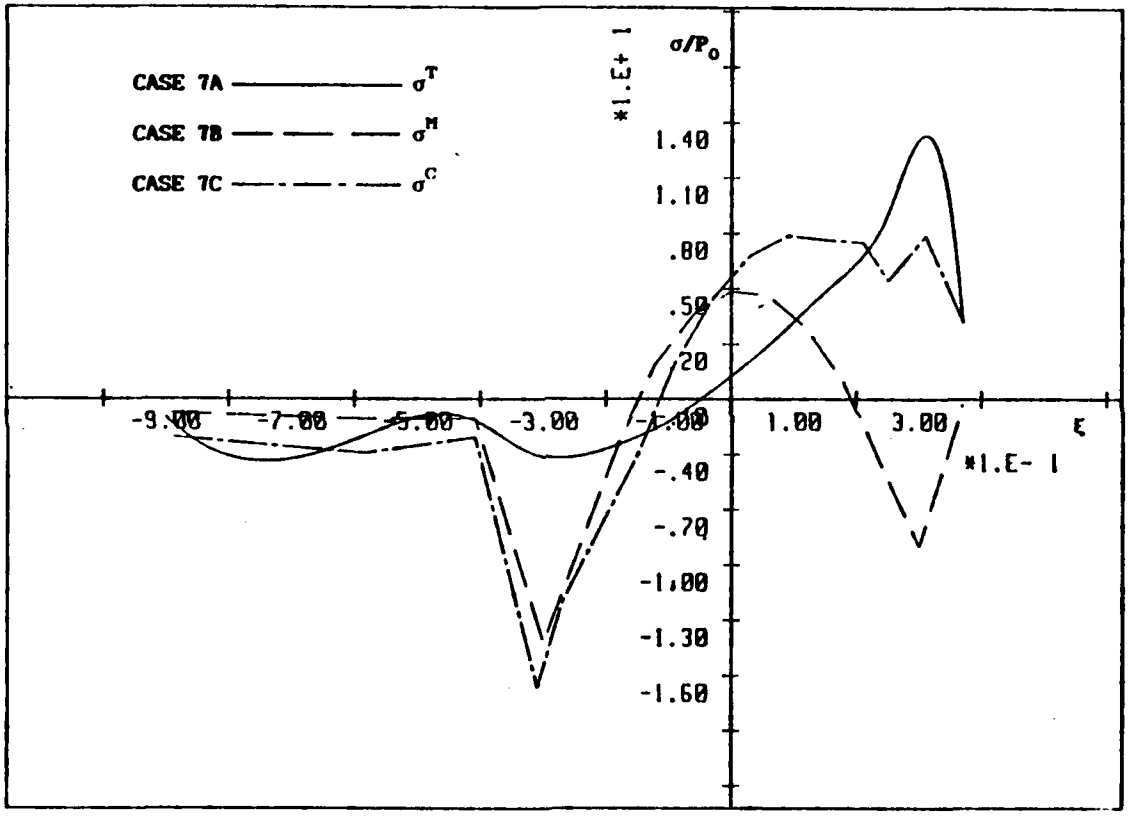

Figure 12. **Thermal, mechanical and combined principal stress (cases 7A, 7B, 7C), L=0.094 and η=0.06 above the top edge of the cavity for all cases.**

same as Stellite III except that Young's modulus is twice that of Stellite III. This figure establishes that, while the tensile thermal stress is larger than the tensile mechanical stress, the mechanical stress field is not negligible as in the no cavity case.

When the cavity location, or the ligament thickness, is smaller than the critical depth of the coating material, the largest tensile stress will occur at the top trailing corner of the cavity. The maximum value occurs when the ligament thickness, the coating thickness in the present section, reaches a critical value. Figure 13 shows the critical ligament thickness of a coated medium with a cavity. From this figure, one can see that the maximum tensile stress occurs when the ligament thickness L=0.094, which is the same as the critical ligament thickness of a single material. Figure 14 compares the critical depth (η_{cr}) of a coated medium with no cavity with the critical ligament thickness (L_{cr}) of a coated medium with a rectangular cavity. From this figure, one can see that, for the same Peclet number (R_I), η_{cr} is always larger than L_{cr}.

Figures 15 and 16 demonstrate the effects of Young's modulus of the coating layer and the substrate on the thermal stress field. In Figure 15, the material of the substrate is Stellite III for all cases. Young's modulus E_I of the surface layer is to vary; that is, E_I is the same as Stellite III (case 1), E_I is twice that of Stellite III (case 7A), and E_I is, respectively, one-half (case 9A) and three times (case 9B) that of Stellite III. In Figure 16, the material of the coating layer is Stellite III for all cases. Young's modulus of the substrate is one-fifth (case 10A), one-half (case 10B), and five times (case 10C) that of Stellite III. From these figures, it is shown that, when the coating is stiffer than the substrate, the thermal stress at the critical ligament thickness is increased in proportion. Figure 17 compares the effect of Young's modulus on the thermal stress field from a single material and from a coated medium with a stiffer surface layer. In the figure, dashed lines represent the case of a single material with a cavity, while solid lines represent the case of a hard coated medium with a cavity. From this figure, we observe that the thermal stress

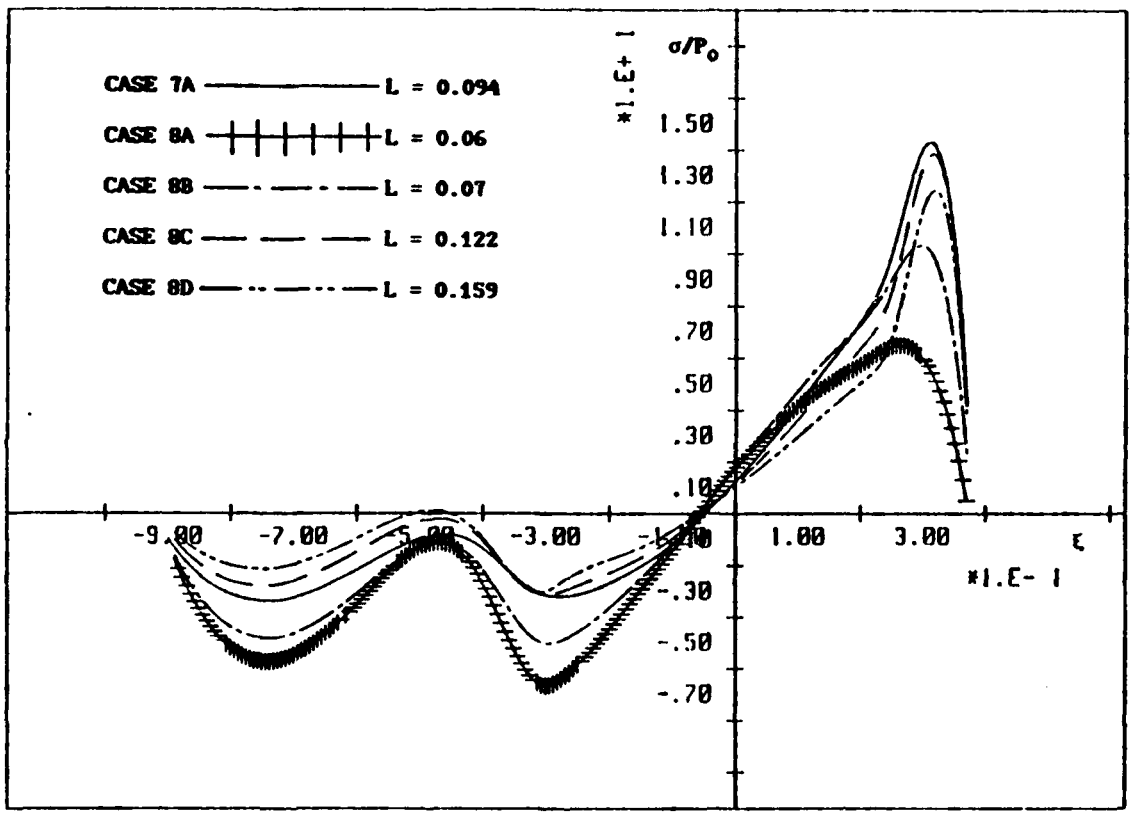

Figure 13. **Thermal principal stress, η=0.06 above the top edge off the cavity for all cases**

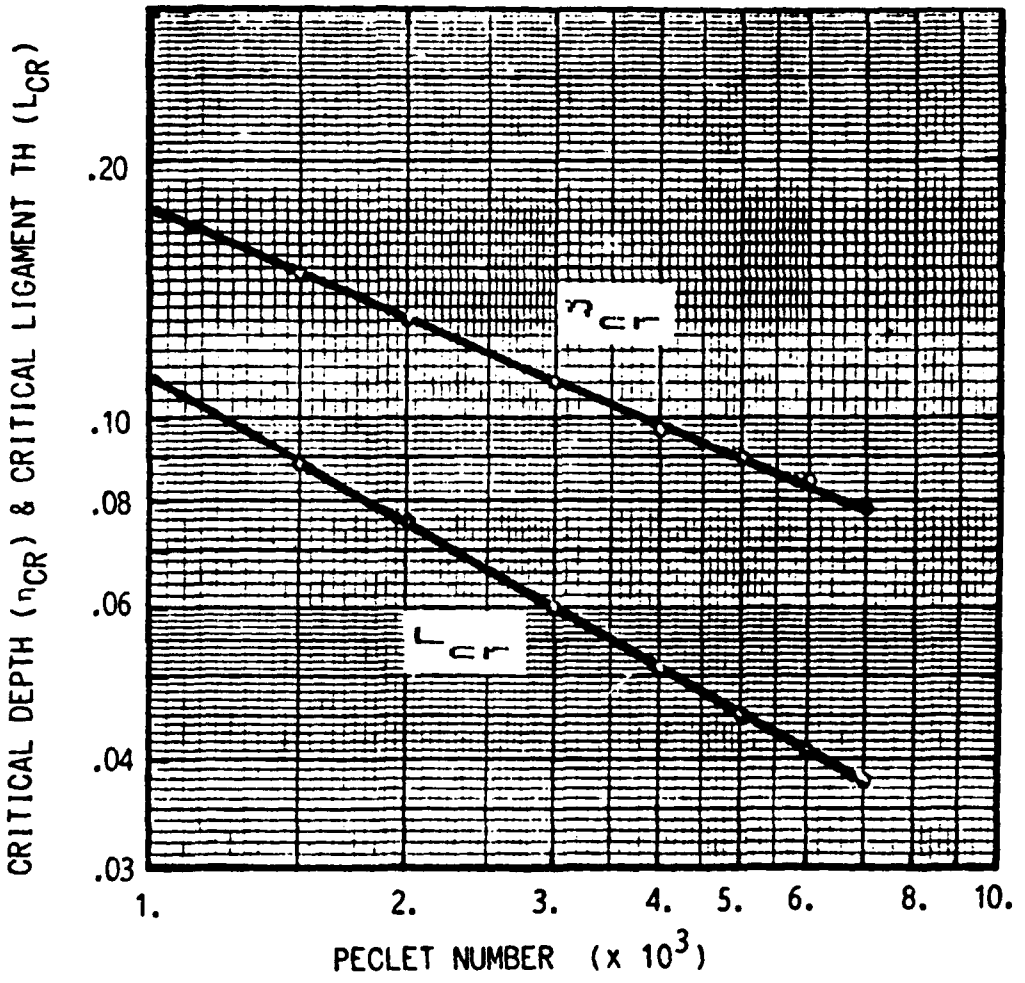

Figure 14. **The effect of Peclet number on the critical depth and the critical ligament thickness**

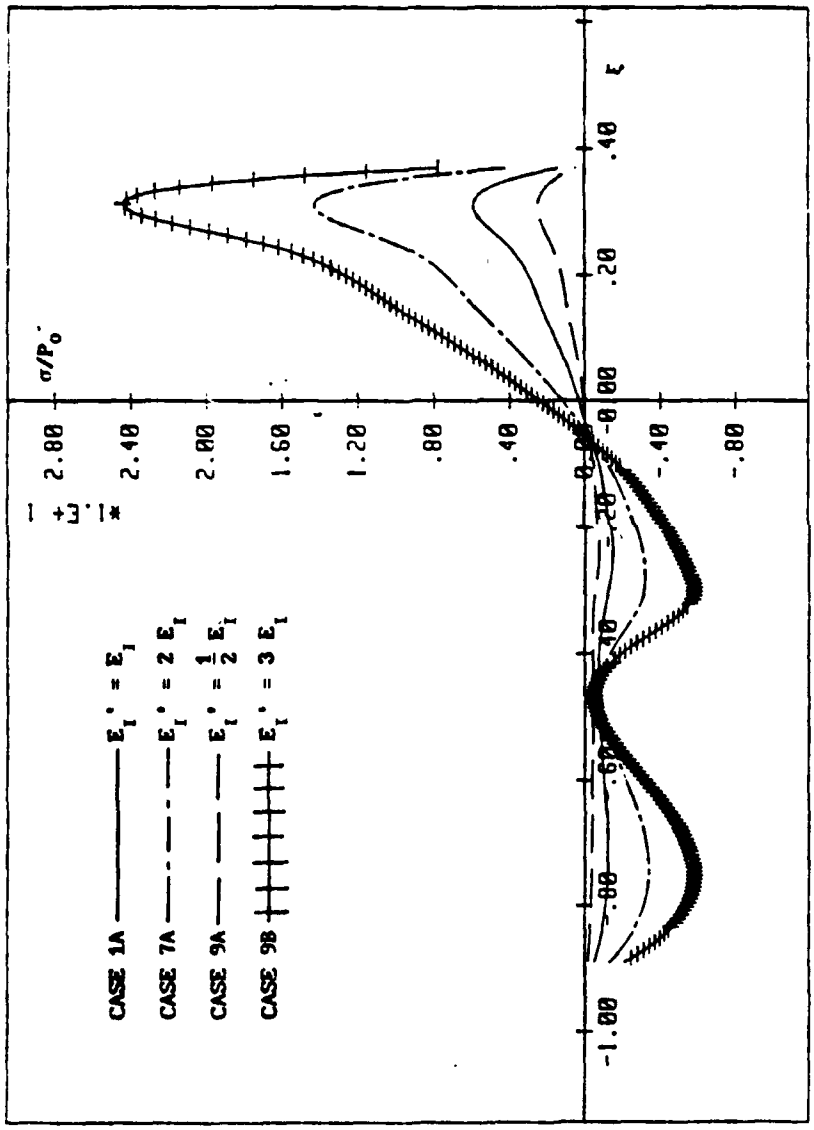

Figure 15. Thermal principal stress, L=0.094 and η=0.06 above the top edge of the cavity for all cases

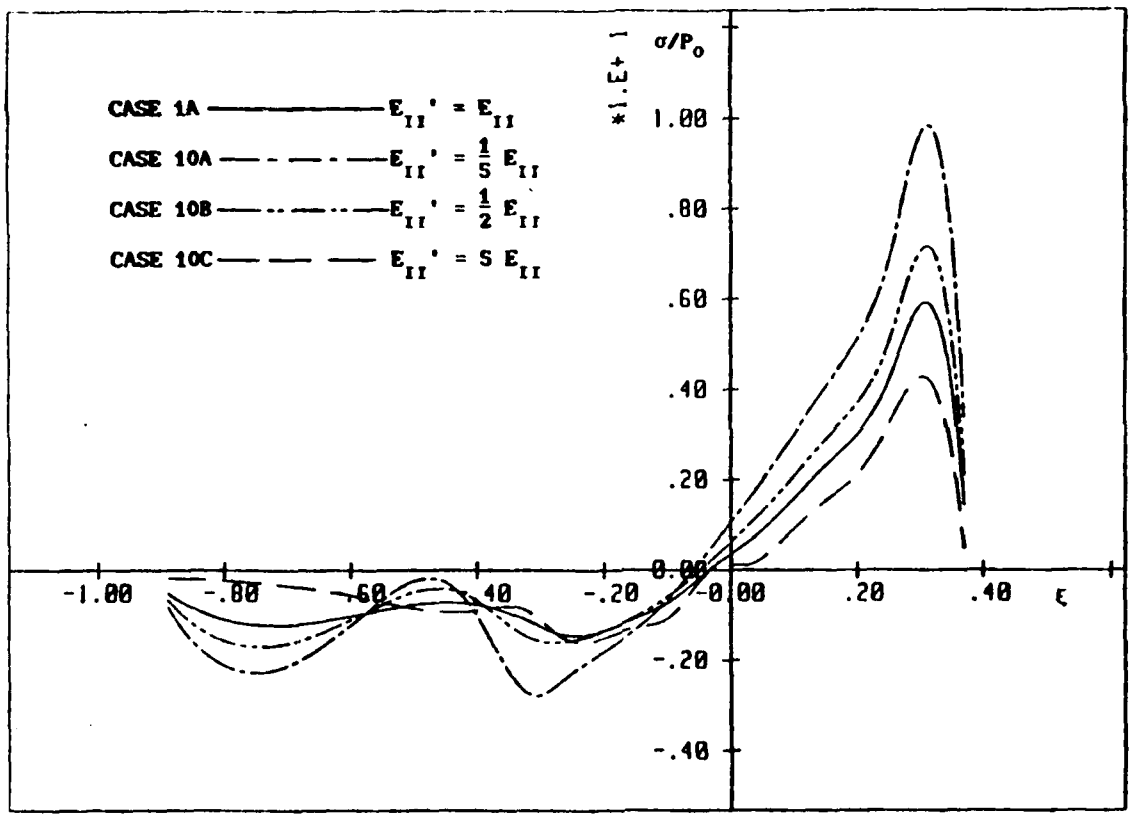

Figure 16. **Thermal principal stress L=0.094 and η=0.06 above the top edge of the cavity for all cases**

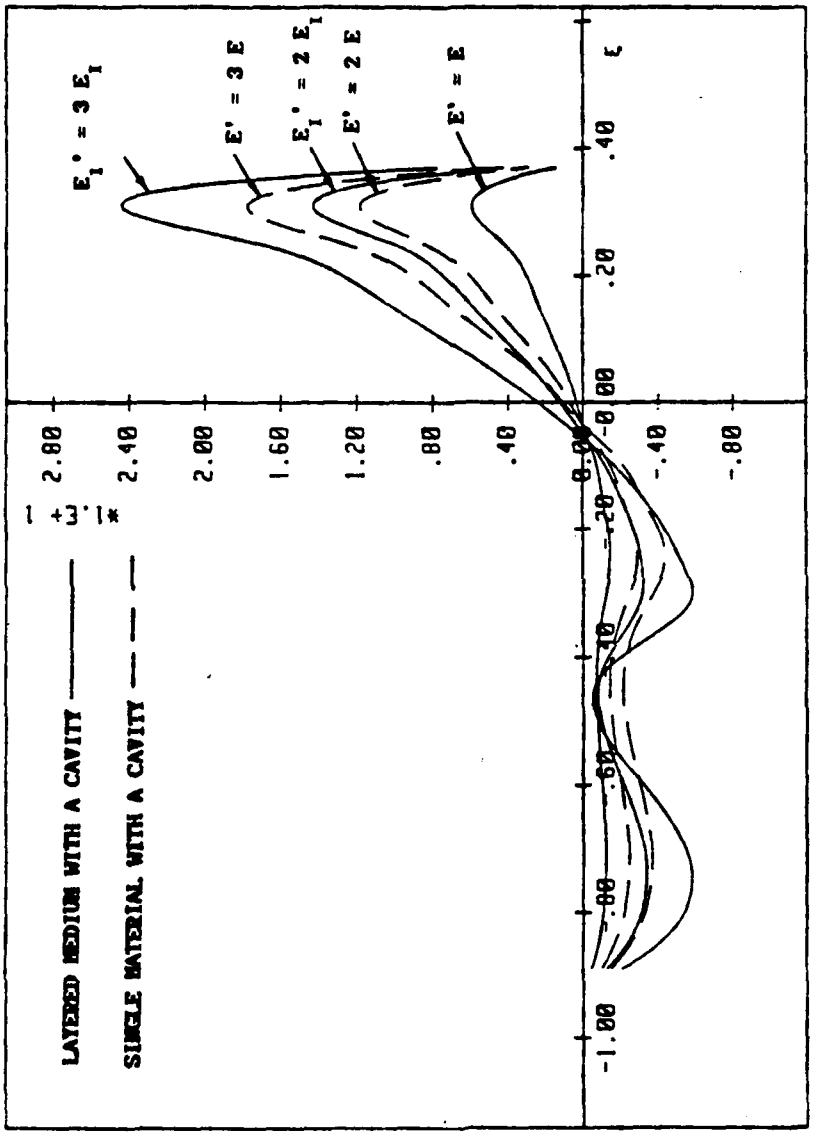

Figure 17. Thermal principal stress, L=0.094 and η=0.06 above the top edge of the cavity for all cases

increases linearly in proportion to Young's modulus for the single material case. For the coated medium case, however, increasing Young's modulus in the coating layer by the same amount will result in higher thermal stress than in the case of a single material. This is because we will have a relatively softer substrate by increasing Young's modulus in the coating layer.

The effects from thermal conductivity and the coefficient of thermal expansion are presented in Figures 18 and 19. These effects are similar to those found in the case of a single material with a cavity.

From the failure specimen for the case of a single material with no cavity, it is observed that the thermo-mechanical cracking occurs on a plane nearly perpendicular to the wear surface. However, Ju et al (1984, 1988) showed that, in the case of a layered medium with no-cavity, shear delamination (cracking is parallel to the wear surface) may occur, caused by the change in the principal directions (larger angle of principal direction); therefore, it is important to understand what will affect principal directions. Figure 20 shows the effect of the ligament thickness (cavity location) on principal directions at a point in the neighborhood of the top trailing corner of the cavity (ξ=0.3 and η=0.006 above the cavity corner). The angle of principal direction reaches a maximum at the critical ligament thickness when L_{cr}=0.094. Figures 21 and 22 compare the effect of Young's modulus on principal directions for the case of a single material with a cavity (dashed line) and for the case of a layered medium with a cavity (solid line). These two figures establish that decreasing Young's modulus in the coating layer (E_I) or increasing Young's modulus in the substrate (E_{II}) will increase the angle of principal direction. Nevertheless, changing Young's modulus in the case of a single material with a cavity will not affect the principal directions. Figures 23 and 24 illustrate the effects of the thermal conductivity and the coefficient of thermal expansion on principal directions for the case of a single material with a cavity (dashed line) and the case of a coated medium with a cavity (solid line). These two figures illustrate that thermal conductivity and the coefficient of thermal expansion will not influence principal

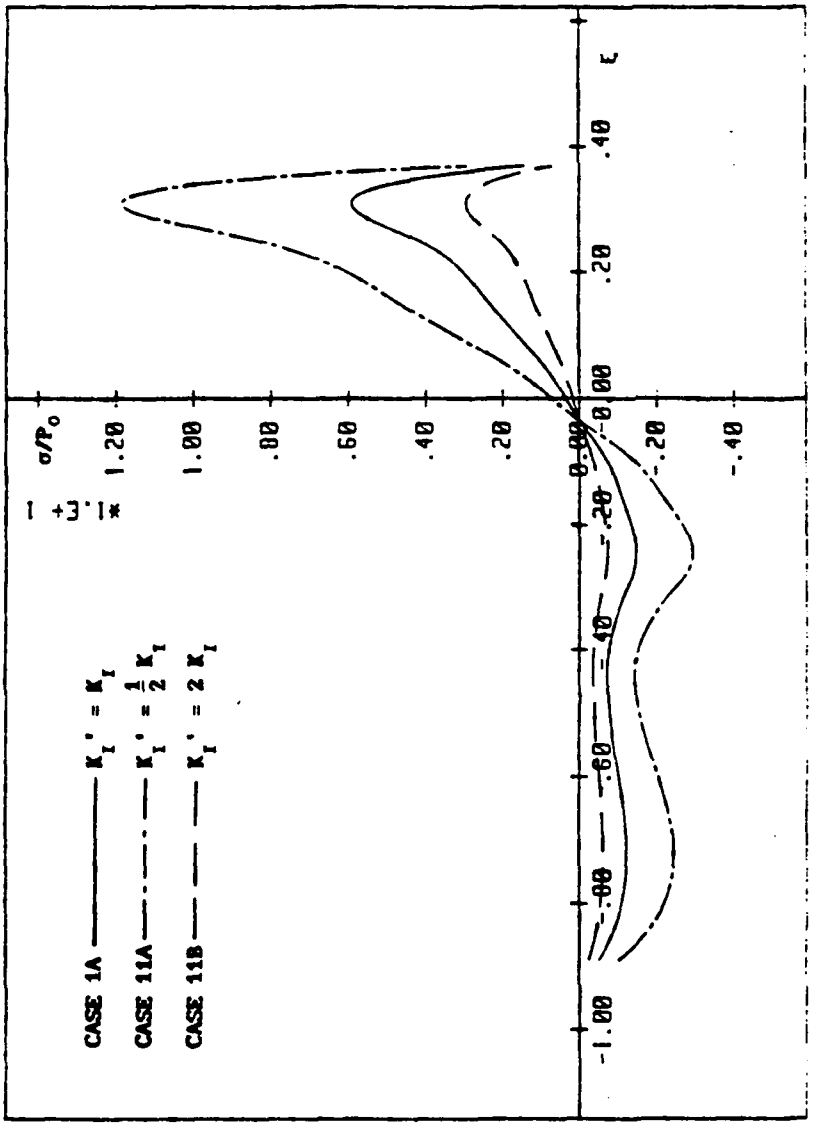

Figure 18. **Thermal principal stress L_c=0.094 and η=0.06 above the top edge of the cavity for all cases**

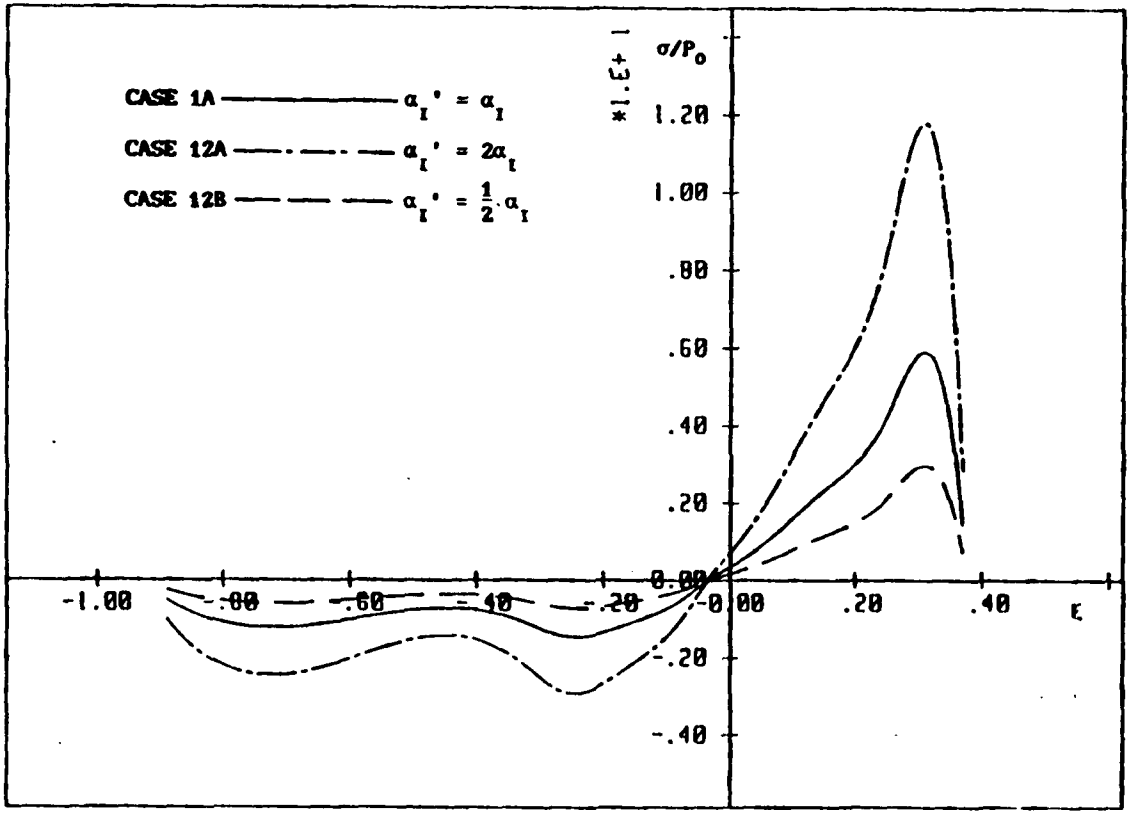

Figure 19. **Thermal principal stress, L=0.094 and η=0.06 above the top edge of the cavity for all cases**

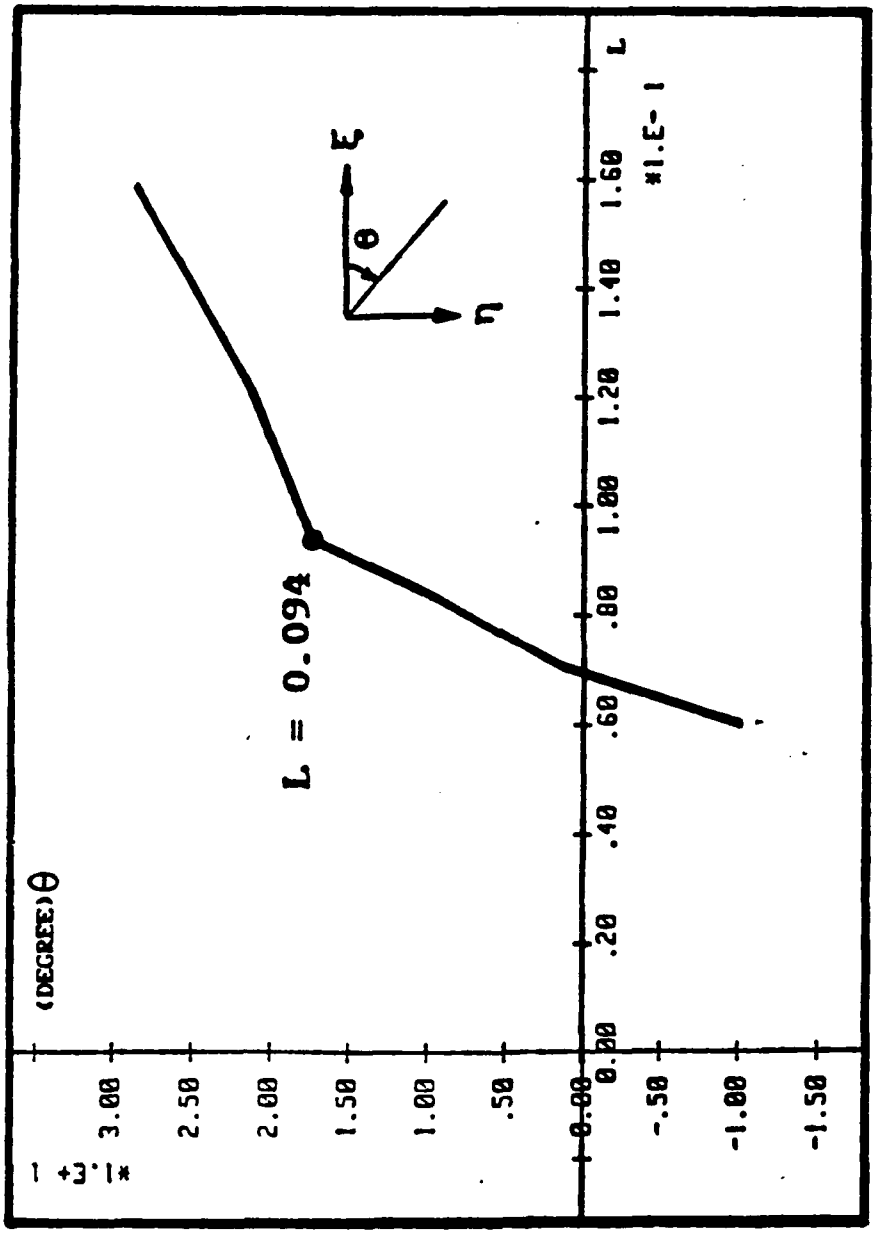

Figure 20. The effect of the ligament thickness on the angle of principal direction of the thermal stress field

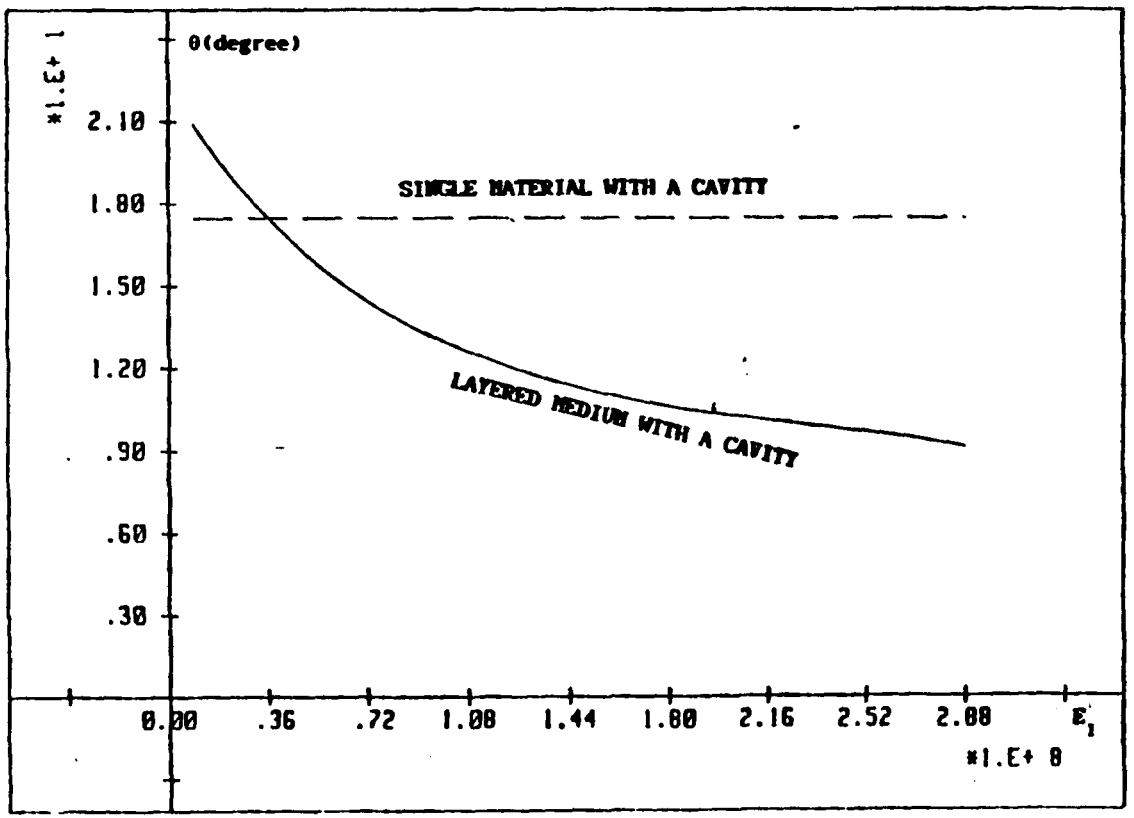

Figure 21. **The effect of Young's modulus of the coating layer on the angle of principal direction of the thermal stress field**

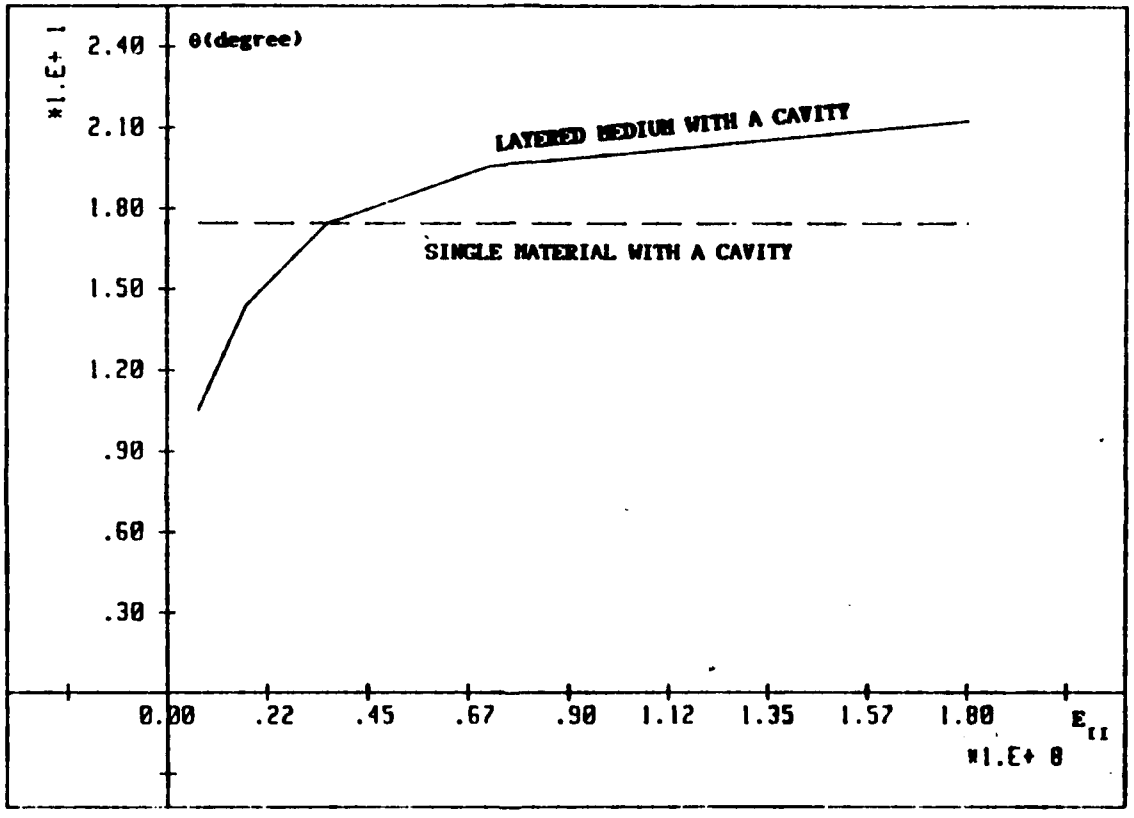

Figure 22. **The effect of Young's modulus of the substrate on the angle of principal direction of the thermal stress field**

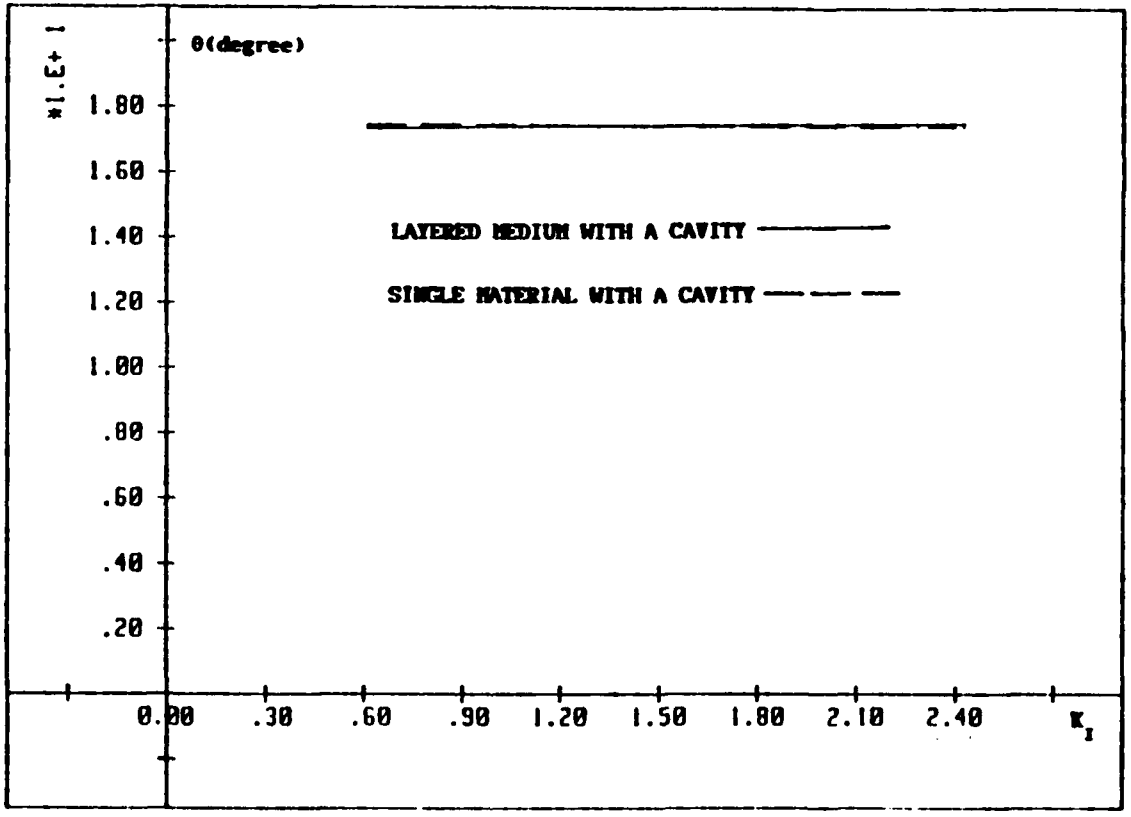

Figure 23. **The effect of thermal conductivity of the coating layer on the angle of principal direction of the thermal stress field**

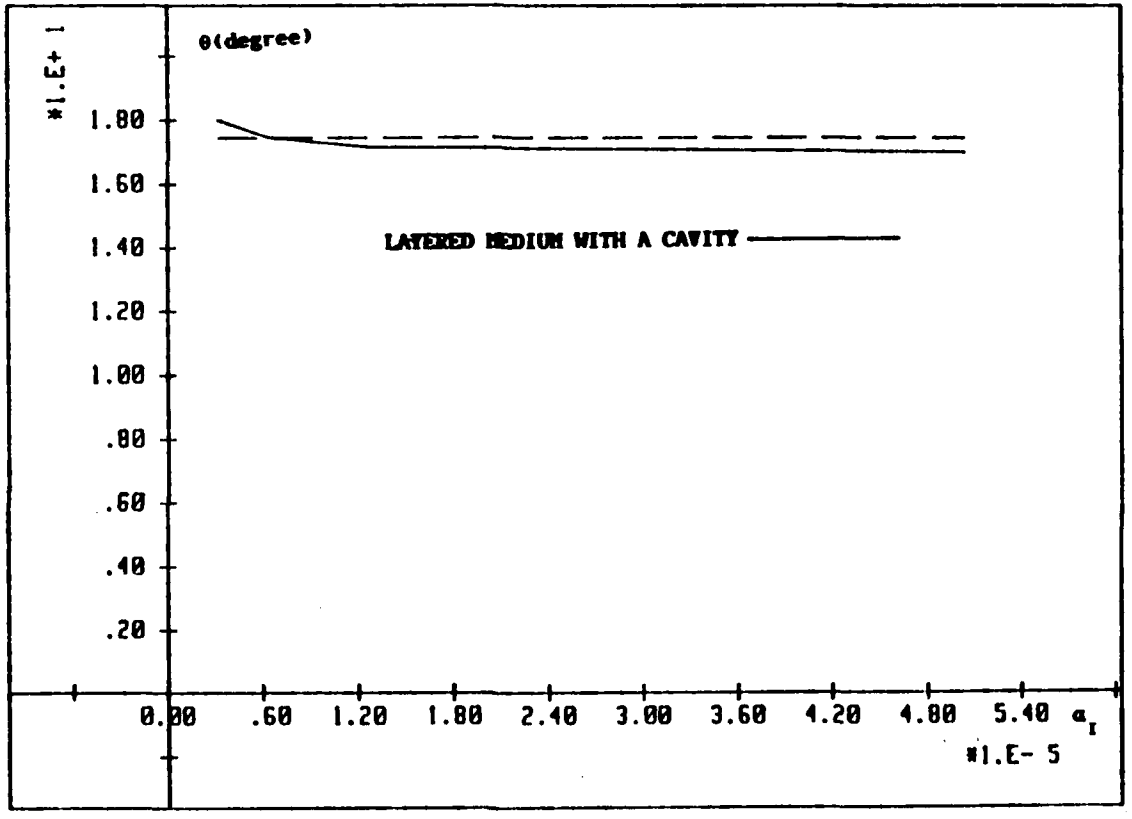

Figure 24. **The effect of thermal conductivity of the substrate on the angle of principal direction of the thermal stress field**

directions significantly.

5.1.4 SUMMARY

This section discusses thermo-mechanical cracking arising from a moving frictional load in coated media with a interfacial cavity. The present section demonstrates that, when cavities exist at the coating/substrate interface, the resulting thermal stress which determines the failure phenomenon is much more severe than that in the no cavity case.

Like most numerical solutions, functional relationships can not be obtained without voluminous computations. However, significant conclusions can be reached through a carefully selected set of pertinent parametric values. The conclusions of the present problem are:

(i) the effects of the mechanical and thermal properties on the stress field are consistent with those obtained in the no-cavity case by Ju and Chen (1984). These effects may be summarized as follows: thermal stress can be reduced by decreasing Young's modulus in the coating layer, increasing Young's modulus in the substrate, increasing thermal conductivity and thermal capacity of the coating layer, and decreasing the coefficient of thermal expansion of the coating layer.

(ii) the location of the cavity influences thermal stress, which reaches a maximum, for Stellite III, at the critical ligament thickness of L_{cr}=0.094 for both cases of a single material with a cavity and a layered medium with a cavity.

(iii) for the same Peclet number (R_I), the critical ligament thickness (L_{cr}) is smaller than the critical depth (η_{cr}) of a coating material. When the coating thickness is designed to avoid the critical depth of the coating material, consideration must be extended to the possibility of interfacial voids. Hence, the coating thickness should not be in the neighborhood of the critical ligament thickness.

(iv) for a thin coated medium, the cavity location and the material properties matching (especially Young's modulus) will influence the principal directions of the thermal stress field. In particular, the obliqueness of the principal axis reaches a maximum when the coating thickness is at the critical ligament thickness. The phenomenon implies a large shearing stress at the coating/substrate interface, leading toward delamination of the coating.

5.2 EFFECTS OF THE LINE CRACK

It is demonstrated that when heat flow is disturbed by the presence of defects, there is a high local intensification of temperature and its gradients in the vicinity of the defects (Chen and Ju, 1987), causing very high thermal stresses around the defects. Such phenomenon eventually results in growth of the defects and may lead to failure. The earlier paper (Chen and Ju, 1987) considered a near-surface cavity defect and a moving line heat source which traverses over the surface at a moderately high speed. The current section will address the thermal phenomenon of a half-space with a near-surface line crack defect. The excitation again is a moving line heat source.

For the fracture mechanics problems, although analytical techniques are very important, but they are very difficult or even impossible to obtain. For complex geometries and loading conditions, numerical techniques are increasingly being used. Since the late 1960's, the finite element methods have been used for such complex fracture mechanics problems. Initially, finite element methods in fracture mechanics employed conventional elements, requiring an extremely fine mesh in the vicinity of the crack tip to obtain accurate stress intensity factors. Later, Byskov (1970), Walsh (1971) and Wilson (1971) introduced special crack tip elements, which directly modeled the $r^{-1/2}$ singularity near the crack tip, combined with conventional elements covering the rest of the domain, to solve linear fracture mechanics problems. This method reduces the total number of elements needed by using relatively large singular elements near the crack tip and

conventional elements in remaining regions. It was proven that this method is efficient and can yield a very accurate solution. Recently, Chen and Ju (1988) extended the special elements concept to the finite difference method and successfully solved the problem of a semi-infinite body containing a rectangular cavity. In this research, the finite difference method used by Chen and Ju (1988) will be modified to solve the line crack problem.

Once a finite difference solution is obtained, the value of the stress intensity factor can be estimated by the use of the established crack tip elements. There are many practical methods which can be used to evaluate stress intensity factors. The present section will use the displacement extrapolation method due to its relative simplicity, ease of interpretation and ready extension of the discrete data.

5.2.1 ANALYTICAL MODEL

The geometry of the medium may be approximated by a semi-infinite body containing a line crack. The excitation of the surface is a moving heat source as shown in Figure 25. Since the existence of the line crack disrupts the homogeneity condition in the direction of traversing of the heat source, the material coordinate system which is fixed to the medium must be employed. With reference to previous work (Chen and Ju, 1988, Ju and Huang, 1982, and Ju and Liu, 1988a), the uncoupled thermoelastic theory can be applied.

The governing equation for the temperature field is the Fourier equation, Equation (1). The temperature field satisfies the zero initial condition and the regularity condition at infinity. On the surface, heat flux is prescribed over a moving contact area. Due to the high-speed of the moving heat source and the size of the line crack, the heat flux is not expected to cross over the crack surfaces. Therefore, the crack surfaces are postulated to be adiabatic. The adiabatic conditions on the crack surfaces will result in an upper bound solution of the temperature field.

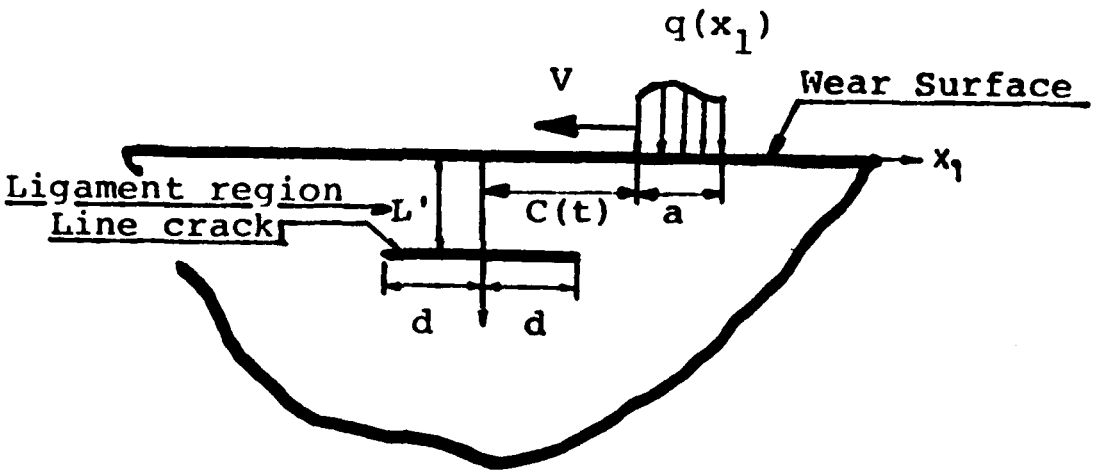

Figure 25. Two-dimensional model

For the thermal stress field, the thermoelastic Navier's equations and the Hooke's law are used, Equations (2, 5). The medium is initially unstressed. Boundary conditions for the thermal stress field are:

(i)the surface boundary and the crack surface are traction free;

(ii)at infinity, the regularity conditions hold.

5.2.2 SOLUTION TECHNIQUE

Due to the complexity of the geometry and the boundary conditions, the finite difference method is employed to solve both the temperature field and the thermal stress field. The difference scheme will now be presented.

(i) Temperature Field

To obtain the solution of the temperature field, an explicit finite difference scheme incorporating the energy balance method is used. The explicit finite difference scheme, the stability criteria and the energy balance method on the surface boundary are discussed by Chen and Ju (1987). The procedure of the energy balance method at the crack tip is (Figure 26)

$$Q_{W\to P} = k\,(\Delta y/2)\,\{[T^{+}(i-1,j,n)-t(i,j,n)]/\Delta x + [T^{-}(i-1,j,n)-T(i,j,n)]/\Delta x\}, \quad (24)$$

$$Q_{S\to P} = k\,(\Delta x)\,[T(i,j-1,n)-T(i,j,n)]/\Delta y, \quad (25)$$

$$Q_{Z\to P} = k\,(\Delta y)\,[T(i+1,j,n)-T(i,j,n)]/\Delta x, \quad (26)$$

$$Q_{N\to p} = k\,(\Delta x)\,[T(i,j+1,n)-T(i,j,n)]/\Delta y, \quad (27)$$

where Q is the heat flux, indexed by the flow direction, T^{+} and T^{-} represent the temperatures of the upper and lower surfaces of the crack, respectively.

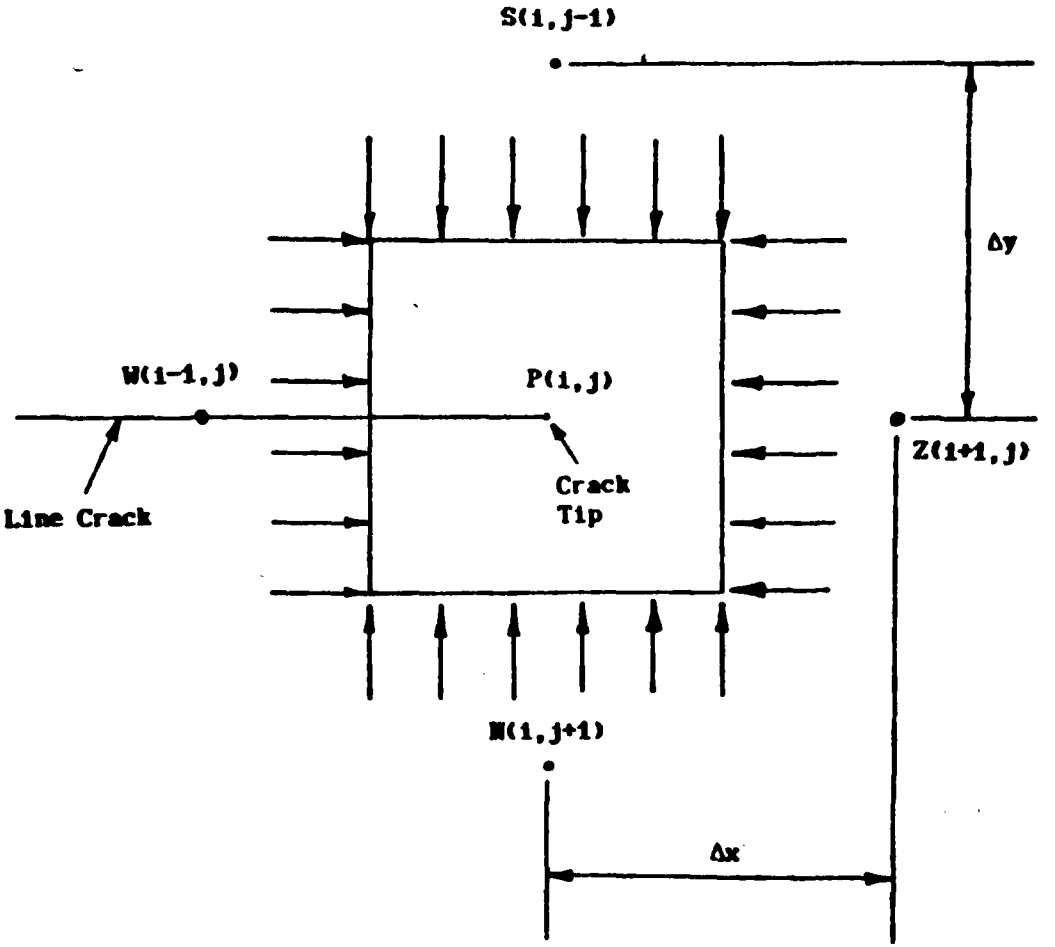

Figure 26. Energy balance at crack tip

The rate of change of internal energy $\dot{U}$ in the time interval Δt at the point P(i,j) is

$$\dot{U}_P = \rho c\ (\Delta x \Delta y)\ [T(i,j,n+1)-T(i,j,n)]/\Delta t\ . \qquad (28)$$

Conservation of energy requires that the algebraic sum of the heat flowing to the point P is equal to the rate of change of internal energy at the same point, i.e., $Q_{SUM} = \dot{U}_P$. From conservation of energy, one can obtain the equation for the crack tip. The dimensionless equation for the crack tip is

$$\phi(i,j,n+1) = \phi(i,j,n) + \frac{\Delta\tau}{R\Delta\xi^2}\ \{[\phi^+(i-1,j,n) +$$
$$+ \phi^-(i-1,j,n)]/2 - 2\phi(i,j,n) + \phi(i+1,j,n)\} +$$
$$+ \frac{\Delta\tau}{R\Delta\eta^2}\ [\phi(i,j-1,n)-2\phi(i,j,n) + \phi(i,j+1,n)]. \qquad (29)$$

Similarly, the equations for the crack surfaces can be obtained by using the energy balance method.

(ii) Stress Field

For hard wear material such as Stellite III and a typical asperity speed, the Mach number for the thermal stress field is of the order of 10^{-3}. Since M^2 is a small parameter, the solution for the thermal stress field can be obtained by the perturbation method (Chen and Ju, 1988), using M^2 as the perturbation parameter. Using the technique introduced by Chen and Ju (1988), for the present case, the contribution of the higher order terms may be shown to be insignificant. Therefore, only the zeroth order solution is presented here.

Since high temperature and high temperature gradient are found in the vicinity of the crack, a fine mesh must be used near the line crack and a relative coarse mesh can be used in the regions away from the crack. This non-uniform mesh can be transformed parametrically to the

uniform mesh and solved in the transformed plane. Discussion of the conventional finite difference equations and the coordinates transformation are referred to Chen and Ju (1988) and Anderson et al. (1984).

(iii) Special Crack Tip Elements

Since the presence of heat flow produces no additional singularities (Sih, 1962), the local character of the thermal stress singularity at the crack tip is of the same nature as that of the mechanical stress; i.e., $r^{-1/2}$. For plane thermoelastic loading conditions, the displacement field associated with the tip is described by the asymptotic equations (Owen and Fawkes, 1983)

$$u = \sum_{n=1}^{\infty} \frac{r^{n/2}}{2\mu} \{a_n^1[(\kappa' + \frac{n}{2} + (-1)^n)\cos(\frac{n}{2})\theta - \frac{n}{2}\cos(\frac{n}{2} - 2)\theta] - a_n^2[(\kappa' + \frac{n}{2} - (-1)^n)\sin(\frac{n}{2})\theta - \frac{n}{2}\sin(\frac{n}{2} - 2)\theta]\} , \quad (30)$$

and

$$v = \sum_{n=1}^{\infty} \frac{r^{n/2}}{2\mu} \{a_n^1[(\kappa' - \frac{n}{2} - (-1)^n)\sin(\frac{n}{2})\theta + \frac{n}{2}\sin(\frac{n}{2} - 2)\theta] + a_n^2[(\kappa' - \frac{n}{2} + (-1)^n)\cos(\frac{n}{2})\theta + \frac{n}{2}\cos(\frac{n}{2} - 2)\theta]\} . \quad (31)$$

where r is the distance measured from the crack tip, $\kappa'=3-4\nu$ for plane strain problem, ν is Poisson's ratio, a_n^1 and a_n^2 are constants to be determined. From equations (30, 31), it can be seen that the first terms of the displacement series yield stresses as a function of $r^{-1/2}$, which characterizes the stress singularity at the crack tip. In the numerical scheme, for small r, the first few terms of the displacement series dominate. The conventional finite difference equations and the special elements constitute a complete set of difference equations for finding the thermal stress field solution.

5.2.3 NUMERICAL RESULTS

Because of the moving heat source, the thermal stress field is unsymmetrical. Hence, the mixed mode stress intensity factors are to be evaluated. Numerical computations are carried out for the following values of the parameters: V=15 m/s, a=0.3d, d=1mm. The material properties are those of Stellite III. The smallest mesh size used under the moving heat source and near the crack tips is $\Delta\xi$=0.01 and $\Delta\eta$=0.005. But the mesh sizes are rapidly increased away from these two regions.

Figure 27 compares the temperature fields of the medium with and without a line crack when the heat source is directly over the crack. The ligament thickness (thickness between the wear surface and the crack surface) for the medium with a line crack is L=0.022. In the figure, solid lines are for the medium with a line crack and dashed lines are for the medium with no crack. The temperature field and the temperature gradient of the medium containing a line crack is much higher than those of the medium with no crack. This high temperature field and its gradients are the source of the high thermal stresses.

The plane strain displacement equations are

$$u = \frac{K_I}{4\mu}(r/2\pi)^{1/2}[(2\kappa'-1)\cos(\theta/2)-\cos(3\theta/2)] - \frac{K_{II}}{4\mu}(r/2\pi)^{1/2}[(2\kappa'+3)\sin(\theta/2)+\sin(3\theta/2)] , \quad (32)$$

and

$$v = \frac{K_I}{4\mu}(r/2\pi)^{1/2}[(2\kappa'+1)\sin(\theta/2)-\sin(3\theta/2)] - \frac{K_{II}}{4\mu}(r/2\pi)^{1/2}[(2\kappa'+3)\cos(\theta/2)+\cos(3\theta/2)] , \quad (33)$$

in which K_I and K_{II} are the mode I and the mode II stress intensity factors, and μ is the shear modulus. Substituting the values of r and u or v for nodal points along the crack surfaces emanating from the crack tip allows a plot of K_I and K_{II} against radial distance r. The

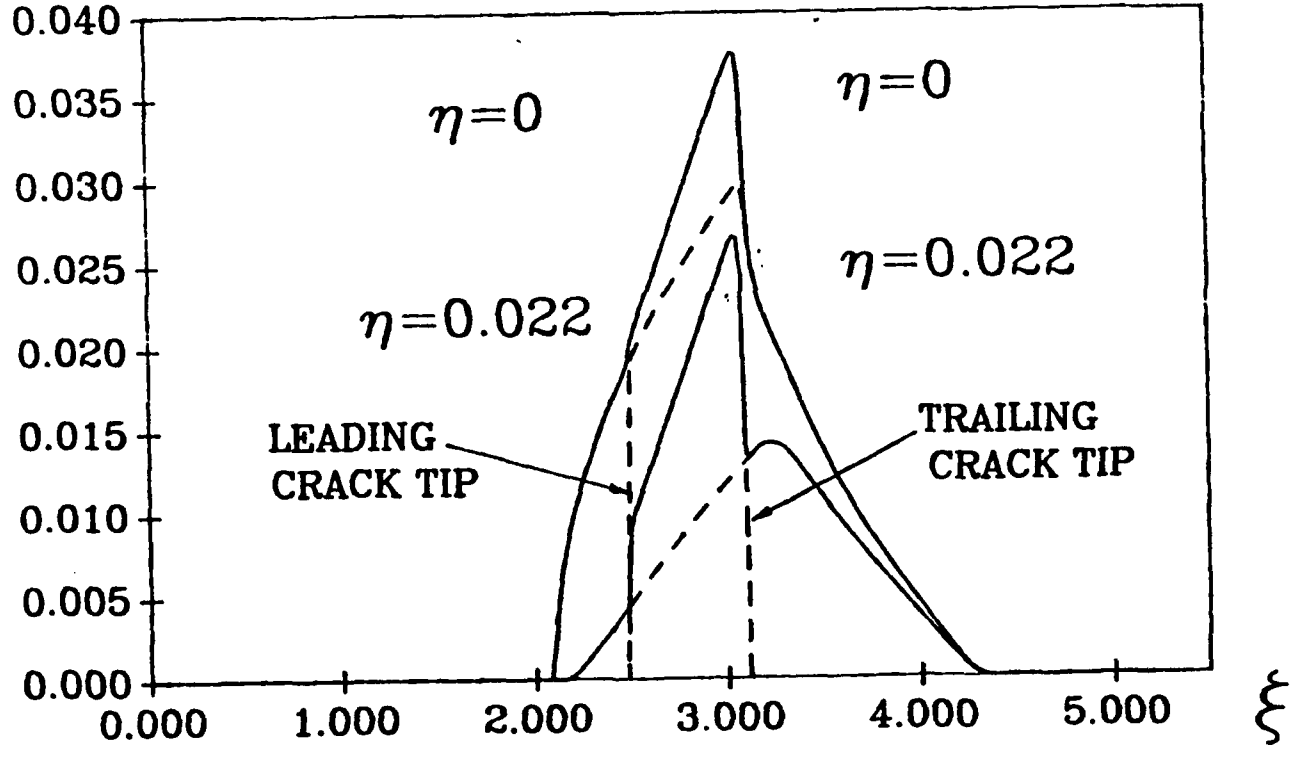

Figure 27. Temperature distribution, L=0.022

approximate values of K_I and K_{II} are thus obtained by extrapolation to r=0. Figure 28 show the effect of the location of the moving heat source on the stress intensity factors, where $k_1=K_I/\sigma_0\sqrt{d}$ is the dimensionless stress intensity factors, d is the contact width of the moving heat source, and σ_0=1 unit. At the time τ=1.2, when the moving heat source is right above the line crack, both k_1 and k_2 reach a maximum value. This figure thus establishes that, when the moving heat source is right above the line crack, not only the thermal stress field but also the stress intensity factors will reach the worst state.

Figures 29 to 33 present the effects of the mechanical and thermal properties on the stress intensity factors when the moving heat source is right above the line crack. Figures 29 and 30 present the effects of the Young's modulus (E) and the coefficient of thermal expansion (α). From these two figures, it can be observed that both k_1 and k_2 are linearly proportional to the Young's modulus E and the coefficient of thermal expansion α. The result can be expected from the Navier's equation. Figure 31 illustrates the effect of thermal conductivity (k). In this figure, thermal diffusivity (κ) is fixed. This figure shows that both k_1 and k_2 are inversely proportional to thermal conductivity. This is simply because larger thermal conductivity will result in a lower temperature field. Figure 32 demonstrates the effect of thermal capacity (ρc) on stress intensity factors. In this figure, thermal conductivity is fixed. The figure establishes that, as the thermal capacity is decreased, the mode I stress intensity factor k_1 is decreased, but the mode II stress intensity factor k_2 is increased.

The presence of defects will change the pattern of the temperature distribution. Consequently, the critical depth, at which thermal principal stress reaches a maximum, is changed. Ju and Liu (1988a) established that, for a medium with no defect, the critical depth, at which the principal tensile stress reaches a maximum, is η_{cr}=0.16 for Stellite III. However, when there is a rectangular cavity, the principal tensile stress is the highest at the top trailing corner of the rectangular cavity and reaches a maximum at the critical ligament thickness L_{cr}=0.094. In the present section, it is found that the

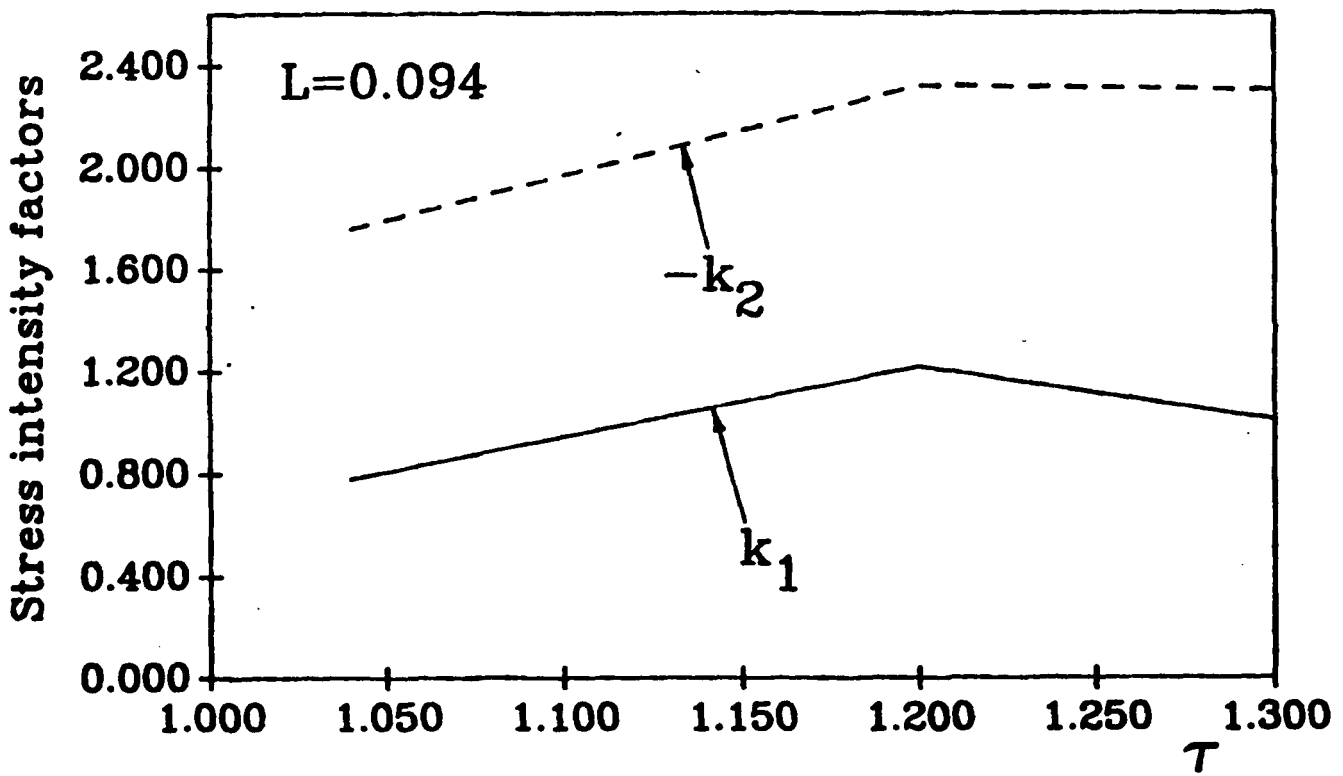

Figure 28. **Effect of the location of the moving heat source on stress intensity factors**

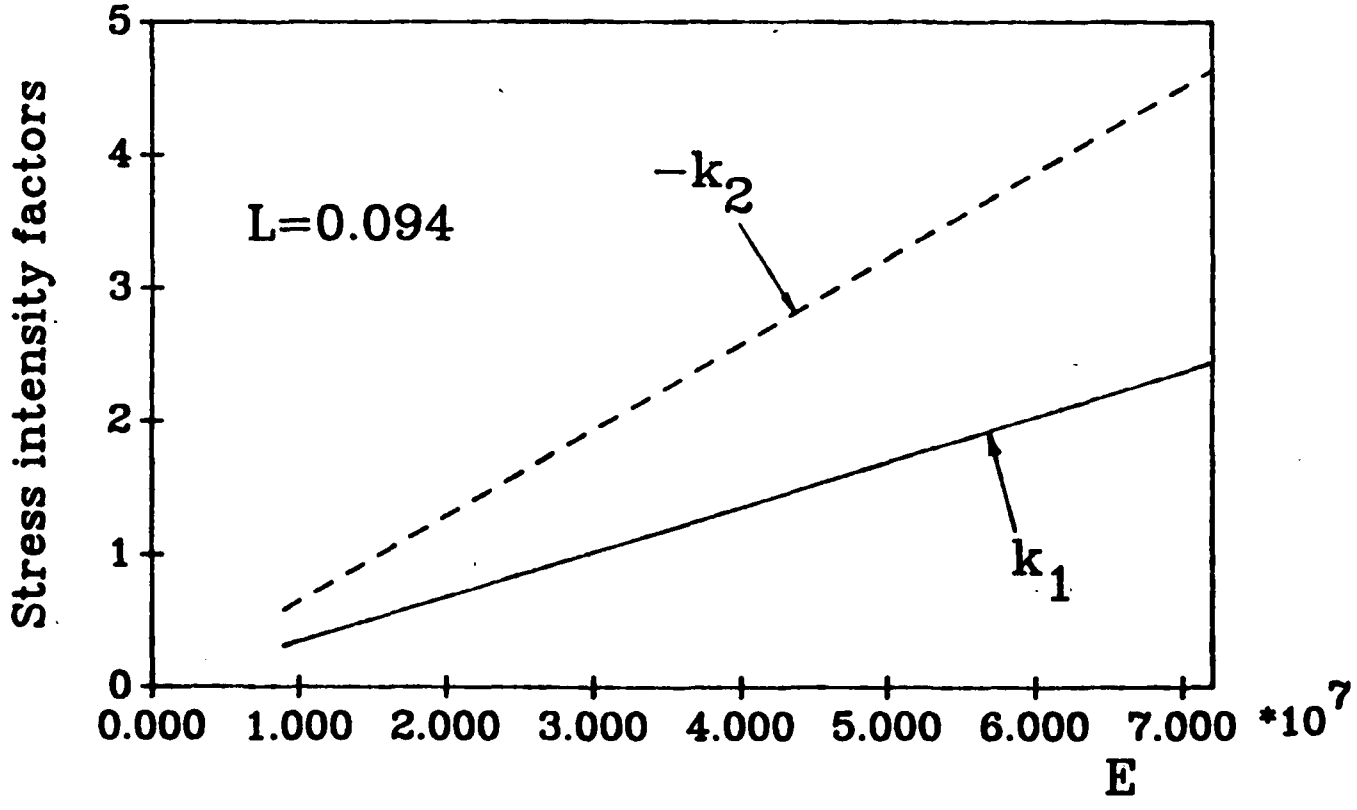

Figure 29. Stress intensity factors vs Young's modulus

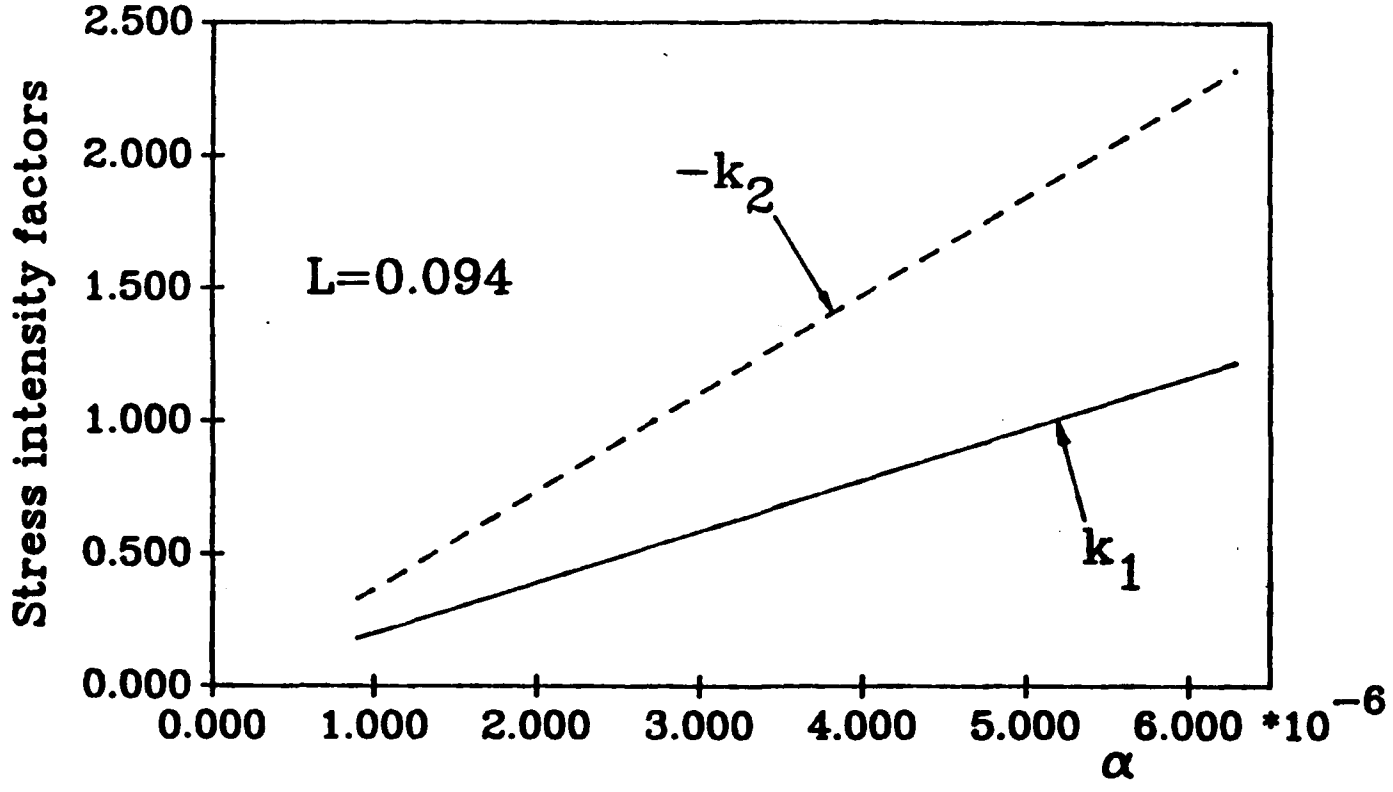

Figure 30. **Stress intensity factors vs the coefficient of thermal expansion**

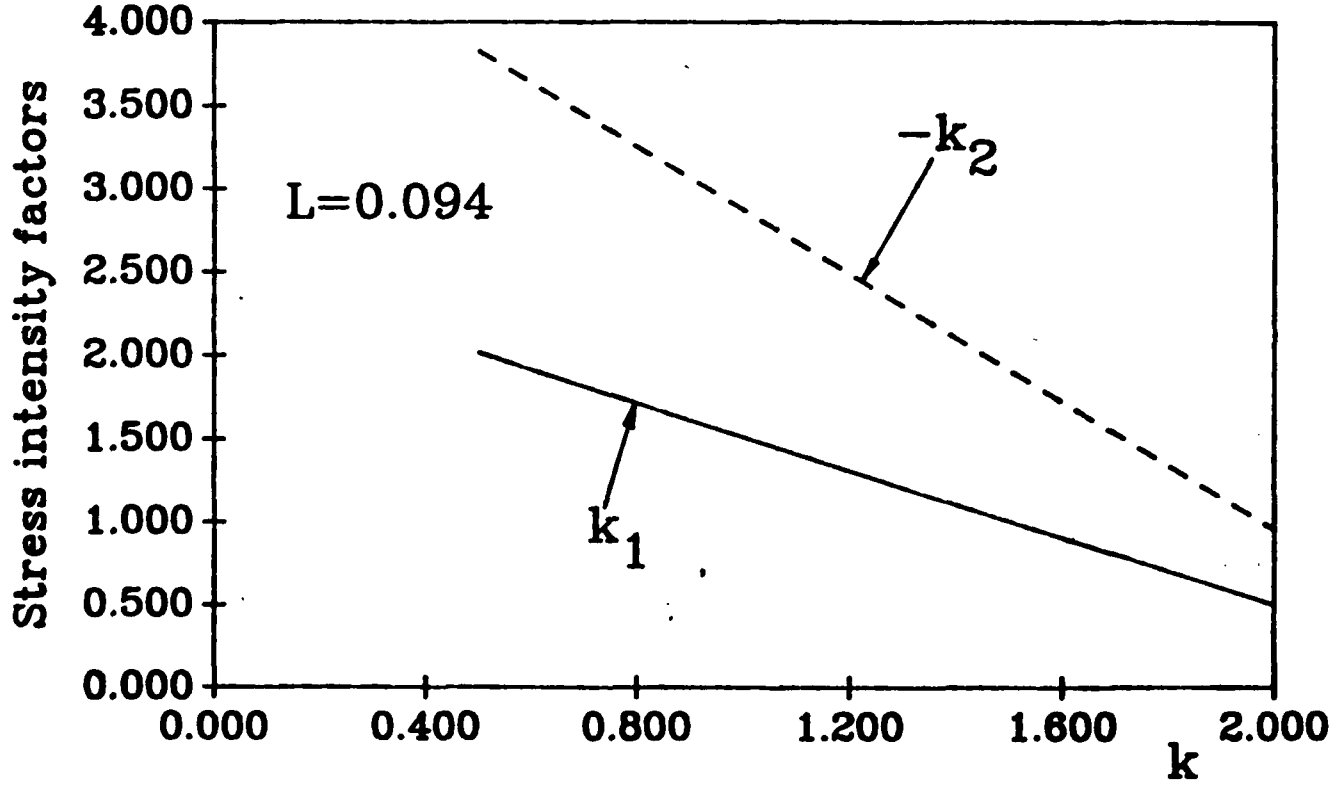

Figure 31. **Stress intensity factors vs thermal conductivity**

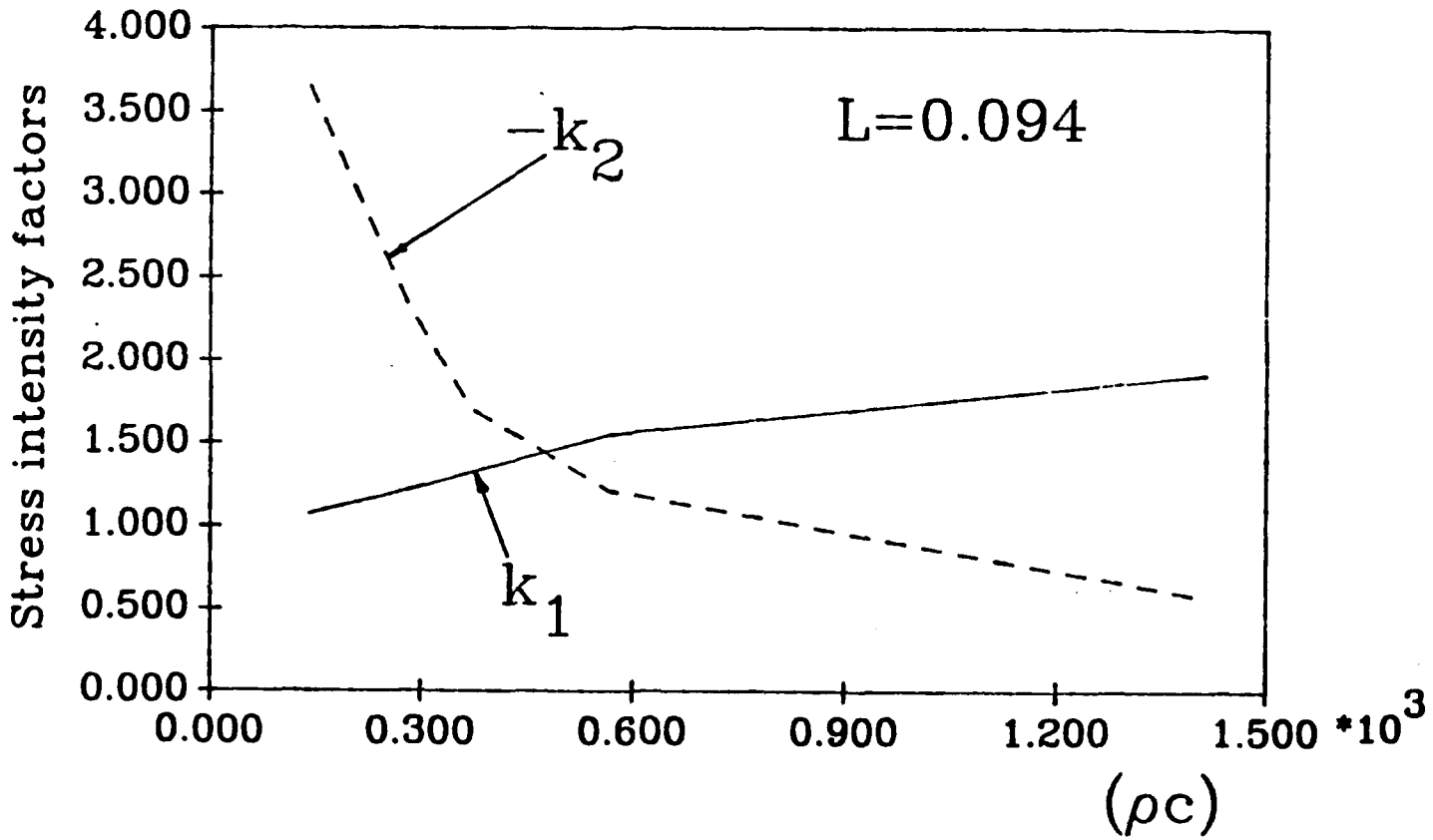

Figure 32. **Stress intensity factors vs thermal capacity**

geometry of the defect will influence the critical ligament thickness. As illustrated in Figure 33, both k_1 and k_2 reach a maximum when the ligament thickness is at L=0.08.

5.2.4 SUMMARY

The present section demonstrates the use of the finite difference method, supplemented with a special computational procedure, to determine the stress intensity factors at the crack tip. The mixed mode stress intensity factors for a thermoelastic problem with a moving heat source excitation were considered in both the derivations and examples. The procedures developed can readily be extended to different loading conditions and different crack geometry. The perturbation method mentioned in the section allows one to consider the various order solutions in the numerical calculations depending on the magnitude of the Mach number. For the current application, because of the smallness of the Mach number, the zeroth order solution is adequate.

According to the numerical results, the conclusions of this work are as follows.

(i) Because of the poor heat transfer characteristics of the crack surface, temperature and its gradients in the vicinity of a line crack are much higher than that of the medium with no defect. This high temperature and high temperature gradients are the source of large thermal stresses.

(ii) Increasing Young's modulus, the coefficient of thermal expansion and decreasing thermal conductivity will result in larger stress intensity factors, leading to earlier crack propagation.

(iii) Decreasing thermal capacity will result in smaller k_I, but larger k_{II}.

(iv) For the moving asperity problem, there is a critical depth at which the principal thermal stress reaches a maximum (Ju and Liu, 1988a). For Stellite III, the critical depth is η_{cr}=0.16. However, when there is a defect, the depth at which the maximum value of stress occurs is changed, depending on the location of the defect (Chen and Ju, 1988). For a rectangular cavity, the maximum thermal stress occurs at

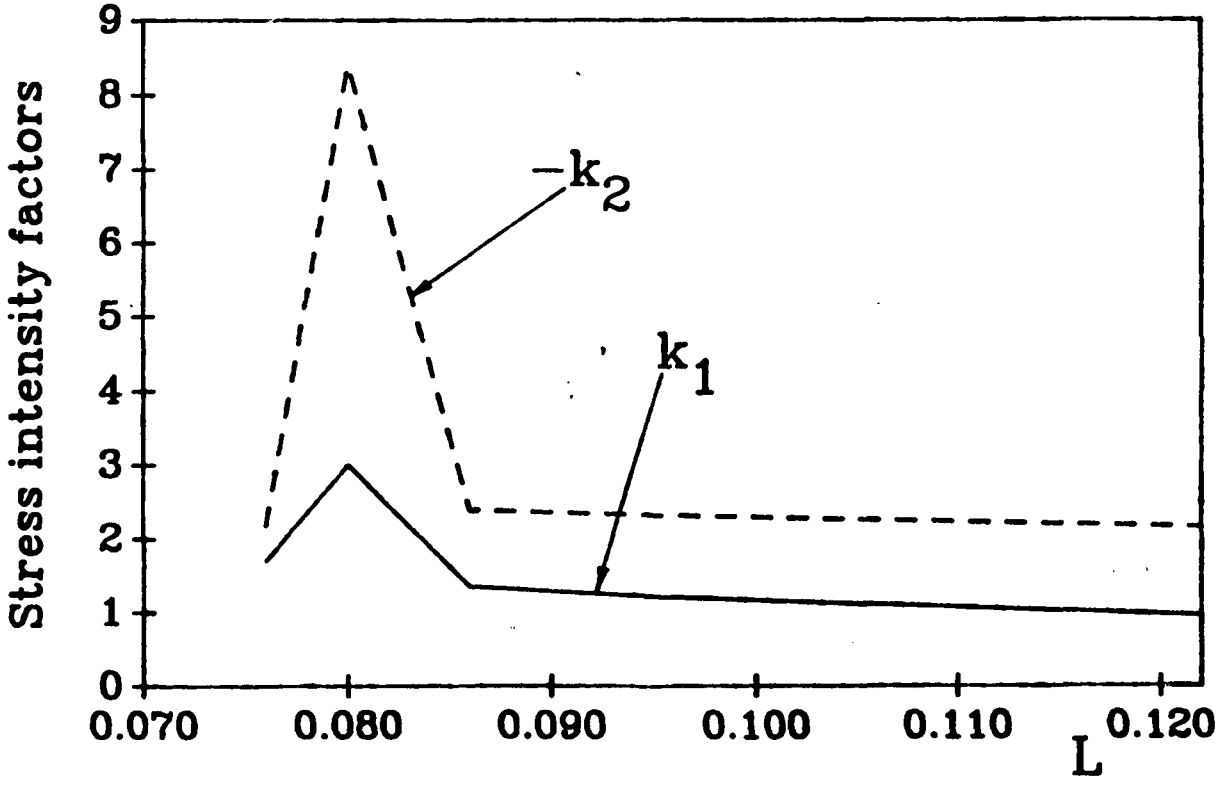

Figure 33. **Effect of ligament thickness on stress intensity factors**

the ligament thickness L_{cr}=0.094. In this section, we established that the geometry of the defect will also influence the critical ligament thickness. For Stellite III, the critical ligament thickness for a line crack is at L_{cr}=0.08.

5.3 EFFECTS OF THE RANDOM VARIATION IN COATING THICKNESS

This section presents the temperature field solution in a coated medium, induced by the excitation of a fast-moving asperity over the wear surface of the coating. The coating thickness is uniform for individual specimens. However, random variation in thickness exists in a sample set Ω. Such random variation in coating thickness arises from a myriad of source such as fabrication tolerances and wear during services. Since the concept of deterministic temperature field no longer applies in analyzing such thermo-mechanical problems, there arises a new class of problems in which one is confronted with determining a random temperature field. The use of the theory of random processes becomes a necessity.

The random characteristics of heat transfer have not been fully studied. Some representative works are noted here. Samuels (1966) approached heat conduction in solids considering a linear system with stationary Gaussian processes and solved several one-dimensional problems. Ling (1972) studied heat conduction in a semi-infinite solid involving Gaussian processes as forcing functions. Ahmadi (1974) studied heat conduction in solids with random initial conditions. He also applied the perturbation method to investigate heat conduction in solids with random thermal conductivity (1978). Tzou (1988) used the stochastic analysis to study the temperature field in a solid with random thermal conductivity. He (1989) also developed an one-dimensional stochastic model to solve that contact problem in heat conduction.

In the present study, we consider first the case that for individual sample the coating thickness and its wear are uniform. Random variation in thickness, however, exists in an assemblage of such

coatings, called the sample space. The coefficient of variation of the thickness is small. We can then use a special perturbation techniques and formulate the coating thickness a sample random variable. In other words, the coating thickness varies from one specimen to another in the sample space Ω. In a single specific specimen, the coating thickness is uniform. The solution for the temperature is expressed in the form of a series expansion in a parameter ϵ which is small in view of slight random variations in the coating thickness. By truncating the series solution which depends on the magnitude of ϵ, we can compute the mean temperature as well as the variance of the temperature on a large sample of the coating media.

5.3.1 Formulation Of The Problem

With reference to Figure 1, a heat source moves at constant speed V over a semi-infinite solid with a surface coating of a uniform thickness H. The strength of the heat source is assumed constant in time and uniform over its width 2a. Furthermore, the heat source is of sufficient depth normal to the plane, such that the plane theory applies. The coating thickness H is considered to be only a function of the sample variable α. The variable α ranges over a probability space Ω composed of all the specimens. The probability density $D(\alpha)$ in Ω is assumed to be measurable. Hence, all of the statistical quantities (such as expected value, standard deviation, etc.) in the present analysis are well-defined.

Referring to Figure 1, and using the material coordinates x'-y', the temperature in each region (I or II), for t>0, must satisfy Fourier's law of the heat conduction in a solid (no sum on the repeated indices).

$$\rho_\beta c_\beta \partial_t T^\beta = k_\beta \nabla^2 T^\beta, \quad -\infty<x'<\infty, \quad 0<y'<H_0+\epsilon' f(\alpha), \tag{34}$$

in which ∇^2 is the Laplacian operator, ρc constitutes the thermal capacity, and $\partial_t=\partial/\partial t$, β designates the coating layer (I) or the

substrate (II). The thermal capacity is deterministic and constant in the analysis. The term $\epsilon' f(\alpha)$ accounts for the random fluctuation of the coating thickness. Taking into consideration a well-controlled manufacturing process for depositing the coating or the hardness of the coating material, the parameter ϵ' is postulated to be a small number, i.e. $\epsilon' << 1$.

The time dependent governing Equations (34), can be transformed into a steady state formulation by using the convective coordinates (x-y), which are fixed to the moving heat source. With the transformation x'=x+Vt, y'=y, Equation (34) becomes

$$\kappa_\beta \nabla^2 T^\beta = V \partial_x T^\beta, \tag{35}$$

where κ is the thermal diffusivity, and $\partial_x = \partial/\partial x$.

As the asperity moves, the contact friction results in heat input, which is constant in the convective reference frame. Hence, the boundary condition on the surface is expressed as:

$$k_I \partial_y T^I = \begin{cases} q(x) & \text{within the contact area} \\ 0 & \text{elsewhere,} \end{cases} \tag{36}$$

where q(x) is the heat input over the contact area.

Regularity conditions hold at infinity; that is, at infinity, $x^2+y^2 \rightarrow \infty$, and

$$T^{II} = 0. \tag{37}$$

At the interface, $y=H_0+\epsilon' f(\alpha)$, continuity conditions must be satisfied for both the temperature and the heat flux.

$$T^I = T^{II}, \tag{38-a}$$

$$k_I \partial_y T^I = k_{II} \partial_y T^{II}. \qquad (38\text{-b})$$

To facilitate a parametric analysis, the following non-dimensional quantities are defined

$$\xi = x/a,\ \eta = y/a,\ d = H/a,\ d_0 = H_0/a,\ \epsilon = \epsilon'/a,$$

$$Q = q/q_0,\ \phi^\beta = (T^\beta - T_0)k_I/q_0 a,\ R_I = Va/\kappa_I,\ R_{II} = Va/\kappa_{II},$$

$\Pi_k = k_I/k_{II}$, q_0 is the average heat input.

Equations (35 - 38) can now be written in terms of these dimensionless variables as follows:

$$\nabla^2 \phi^\beta = R_\beta \partial_\xi \phi^\beta, \qquad (39)$$

$$-\partial_\eta \phi^I = \begin{cases} Q(\xi) \text{ within the contact area} \\ 0 \quad \text{elsewhere,} \end{cases} \qquad (40)$$

$$\phi^I = \phi^{II}, \qquad \eta = d_0 + \epsilon f(\alpha) \qquad (41\text{-a})$$

$$\Pi_k \partial_\eta \phi^I = \partial_\eta \phi^{II}, \qquad \eta = d_0 + \epsilon f(\alpha) \qquad (41\text{-b})$$

$$\phi^{II} \to 0, \qquad \xi^2 + \eta^2 \to \infty. \qquad (42)$$

In the next section, the resulting stochastic temperature distribution in solid media with random thickness is studied by perturbation.

5.3.2 Method of Solution

We recognize the fact that the coefficient ϵ which modulates the random fluctuation function $f(\alpha)$ is to satisfy the condition $|d_0| >> |\epsilon f(\alpha)|$. The quantity ϵ can be the small perturbative parameter for the

perturbation method. For a sample random thickness, ϵ' in the the material coordinate and ϵ in the convective coordinate are the same. $\phi(\xi,\eta;\alpha)$ is then expanded into a asymptotic series in powers of ϵ:

$$\phi^{\beta}(\xi,\eta;\alpha) = \sum_{n=0}^{\infty} \epsilon^{n} \phi_{n}^{\beta}(\xi,\eta;\alpha). \tag{43}$$

Since the continuity conditions (41) are imposed at $\eta = d_0+\epsilon f(\alpha)$, ϵ appears in the argument of ϕ^{β} in Equations (41) as well as in the coefficients of the asymptotic series. To equate coefficients of equal powers of ϵ, at $\eta = d_0+\epsilon f(\alpha)$, ϵ must be removed from the argument of function $\phi_{n}^{\beta}(\xi,d_0+\epsilon f(\alpha);\alpha)$. We shall use the technique of the boundary condition transfer (Nayfeh, 1980). By writing ϕ^{β} at $\eta = d_0+\epsilon f(\alpha)$ in Equation (41-a) as $\phi^{\beta}(\xi,d_0+\epsilon f(\alpha))$, and expanding ϕ^{β} into a Taylor series about $\eta = d_0$, we have

$$\phi^{\beta}(\xi,d_0+\epsilon f(\alpha)) = \sum_{n=0}^{\infty} \frac{1}{n!} [\epsilon f(\alpha)]^{n} \partial_{\eta}^{n} \phi^{\beta}(\xi,d_0). \tag{44-a}$$

Similarly, $\partial_{\eta}\phi^{\beta}$ at $\eta = d_0+\epsilon f(\alpha)$ can be expressed as

$$\partial_{\eta}\phi^{\beta}(\xi,d_0+\epsilon f(\alpha)) = \sum_{n=0}^{\infty} \frac{1}{n!} [\epsilon f(\alpha)]^{n} \partial_{\eta}^{n+1} \phi^{\beta}(\xi,d_0). \tag{44-b}$$

By substituting these Taylor series expansions (44-a and b) into the continuity conditions, we obtains from Equations (41-a and b), respectively, the equations

$$\sum_{n=0}^{\infty} \frac{1}{n!} [\epsilon f(\alpha)]^{n} \partial_{\eta}^{n} \phi^{I}(\xi,d_0) =$$

$$= \sum_{n=0}^{\infty} \frac{1}{n!} [\epsilon f(\alpha)]^n \partial_\eta^n \phi^{II}(\xi, d_0), \qquad (45\text{-a})$$

$$\sum_{n=0}^{\infty} \frac{1}{n!} [\epsilon f(\alpha)]^n \partial_\eta^{n+1} \phi^{I}(\xi, d_0) =$$

$$= \sum_{n=0}^{\infty} \frac{1}{n!} [\epsilon f(\alpha)]^n \partial_\eta^{n+1} \phi^{II}(\xi, d_0). \qquad (45\text{-b})$$

The continuity conditions are effectively transferred from $\eta = d_0 + \epsilon f(\alpha)$ to $\eta = d_0$ by removing ϵ from the argument of $\phi^\beta(\xi, d_0 + \epsilon f(\alpha); \alpha))$ and $\partial_\eta \phi^\beta(\xi, d_0 + \epsilon f(\alpha); \alpha)$.

Substituting Equation (43) into Equations (39, 40, 42, 45), a system of equations may now be obtained by matching the terms of various orders of ϵ.

For the 0^{th} order:

$$\partial_{\xi\xi} \phi_0^I + \partial_{\eta\eta} \phi_0^I = R_I \partial_\xi \phi_0^I, \qquad (46\text{-a})$$

$$\partial_{\xi\xi} \phi_0^{II} + \partial_{\eta\eta} \phi_0^{II} = R_{II} \partial_\xi \phi_0^{II}, \qquad (46\text{-b})$$

subject to the conditions:

$$-\partial_\eta \phi_0^I = \begin{cases} Q(\xi) & \text{within the contact area} \\ 0 & \text{elsewhere} \end{cases}, \quad \eta = 0, \qquad (47)$$

$$\phi_0^I = \phi_0^{II}, \qquad \eta = d_0, \qquad (48\text{-a})$$

$$\Pi_k \partial_\eta \phi_0^I = \partial_\eta \phi_0^{II}, \qquad \eta = d_0, \qquad (48\text{-b})$$

$$\phi_0^{II} \to 0, \qquad \xi^2 + \eta^2 \to \infty. \qquad (49)$$

For the n^{th} order; n = 1, 2, 3,...

$$\partial_{\xi\xi}\phi_n^I + \partial_{\eta\eta}\phi_n^I = R_I\partial_\xi\phi_n^I, \tag{50-a}$$

$$\partial_{\xi\xi}\phi_n^{II} + \partial_{\eta\eta}\phi_n^{II} = R_{II}\partial_\xi\phi_n^{II}, \tag{50-b}$$

subject to the conditions:

$$-\partial_\eta\phi_n^I = 0, \qquad \eta = 0, \tag{51}$$

$$\sum_{i=0}^{n}\frac{1}{i!}\,f^i(\alpha)\partial_\eta^i\phi_{n-i}^I = \sum_{i=0}^{n}\frac{1}{i!}\,f^i(\alpha)\partial_\eta^i\phi_{n-i}^{II}, \qquad \eta = d_0, \tag{52-a}$$

$$\Pi_k\sum_{i=0}^{n}\frac{1}{i!}\,f^i(\alpha)\partial_\eta^{i+1}\phi_{n-i}^I =$$

$$= \sum_{i=0}^{n}\frac{1}{i!}\,f^i(\alpha)\partial_\eta^{i+1}\phi_{n-i}^{II}, \qquad \eta = d_0, \tag{52-b}$$

$$\phi_n^{II} \to 0, \qquad (\xi^2+\eta^2)^{1/2} \to \infty. \tag{53}$$

The set of the zeroth order equations (46 - 49) is the corresponding deterministic problem with ϵ being zero when there is no random variation in thickness. It is then clear that the effects of the higher order terms will gradually enter the problem as the contributions of ϕ_n^β (n = 1, 2,$\cdots$), and are summed into the perturbation series (43). The random feature of the perturbation system can be observed, from the continuity conditions (52), that the fluctuation function now is the coefficient of each summed-up term.

By applying the Fourier transform to Equations (46 - 53) with respect to ξ-coordinate, these equations become ordinary differential

equations of the transformed temperature $\tilde{\phi}^{\beta}(s,\eta;\alpha)$ in the transform space, where s is the transform parameter. The analytical solutions for various orders in the perturbation system in the transform space can be obtained in sequence. Because of the complexity of the solution, they are given in the Appendix. The expressions for $\tilde{\phi}_0^{\beta}(s,\eta)$, $\tilde{\phi}_1^{\beta}(s,\eta;\alpha)$, and $\tilde{\phi}_2^{\beta}(s,\eta;\alpha)$ (Appendix) can be expressed as:

$$\tilde{\phi}_n^{\beta}(s,\eta;\alpha) = f^n(\alpha)\tilde{W}_n^{\beta}(s,\eta) \quad \text{for } n = 0, 1, 2,\cdots \tag{54}$$

The form in Equation (54) can be obtained due to the homogeneous governing equations subject to the non-homogeneous continuity conditions. Therefore, the temperature distribution in the solid may be written as

$$\tilde{\phi}^{\beta}(s,\eta;\alpha) = \sum_{n=0}^{\infty} \epsilon^n f^n(\alpha)\tilde{W}_n^{\beta}(s,\eta). \tag{55}$$

Let ϵ be associated with the design tolerance of the coating thickness, say, 0.5% of the design value. According to Equation (55), the accuracy of the analysis could be in the order of 0.1% if the perturbation system is solved up to the second order. Consequently, in the physical domain $(\xi,\eta;\alpha)$, the solution may be adequately expressed, with second order approximation, as

$$\phi^{\beta}(\xi,\eta;\alpha) = \sum_{n=0}^{2} \epsilon^n f^n(\alpha)W_n^{\beta}(\xi,\eta), \tag{56}$$

where

$$W_n^{\beta}(\xi,\eta) = \int_{-\infty+ic}^{\infty+ic} \tilde{W}_n^{\beta}(s,\eta)\exp(-i\xi s)ds. \tag{57}$$

The advantage of the present formulation to describe the diffusion

phenomenon with geometrical randomness is readily evident from (56). By applying an statistical operator to (56), for example the expected value and the variance, we obtain

$$E_\alpha[\phi^\beta(\xi,\eta,;\alpha)] = \sum_{n=0}^{2} \epsilon^n E_\alpha[f^n(\alpha)] W_n^\beta(\xi,\eta), \tag{58}$$

$$\begin{aligned} Var_\alpha[\phi^\beta(\xi,\eta,;\alpha)] = {} & \epsilon^2 W_1^2 Var_\alpha[f(\alpha)] + 2\epsilon^3 W_1 W_2 \Big(E_\alpha[f^3(\alpha)] - \\ & - E_\alpha[f(\alpha)] E_\alpha[f^2(\alpha)] \Big) + \epsilon^4 W_2^2 Var_\alpha[f^2(\alpha)]. \end{aligned} \tag{59}$$

Accordingly, Equations (58, 59) indicate that the statistical order of the random response of the system is the same as that of the random fluctuation function under the present formulation. In other word, the mean value of the random response depends only upon the mean value of the random fluctuation function and the same situation holds for the variance.

5.3.3 Numerical Results

To illustrate the application of the proposed formulation, a cyclic function is chosen to be the random variation of the coating thickness in a collection of samples; i.e.

$$f(\alpha) = \sin(\alpha p). \tag{60}$$

The Gaussian distribution is the corresponding probability density function of the process;

$$D(\alpha) = \frac{1}{\sqrt{2\pi}\, b} \exp\left(-\frac{\alpha^2}{2b^2}\right), \quad -\infty \le \alpha \le \infty, \tag{61}$$

where b is the standard deviation of a random variable with Gaussian distribution. The expected value for different orders of $f(\alpha)$ and the variance can be evaluated as:

$$E_a[f(a)] = 0,$$

$$E_a[f^2(a)] = \left(1-\exp(-2b^2p^2)\right)/2,$$

$$E_a[f^3(a)] = 0,$$

$$E_a[f^4(a)] = \left(3-4\exp(-2b^2p^2)+\exp(-8b^2p^2)\right)/8,$$

$$Var_a[f(a)] = E_a[f^2(a)] - E_a^2[f(a)],$$

$$Var_a[f^2(a)] = E_a[f^4(a)] - E_a^2[f^2(a)].$$

The stochastic response for the present problem, with sample-dependent randomness of coating thickness, can thus be obtained.

For numerical computations, the material properties of Stellite III have been chosen. The deterministic quantities involved in the numerical calculations are:

$$a = 0.254 \text{ mm}, \quad k = 9.7 \text{ J/M·sec·K},$$

$$\rho c = 3.5\text{x}10^6 \text{ J/M}^3\text{·K}, \quad V = 15 \text{ M/sec}.$$

b = 2 and p = 0.2 are used in the Gaussian distribution defined in (60, 61). The corresponding coefficient of the variation of coating thickness is computed to be 0.1%.

The following figures of results are all computed at the trailing end of the asperity in the coated solid medium.

CASE I: The mismatch in thermal conductivity, $\Pi_k = k_I/k_{II}$

Figures 34 and 35 show the variation of mean temperature distribution with respect to η (the depth direction) for mean coating thickness d_0, chosen at a thin geometry of 0.03 and 0.05. Figures 36 and 37 show the standard deviation of temperature distribution under the same conditions as Figures 34 and 35. Figures 38 and 39 plot the mean and the standard deviation of temperature distribution at the coating/substrate interface with respect to the mean coating thickness d_0.

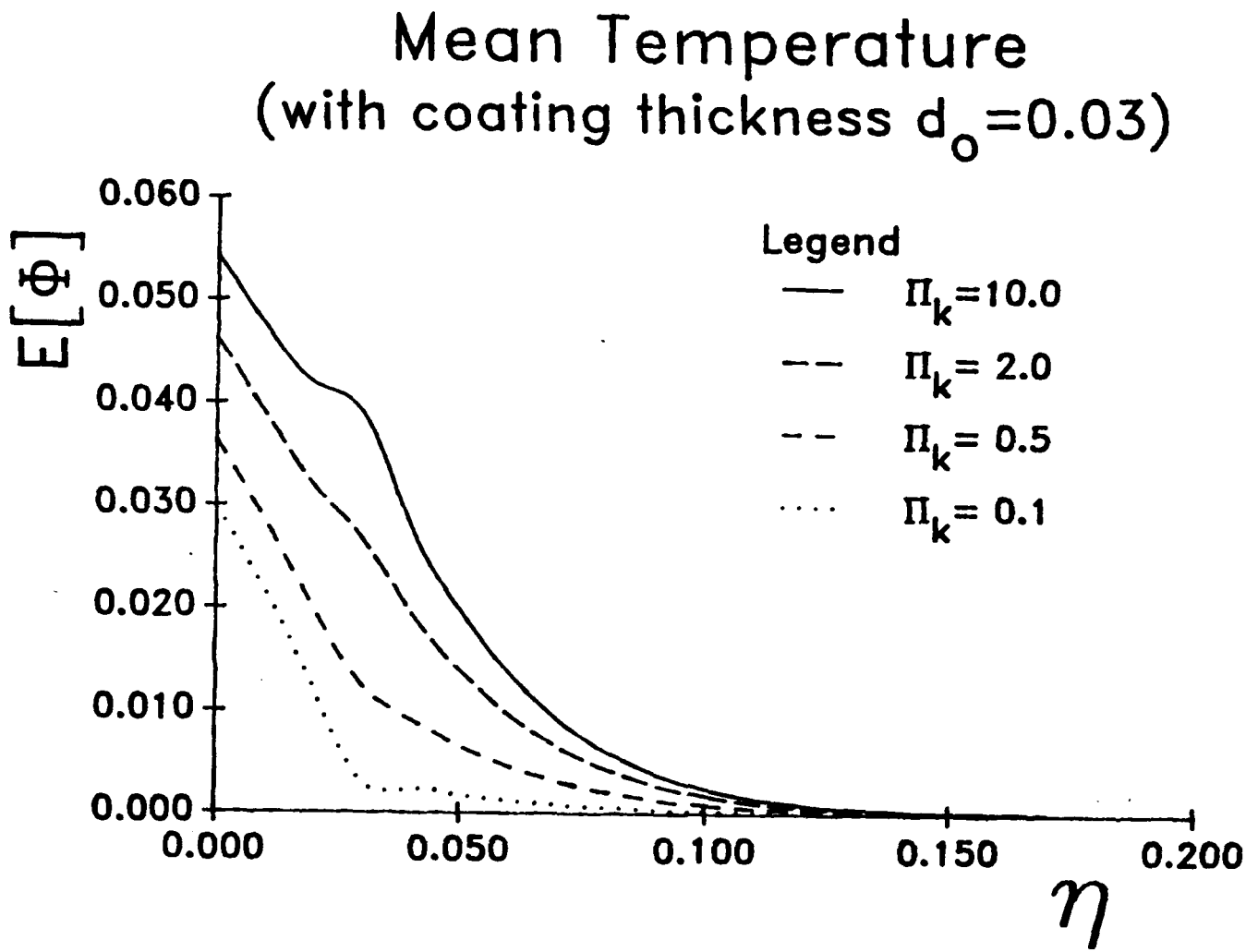

Figure 34. **Mean temperature as a function of η with coating thickness d_0=0.03 for thermal conductivity impedance**

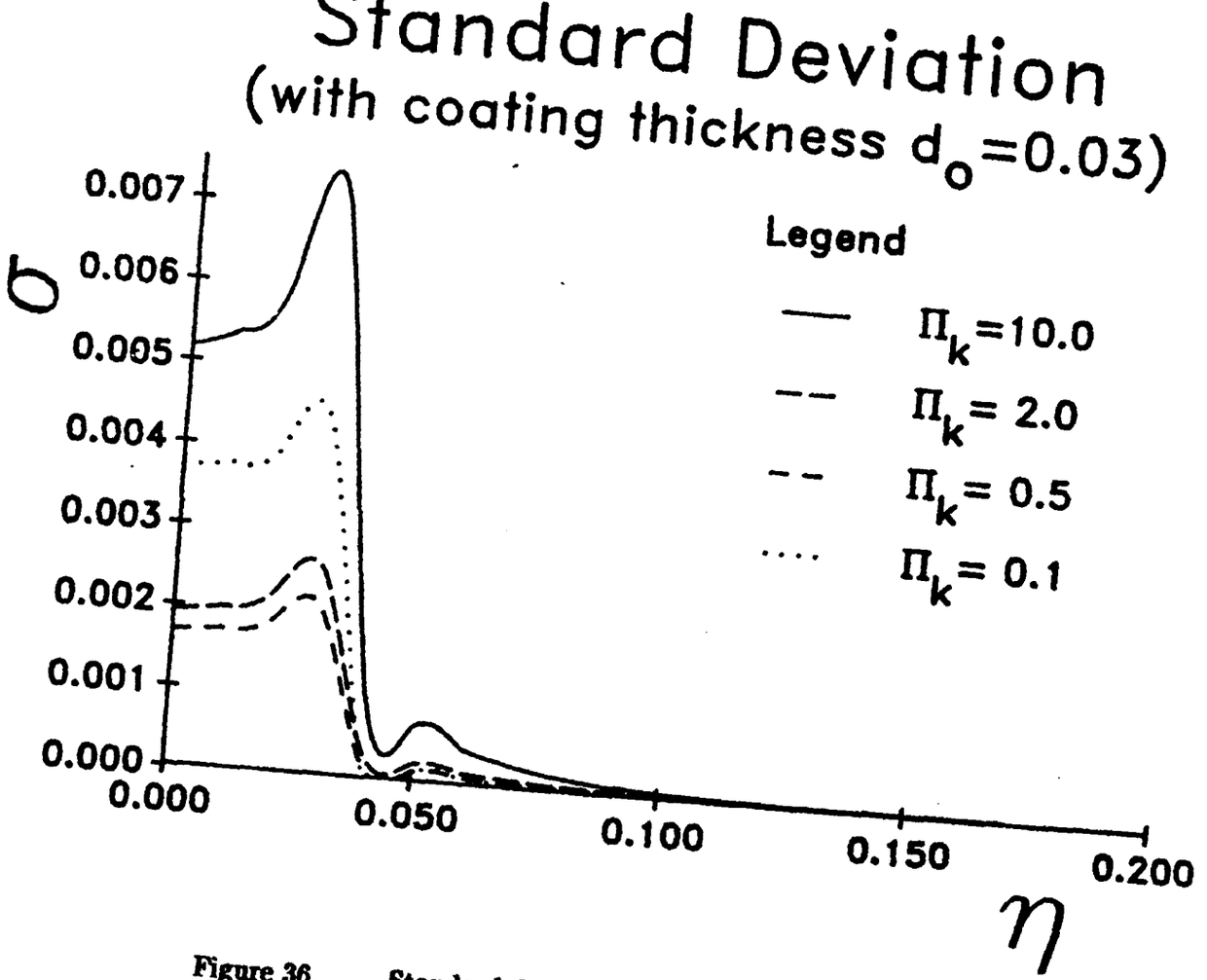

Figure 36. Standard deviation as a function of η with coating thickness d_0=0.03 for thermal conductivity impedance

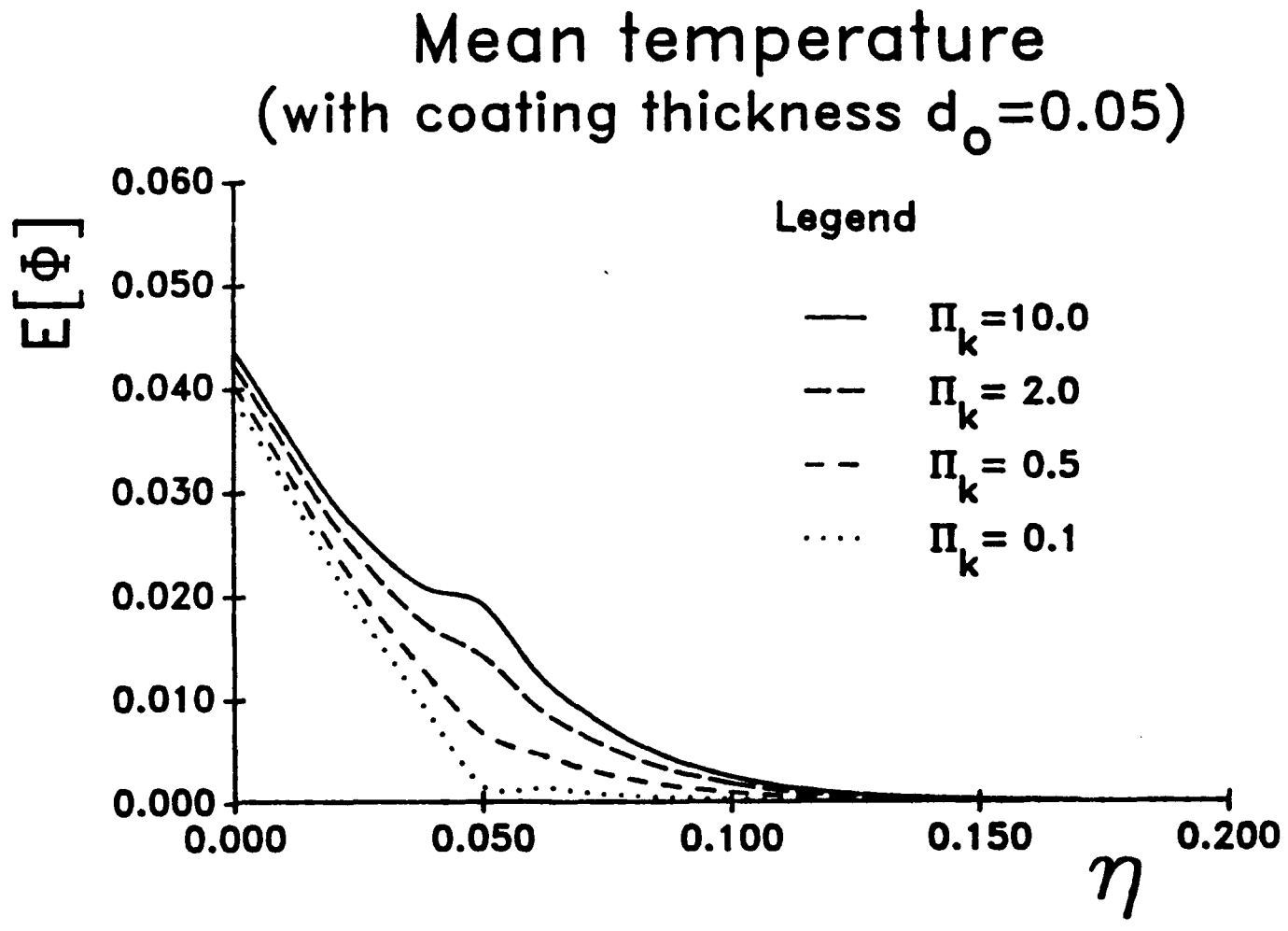

Figure 35. **Mean temperature as a function of η with coating thickness d_0=0.05 for thermal conductivity impedance**

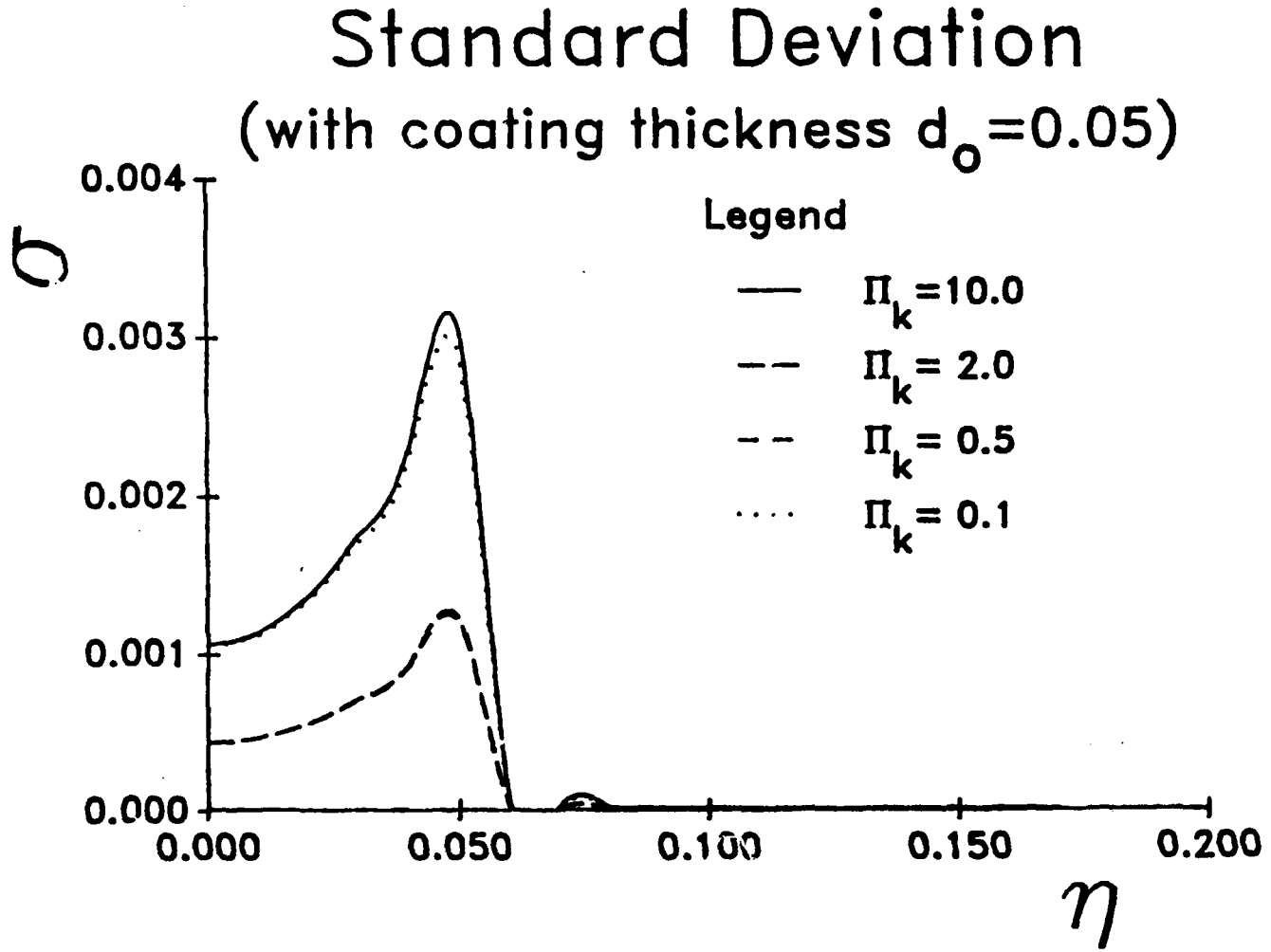

Figure 37. Standard deviation as a function of η with coating thickness d_0=0.05 for thermal conductivity impedance

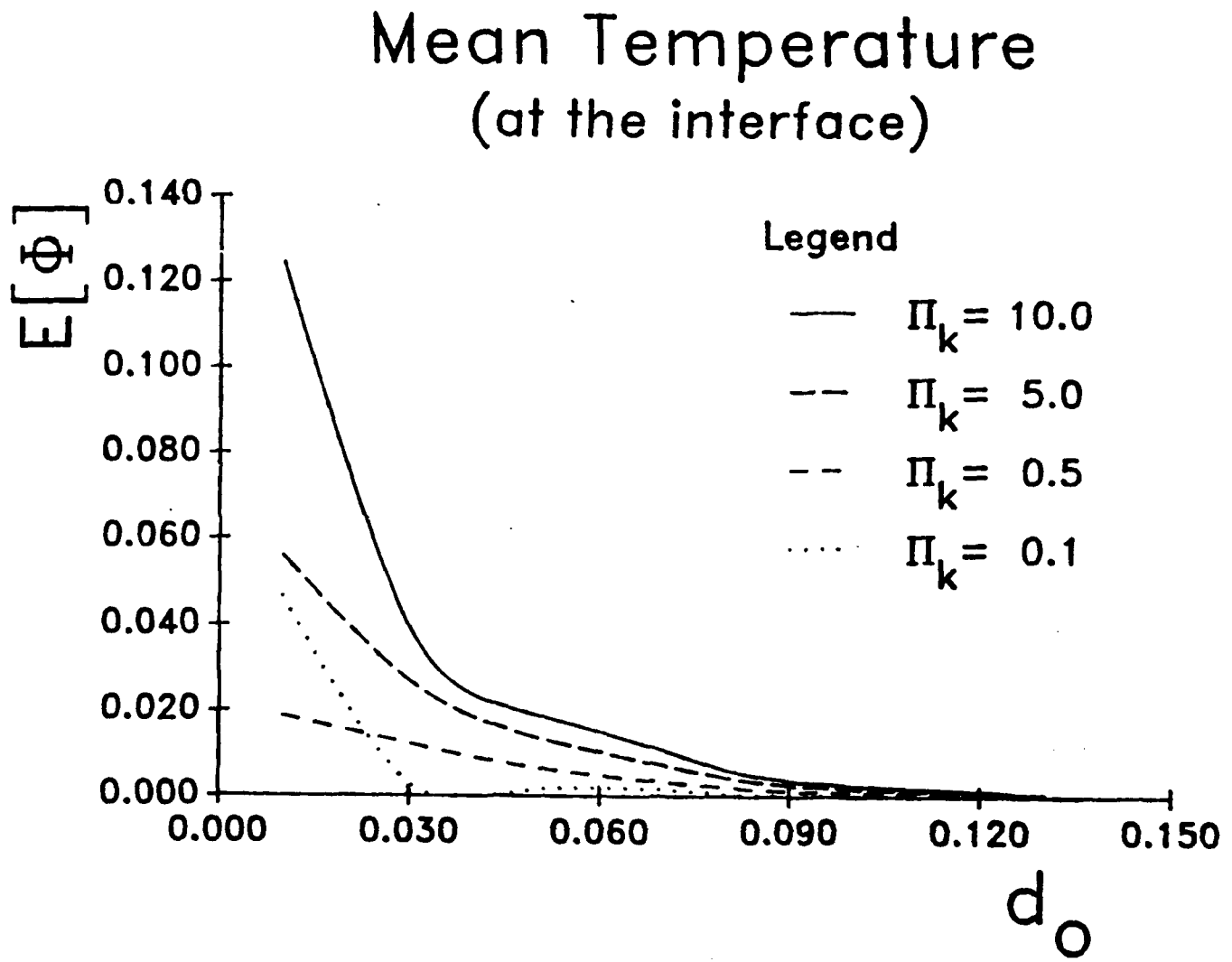

Figure 38. **Mean temperature at the coating/substrate interface as a function of mean coating thickness d_0 for thermal conductivity impedance**

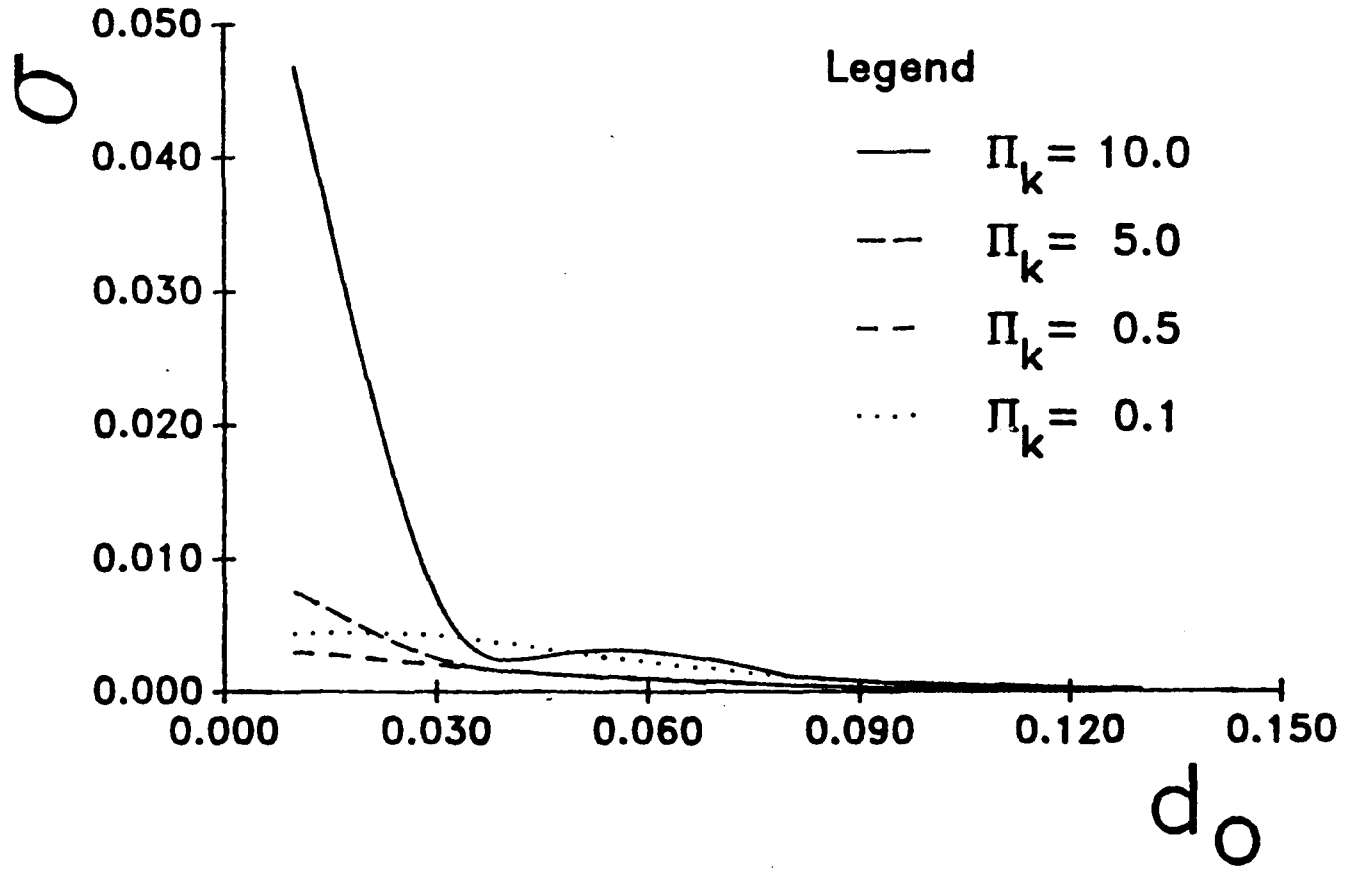

Figure 39. **Standard deviation at the coating/substrate interface as a function of mean coating thickness d_0 for thermal conductivity impedance**

A relative maximum of standard deviation at $\eta = d_0$ can be observed for a thin coating layer (referring to Figures 36, and 37). The coefficient of variation of temperature can reach 18% for thin coatings (referring to Figure 38 and 39) with a thickness randomness of only about 0.1%. This indicates the occurrence of a large deviation of the temperature from its mean value as a result of the small randomness of the coating thickness. Therefore, the amount of deviation from expected values is by no means negligible.

Figures 40 and 41 demonstrate the effect of the "frequency" (p). Figure 40 shows that p has very little effect on the mean response. However, Figure 41 demonstrates that the magnitude of standard deviation increases as p increases up to p = 2, and thereafter becomes constant. These two figures illustrate the contribution of $f(\alpha)$ to the mean value and the standard deviation. The coefficient of variation of the temperature can reach as high as 22% when the mean coating thickness d_0 is about 0.05.

CASE II: The mismatch in thermal capacity, $\Pi_c = (\rho c)_I/(\rho c)_{II}$

Under the same situation as the thermal conductivity case; Figures 42 and 43 show the mean temperature distribution, Figures 44 and 45 show the standard deviation of temperature distribution. By comparing the results with the thermal conductivity case, the temperature distributions are not affected as much by the randomness of the coating thickness from mismatches in thermal capacity. This is due to the fact that $k_I = k_{II}$ and at the interface the heat flux continuity condition also implies continuity in the temperature gradient.

5.3.5. SUMMARY

The effect of the uniformly random coating thickness on the temperature response in a medium with a fast-moving asperity has been analyzed. In the present analysis, we have shown that the amount of the standard deviation of temperature depends upon

(1)the mean coating thickness,

(2)the thermal conductivity,

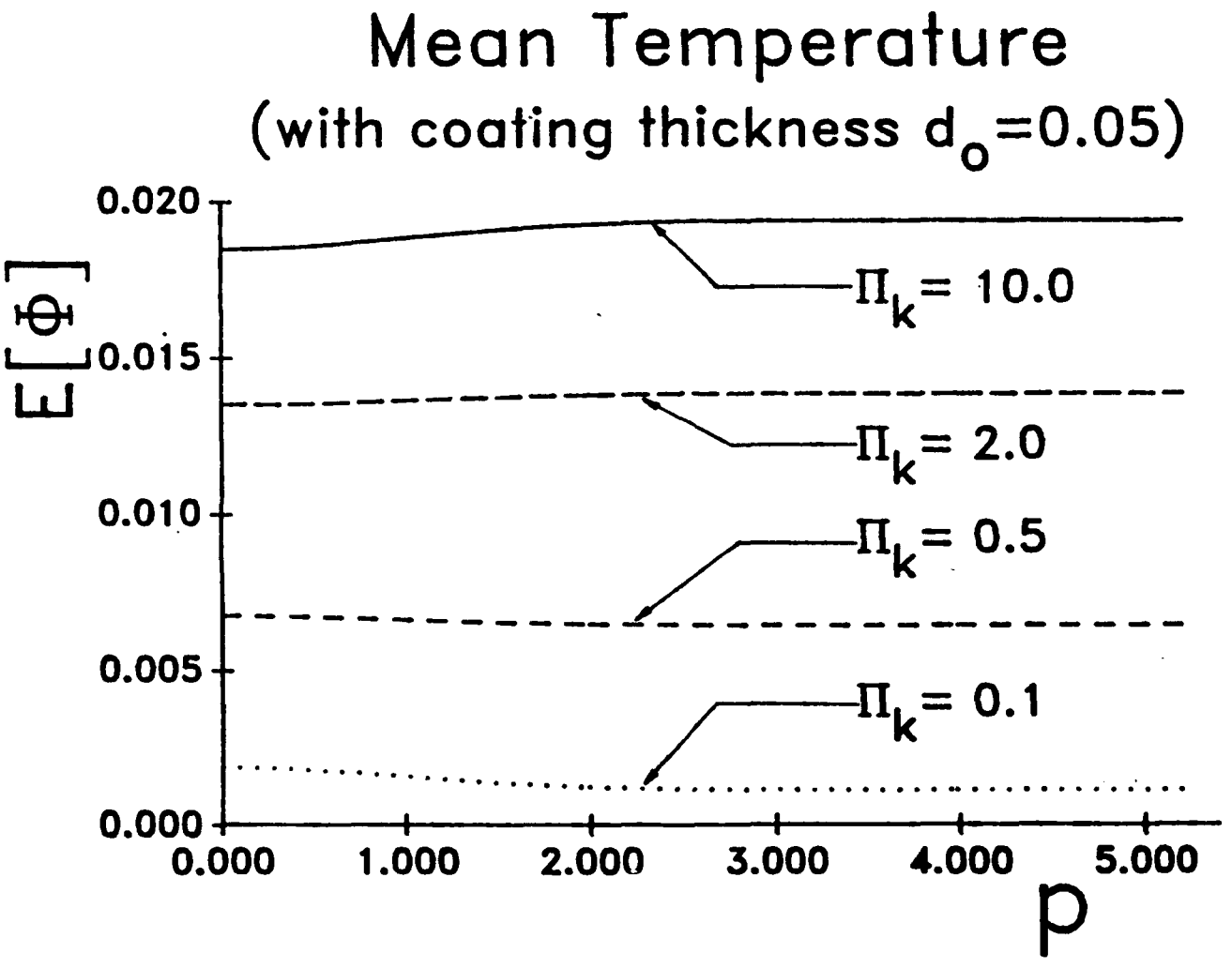

Figure 40. **Mean temperature as a function of the frequency p with coating thickness d_0=0.05 for thermal conductivity impedance**

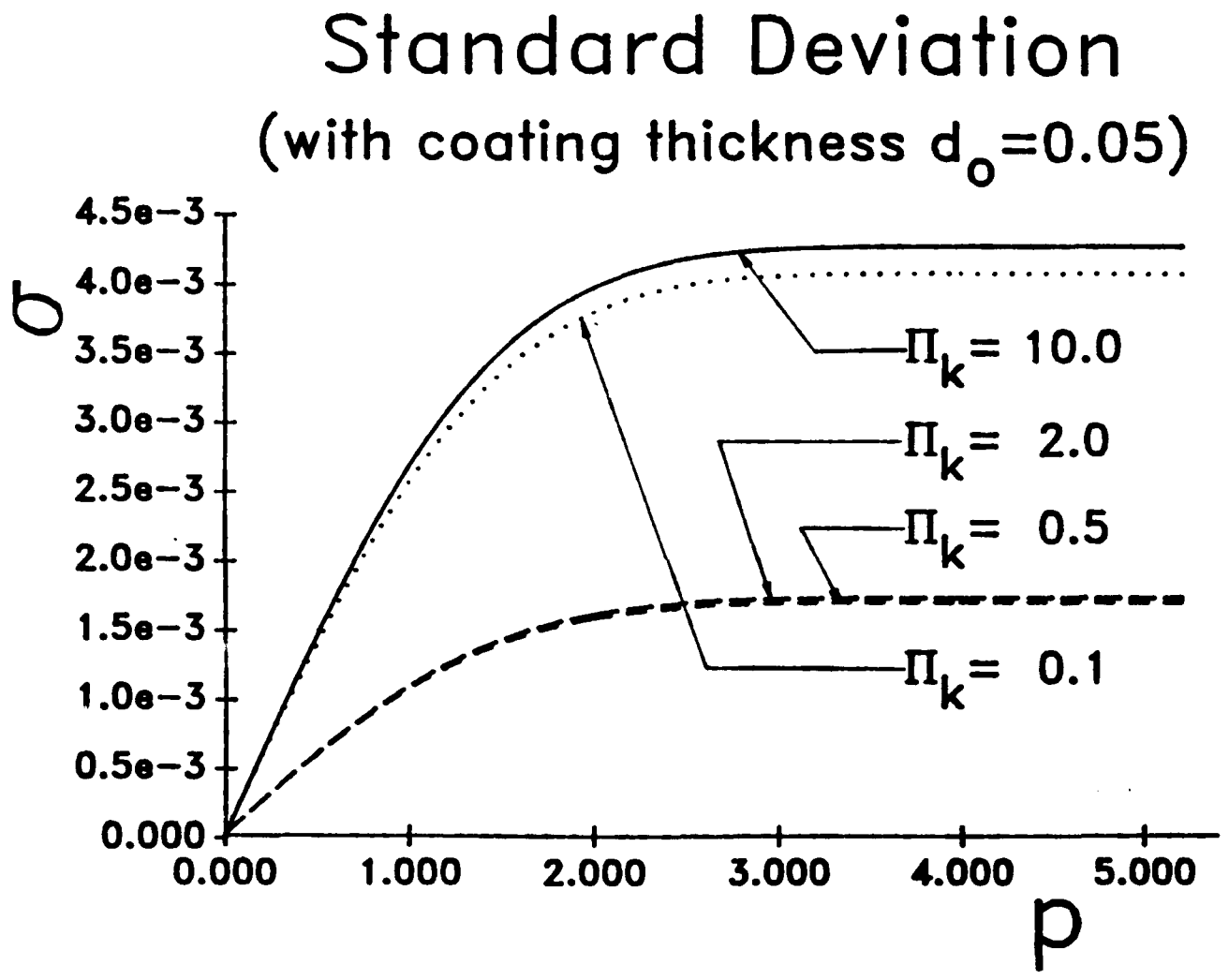

Figure 41. **Standard deviation as a function of the frequency p with coating thickness d_0=0.05 for thermal conductivity impedance**

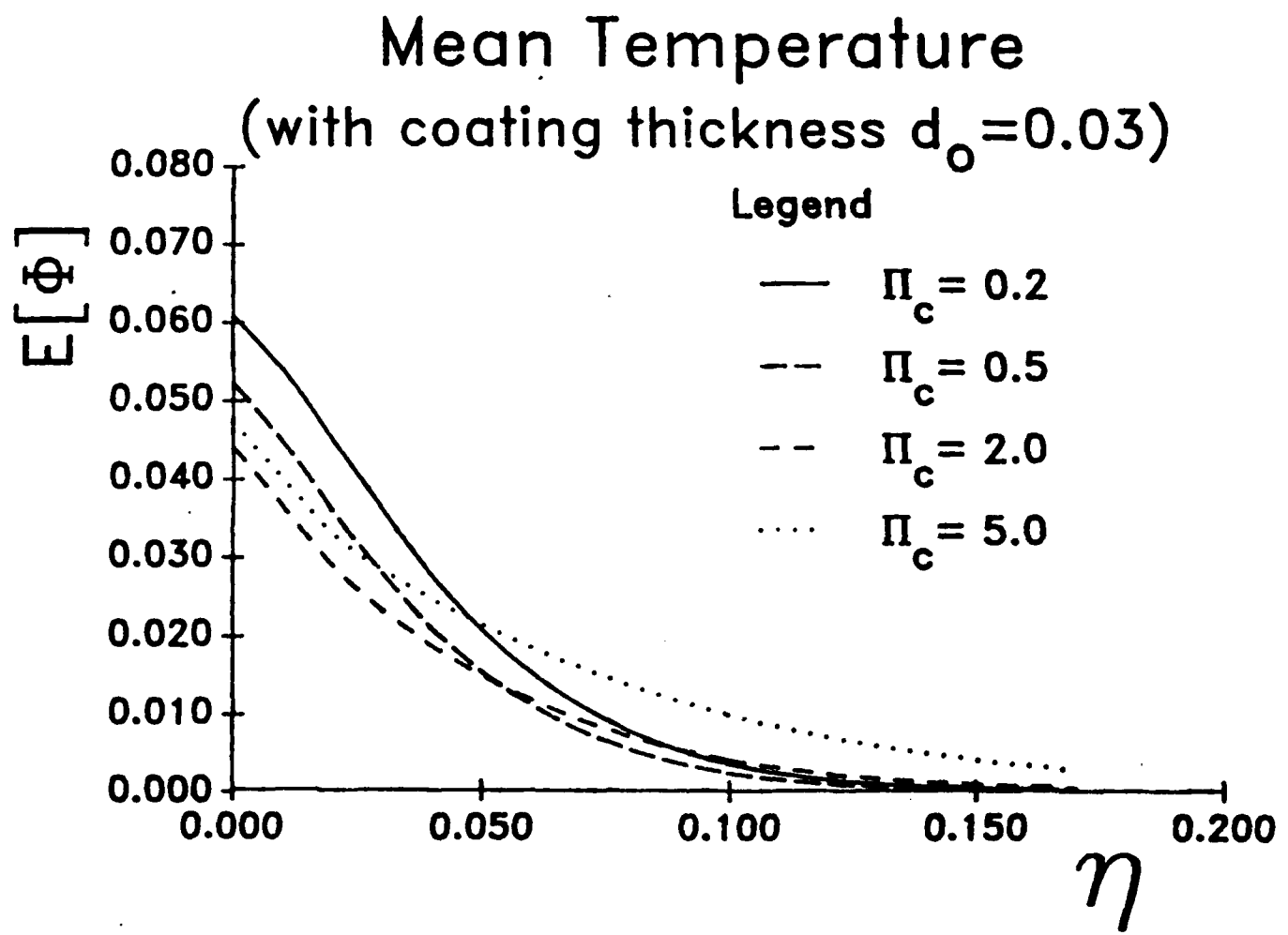

Figure 42. Mean temperature as a function of η with coating thickness d_0=0.03 for thermal capacity impedance

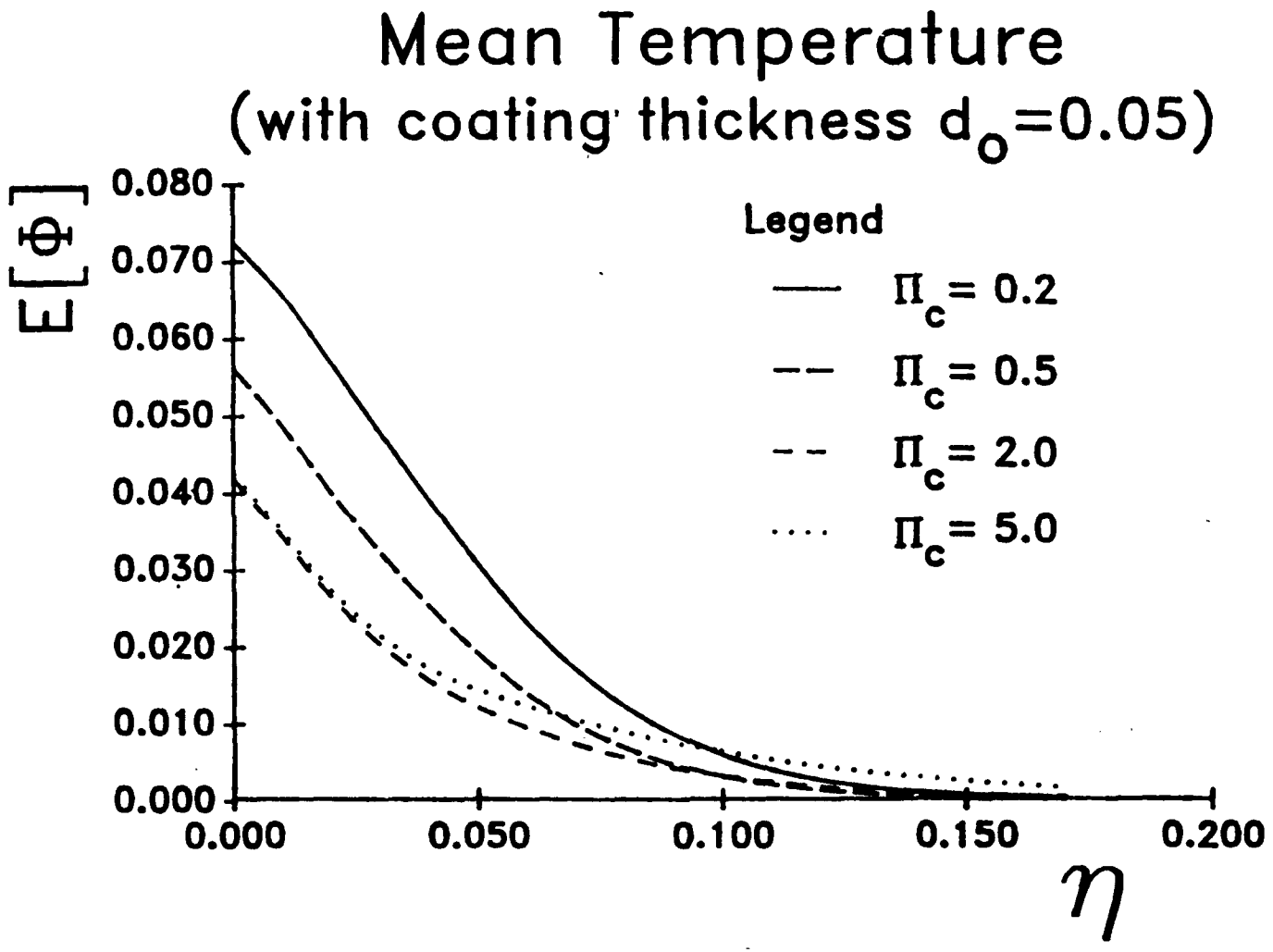

Figure 43. **Mean temperature as a function of η with coating thickness d_0=0.05 for thermal capacity impedance**

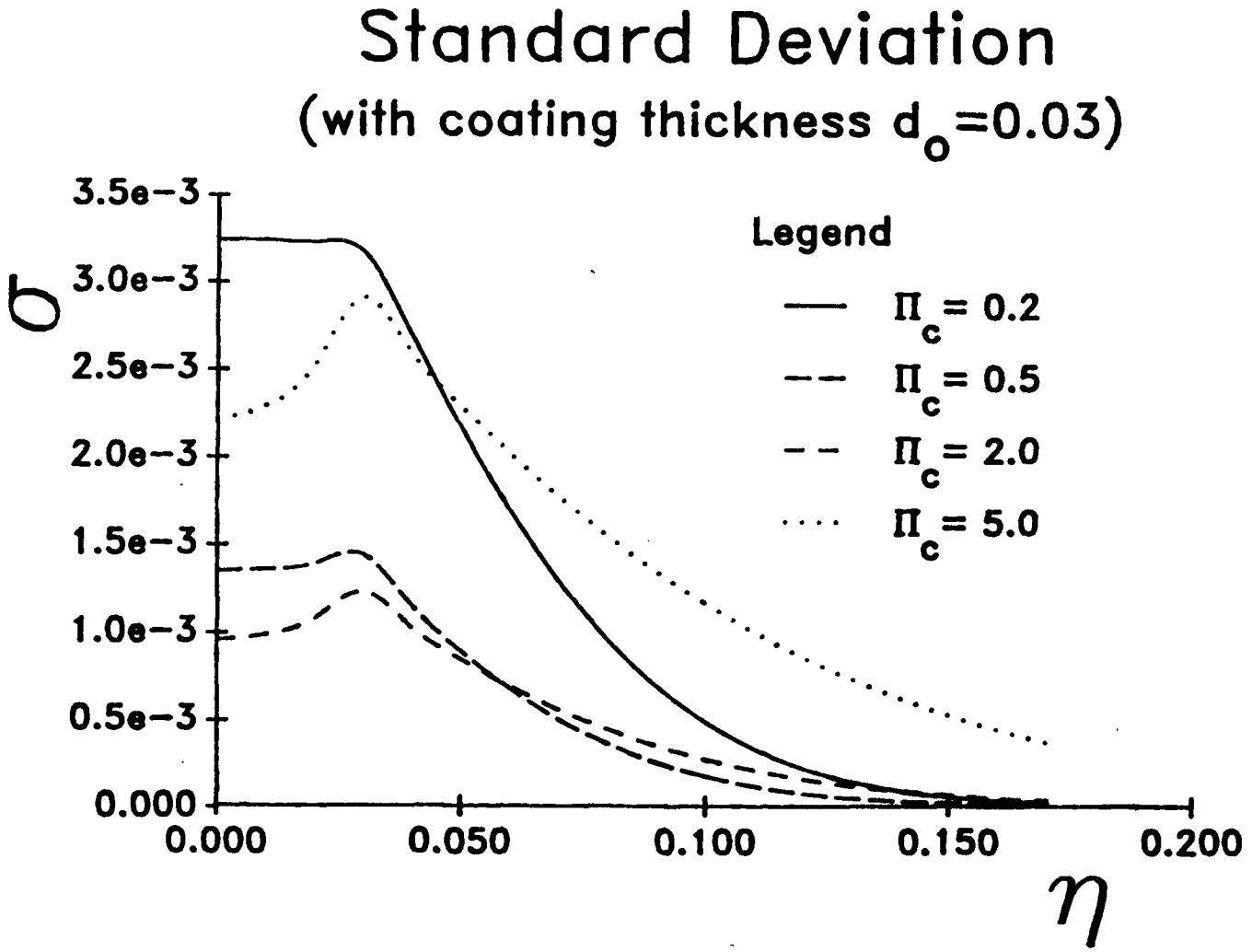

Figure 44. Standard deviation as a function of η with coating thickness d_0=0.03 for thermal capacity impedance

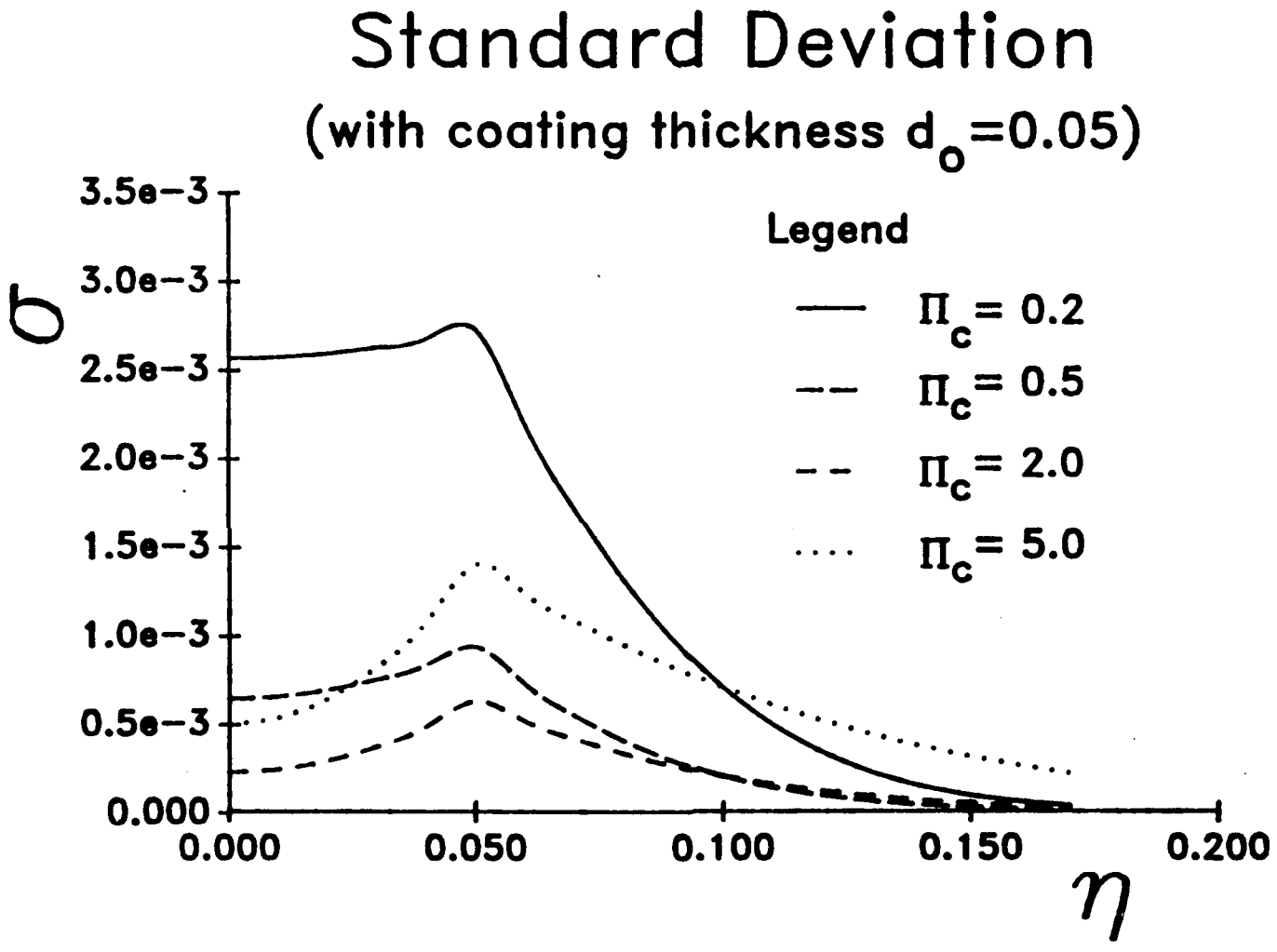

Figure 45. Standard deviation as a function of η with coating thickness d_0=0.05 for thermal capacity impedance

(3)the random fluctuation function $f(\alpha)$.

In the numerical example, a large standard deviation of temperature for a thin coating can be observed. As a consequence, the coating bonding strength , which is selected on the basis of the mean value estimation of temperature, may prove to be unreliable because of the large probability of higher temperature field there. It is expected that the temperature gradient in the neighborhood of thin coating interface has also a significant amount of deviation, which must be considered carefully in the related thermal failure analysis. For the case of position-dependent random coating thickness (i.e., the coating thickness varies from one position to another in one specific specimen) has been understudied.

Finally, it is noted that the analytical results from truncation of the asymptotic series depends on the magnitude of ϵ. For larger values, more terms are needed for accuracy in numerical computation.

6.0. CONCLUSIONS

In the design of hard coating to provide a wear surface for the substrate against high-speed frictional load, the integrity of the coating depends much on the coating thickness and the parametric matching with the substrate. For thick coatings, order of 1 mm, the effect of the substrate on the coating integrity is negligible. Therefore, critical considerations for the appropriate thickness and the interaction of coating and substrate must be given to coating thickness less than 100 microns.

It was found that the principal thermal stress attains a maximum tensile value at a distance from the wear surface, called the critical depth. Discontinuity in material property further aggravates the stress state. For better integrity of the coating, its thickness should avoid to be located in the neighborhood of the critical depth of the coating material. The critical depth is exponentially related to the traversing speed of the asperity and the single material property, the thermal diffusivity. Moreover, if the coating process cannot avoid weak bond that interfacial cavity or crack would develop through use, the coating thickness has another critical thickness to consider. The second thickness that may lead to premature delamination is the critical ligament thickness, which is also controlled by the same parameters as for the critical depth.

The relative stiffness between the coating and the substrate is essential governed by the support that the substrate provides for the coating. The softer the substrate is, the more stress must the coating be subject to the frictional loading. The thermal conductivity of the substrate also is influential in the design for coating integrity. The stress level is lower in the coating, when the substrate is more conductive. Interfacial shearing stress as a criterion for coating delamination is determined by the parameter matching and the coating thickness. The shearing stress rises rapidly as the coating increases in thickness towards the critical depth of the coating material, or when there is an interfacial void.

REFERENCES

Ahmadi, G., 1974, "Heat Transfer in Solids with Random Initial Conditions," ASME *J. of Heat Transfer*, Vol. 11, pp. 474-477.

Ahmadi, G., 1978, "A Perturbation Method for Studying Heat Conduction in Solid with Random Conductivity," *J. of Applied Mechanics*, Vol. 45, pp. 933-934.

Anderson, D.A., Tannehill, J.C. and Pletcher, R.H., 1984, *Computational Fluid Mechanics and Heat Transfer*, McGraw-Hill Book Company, New York.

Archard, J.F., 1959, "The Temperature of Rubbing Surface," *Wear*, Vol. 2, No. 6, pp. 438-455.

Bannerjee, B.N. and Burton, R.A., 1979, "Experimental Studies of Thermoelastic Effects in Hydrodynamically Lubricated Face Seals," *J. Lub. Technol.*, Vol. 101, pp. 275-282.

Blau, P.J., 1980, "The Role of Metallurgical Structure in the Integrity of Sliding Solid Contacts," *Solid Contact and Lubrication*, ASME AMD, Vol. 39, pp 135-191.

Byskov, E., 1970, "The Calculation of Stress Intensity Factors Using the Finite Element Method with Cracked Elements," *Int. J. Fracture Mech.*, Vol. 6, pp. 159-167.

Chen, T.Y. and Jú, F.D., 1987, "Thermal Effect in a Coated Medium (With A Cavity) Due to Friction Heating By A Passing Asperity," *ASLE Transaction*, Vol. 30, No.4, pp. 427-435.

Chen, T.Y. and Ju, F.D., 1988, "Thermo-mechanical Cracking in the Vicinity of a Near-Surface Void due to High-Speed Friction Load," *Jour of Tribology*, Vol. 110, No.2, pp. 306-312.

Chen, T.Y. and Ju, F.D., 1989a, "High-Speed Frictional Heating Effect on the Stress Intensity Factors of a Near-Surface Line Crack," *Advances in Fracture Research*, Ed. K. Salama et al, Vol. 3, Pergamon Press, pp. 2331-2338.

Chen, T.Y. and Ju, F.D., 1989b, "Friction-Induced Thermo-mechanical Cracking in Coated Medium with a Near Surface Cavity," *Jour of Tribology*, Vol. 111, No.2, pp.270-277.

Huang, J.H. and Ju, F.D., 1985, "Thermomechanical Cracking Due to Moving Friction Load," Part I, II, & III, *Wear*, Vol. 102, PP. 81-104.

Huang, J.H. and Ju, F.D., 1987, "The Asperity and Material Parameters in Thermo-mechanical Cracking due to Moving Friction Loads," *Use of New Technology to Improve Mechanical Readiness, Reliability and Maintainability*, Ed. T.R. Shives, Cambridge Univ Press, pp. 205-214.

Ju, F.D. and Huang, J.H., 1982, "Heat Checking in a Contact Zone of a Bearing Seal (A Two-Dimensional Model of a Single Moving Asperity)," *Wear*, Vol. 79, pp. 107-118.

Ju, F.D. and Chen, T.Y., 1984, "Thermo-mechanical Cracking in Layered Media," *Jour of Tribology*, Vol. 106, No.4, pp. 513-518.

Ju, F.D. and Liu, J.C., 1988a, "Effect of Peclet Number in Thermo-Mechanical Cracking due to High-Speed Friction Load," *Jour of Tribology*, Vol. 110, No.2, pp. 217-221.

Ju, F.D. and Liu, J.C., 1988b, "Parameters Affecting Thermo-mechanical Cracking in Coated Media due to High-Speed Friction Load," *Jour of Tribology*, Vol. 110, No.2, pp.222-227.

Kennedy, F.E., 1981, "Surface Temperature in Sliding System--A Finite Element Analysis," ASME *J. of Lub. Tech.*, Vol. 103, pp. 90-96.

Kennedy, F.E. and Karper, S.A., 1982, "Thermocracking of a Mechanical Face Seal," *Wear*, Vol. 79, pp. 21-36.

Kennedy, F.E., Grim, J.N. and Glovsky, R.P., 1983, "Factors Influencing Thermomechanical Failure of Face Seals," II, Interium Report No. 2 (ONR Contact No. N00014-81-k-0090).

Kennedy, F.E. and Grim, J.N., 1984a, "Observation of Contact Conditions in Mechanical Face Seals," *ASLE Trans.*, Vol. 27, pp. 122-128.

Kennedy, F.E., Grim, J.N. and Chuah, C.K., 1984b, "An Experimental/Theoretical Study of Contact Phenomena in Mechanical Face Seals," *Developments in Numerical and Experimental Methods Applied to Tribology*, pp. 285-291.

Ling, F.F. and Mow, V.C., 1965, "Surface Displacement of a Convective Elastic Half-Space Under an Arbitrarily Distributed Fast-Moving Heat Source," *J. Basic Eng.*, pp. 729-734.

Ling, F.F., 1972, *Surface Mechanics*, John Wiley & Sons, New York, pp. 56-61.

Ling, F.F., 1973, *Surface Mechanics*, John Wiley & Sons, Inc..

Liu, J.C., 1986, "The Parametric Effects in Thermo-Mechanical Cracking in Coated Media Due to High Speed Asperity Excitation," Master Thesis, University of New Mexico.

Liu, J.C. and Ju, F.D., 1989, "Asperity Excited Thermo-Mechanical Field in Media with Uniformly Random Coating Thickness," *Jour of Tribology*, Vol. 111, No.1, pp. 129-135.

(References Continue)

Mow, V.C. and Cheng, H.S., 1967, "Thermal Stresses in an Elastic Half-Space Associated with an Arbitrarily Distributed Moving Heat Source," *Z. Angrew. Math. Phys.*, Vol. 18, pp. 500-507.

Nayfeh, A.H., 1980, *Introduction to Perturbation Techniques*, John Wiley & Sons, New York.

Owen, D.R.J. and Fawkes, A.J., 1983, *Engineering Fracture Mechanics: Numerical Methods and Applications*, Pineridge Press Ltd. Swansea, U.K.

Ruff, A.W., and Blau, P.J., 1980, "Studies of Microscopic Aspects of Wear Processes in Metals," National Bureau of Standard, NBSIR 80-2085.

Samuels, J.C., 1966, "Heat Conduction in Solids with Random External Temperature and/or Random Internal Heat Generation," *Int. J. Heat Transfer*, Vol. 9, pp.301-314.

Sih, G.C., 1962, "On the Singular Character of Thermal Stresses Near a Crack Tip," ASME *J. of Applied Mechanics*, Vol. 29, pp. 587-589.

Walsh, P.F., 1971, "The Computation of Stress Intensity Factors by a Special Finite Element Technique," *Int. J. Solids Struct.*, Vol. 7, pp. 1333-1342.

Wilson, W.K., 1971, "Some Crack Tip Finite Elements for Plate Elasticity in Fracture Toughness," *Proc. of Fifth Nat. Symp. on Fract. Mech.*, ASTM STP514.

Williams, M.L., 1952, "Stress Singularities Resulting from Various Boundary Conditions in Angular Corners of Plates in Extension," ASME *J. of Applied Mechanics*, pp. 526-528.

Tzou, D.Y., 1987a, "Stochastic Analysis of Temperature Distribution in the Solid with Random Heat Conductivity," *J. of Heat Transfer*, Vol. 110, pp.23-29.

Tzou, D.Y., 1987b, "Stochastic Modeling for Contact Problems in Heat Conduction," *Int. J. Heat Mass Transfer*, Vol. 32, pp.913-921.

Appendix

Temperature Field Solution

(i)Solution for the 0^{th} order:

$$\tilde{\phi}_0^I = A_0^I \exp(-F_I\eta) + B_0^I \exp(F_I\eta), \tag{A.1}$$

$$\tilde{\phi}_0^{II} = A_0^{II} \exp(-F_I\eta), \tag{A.2}$$

where

$$A_0^I = \frac{\tilde{Q}(F_I+\Pi_k F_{II})}{F_I[(F_I+\Pi_k F_{II})-(F_I-\Pi_k F_{II})\exp(-2F_I d_0)]},$$

$$B_0^I = \frac{\tilde{Q}(F_I-\Pi_k F_{II})\exp(-2F_I d_0)}{F_I[(F_I+\Pi_k F_{II})-(F_I-\Pi_k F_{II})\exp(-2F_I d_0)]},$$

$$A_0^{II} = \frac{2\tilde{Q}\exp[(F_{II}-F_I)d_0]}{[(F_I+\Pi_k F_{II})-(F_I-\Pi_k F_{II})\exp(-2F_I d_0)]},$$

and

$$F_\beta = \sqrt{s^2 - \iota R_\beta s}.$$

(ii)Solution for the 1^{st} order

$$\tilde{\phi}_1^I = A_1^I \exp(-F_I\eta) + B_1^I \exp(F_I\eta), \tag{A.3}$$

$$\tilde{\phi}_1^{II} = A_1^{II} \exp(-F_I\eta), \tag{A.4}$$

where

$$A_1^I = B_1^I = \frac{-2f(\alpha)\tilde{Q}(F_I^2-\Pi_k^2 F_{II}^2)\exp(-2F_I d_0)}{[(F_I+\Pi_k F_I)-(F_I-\Pi_k F_{II})\exp(-2F_I d_0)]^2},$$

$$A_1^{II} = \frac{-2f(\alpha)\tilde{Q}(F_I-F_{II})(F_I+\Pi_k F_{II})\exp[(F_{II}-F_I)d_0]}{[(F_I+\Pi_k F_I)-(F_I-\Pi_k F_{II})\exp(-2F_I d_0)]^2} +$$

$$+ \frac{-2f(\alpha)\tilde{Q}(F_I+F_{II})(F_I-\Pi_k F_{II})\exp[(F_{II}-3F_I)d_0]}{[(F_I+\Pi_k F_I)-(F_I-\Pi_k F_{II})\exp(-2F_I d_0)]^2}.$$

(iii)Solution for the 2nd order

$$\tilde{\phi}_2^I = A_2^I\exp(-F_I\eta) + B_2^I\exp(F_I\eta), \qquad (A.5)$$

$$\tilde{\phi}_2^{II} = A_2^{II}\exp(-F_I\eta), \qquad (A.6)$$

where

$$A_2^I = B_2^I = \frac{2f^2(\alpha)\tilde{Q}F_I(F_I-\Pi_k F_{II})^2(F_I+\Pi_k F_{II})\exp(-4F_I d_0)}{[(F_I+\Pi_k F_I)-(F_I-\Pi_k F_{II})\exp(-2F_I d_0)]^3} +$$

$$+ \frac{2f^2(\alpha)\tilde{Q}F_I(F_I-\Pi_k F_{II})(F_I+\Pi_k F_{II})^2\exp(-2F_I d_0)}{[(F_I+\Pi_k F_I)-(F_I-\Pi_k F_{II})\exp(-2F_I d_0)]^3},$$

$$A_2^{II} = \frac{f^2(\alpha)\tilde{Q}(F_I-F_{II})^2(F_I+\Pi_k F_{II})^2\exp[(F_{II}-F_I)d_0]}{[(F_I+\Pi_k F_I)-(F_I-\Pi_k F_{II})\exp(-2F_I d_0)]^3} -$$

$$- \frac{2f^2(\alpha)\tilde{Q}(F_{II}^2-3F_I^2)(F_I^2-\Pi_k^2F_{II}^2)\exp[(F_{II}-3F_I)d_0]}{[(F_I+\Pi_k F_I)-(F_I-\Pi_k F_{II})\exp(-2F_I d_0)]^3} +$$

$$+ \frac{f^2(\alpha)\tilde{Q}(F_I+F_{II})^2(F_I-\Pi_k F_{II})^2\exp[(F_{II}-5F_I)d_0]}{[(F_I+\Pi_k F_I)-(F_I-\Pi_k F_{II})\exp(-2F_I d_0)]^3}.$$